

https://dspace.org/

Distribution of rare earth elements in the Epembe Carbonatite Dyke, Opuwo Area, Namibia

Kapuka, Ester P.

2019

https://hdl.handle.net/10539/29428

Kapuka, Ester Panduleni (2019) Distribution of Rare Earth Elements in the Epembe carbonatite dyke, Opuwo area, Namibia, University of the Witwatersrand, Johannesburg, <http://hdl.handle.net/10539/29428>

Downloaded from a DSpace repository. https://dspace.org/



FACULTY OF SCIENCE

SCHOOL OF GEOSCIENCES

Distribution of Rare Earth Elements in the Epembe Carbonatite Dyke, Opuwo Area, Namibia

---

Research report submitted to the Faculty of Science, University of Witwatersrand, in partial fulfillment of the requirements for the degree of Masters of Science in Economic Geology (Course Work & Research Report)

BY

Ester P. Kapuka [1535875]

SUPERVISOR: **Professor Paul Nex**

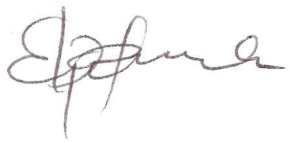
Declaration

I, the undersigned, hereby affirm that this dissertation is the product of my own work that it has not been submitted before for any degree or examination at any other university. Further, I have faithfully acknowledged all sources used and have properly cited these in this thesis.

Date

02/10/2019

Signature



Acknowledgements

I would like to express my profound gratitude to my research supervisor, Professor Paul Nex of the School of Geosciences, University of the Witwatersrand for his endless support, guidance and supervision of this research work. Acknowledgment goes to Kunene Resource Holdings (Pty) and the Gecko Exploration team, particularly Dr. R. Ellmies for having granted me permission to work on their EPL as well as aiding me with literature and data related to the research project. The Geological Survey of Namibia, particularly the department of Regional Mapping and Geo-information for having granting me a car for the fieldwork as well as several data used in this project. This research would have not been of greater value and achievement without the support of GSN.

In addition, I would like to thank my colleagues from GSN Mr. Abner Nghoongholoka and Mr. Iyambo Nekwaya of Gecko Exploration who accompanied me in the field, for their pleasing teamwork during the fieldwork. They had supported me greatly and they were always keen to help me.

I am, indeed, short of words to express my inner-feel to my colleague and friends Mrs. Kaasheka, Mrs. Amutenya and Ms. Pokolo for their constant encouragement, moral support throughout the course of the work and for critical moments. It would not have been possible to complete this research work without their backing. The sponsorship by Namibia Student Financial Assistant Fund (NSFAF) for the study of the master's degree is greatly recognized. It would not be possible without that support.

Lastly but not least, I am very obliged to my beloved family members for standing behind me for all important decisions, particularly for pursuing M.Sc. degree and for constant encouragements throughout research work.

Thank you very much, everybody!

Abstract

The Epembe carbonatite dyke at the Epembe Carbonatite-Syenite Complex in the Kunene region on the northwestern border of Namibia was emplaced along a northwest-trending fault zone, into syenites and nepheline syenites and extends for approximately 6.5 km in a northwest to southeast direction with a maximum outcrop width of 400 m. The Epembe carbonatite has a Mesoproterozoic age of 1184 ± 10 Ma which is slightly younger than their host nepheline syenites (1216 ± 2.4 Ma).

Following the geological data collection and laboratory analysis of whole-rock samples [using optical microscopy, X-ray fluorescence (XRF) and inductively coupled plasma mass spectrometry (ICP-MS)] the collected data was studied in detail in order to determine the geochemical composition of the Epembe carbonatite dyke. This research therefore presents new geochemical data for the Epembe carbonatite in order to describe the distribution and occurrence of rare earth elements of this dyke.

The carbonatite displays a heterogeneous characteristic both texturally and mineralogically highlighting clear successions of at least three magmatic pulses. Irrespective of the changes, all carbonatite phases are inferred to be sourced from the same magma because they are typified by a similar geochemical signature of both major and trace element composition. They are characterised by high concentrations of calcium (CaO: 38.01 - 55.31 wt. %), phosphorus (P) (up to 18076), titanium (Ti) (up to 5122 ppm) strontium (Sr) (up to 12315 ppm) and niobium (Nb) with the (highest value of up to 2022 ppm) alongside low concentrations of iron (FeO: 0.87 - 9.29 wt. %), magnesium (MgO: 0.19 – 1.33 wt. %) silica (SiO_2: 1.30 – 10.89 wt. %) and total alkalis ($K_2O + Na_2O < 2.0$ wt. %) , hence they are regarded as one carbonatite dyke.

The petrography and whole-rock element compositions of major elements have demonstrated the Epembe carbonatite is primarily made up of course-grained calcite (~92%) with a $CaO+MgO+Fe_2O_3+MnO$ ratio of 0.93 relative abundances (in wt. %) and thus is classified as calcio or calcite carbonatite. The total REE content of Epembe carbonatite is high (406 – 912 ppm) with high LaN/YbN value (10.19 -28.49) and thus atypical of calcio-carbonatites. Chondrite normalized REE pattern for the carbonatite exhibit a strong steady decrease (negative slope) from LREEs to HREEs with a slight negative Eu anomaly but those are relatively low compared to global average calcio-carbonatites. Even though the Epembe carbonatite is enriched in Rare Earth Elements, there were no REE-bearing minerals observed at Epembe carbonatite except for monazite in trace amounts. Geochemical results show that the REE are either included in several accessory minerals such as apatite and pyrochlore and possibly in gangue minerals (i.e., silicates [including calcite and zircons] and carbonates) through enrichment processes related to fractional crystalisations and chemical substitution.

Keywords: Rare Earth Elements, Epembe carbonatite

TABLE OF CONTENTS

Declaration i

Acknowledgements ii

Abstract iii

List of Figures vi

List of Tables ix

List of Acronyms x

1 CHAPTER 1: INTRODUCTION AND PROJECT DETAILS 1

1.1 General introduction 1

1.1.1 Rationale 2

1.1.2 Problem statement 2

1.1.3 Location of the study area 3

1.1.4 Objectives of the study 3

1.2 Regional geology of the study area 4

1.2.1 Epupa Metamorphic Complex (EMC) (also Epupa Complex [EC]) 5

1.2.2 Kunene Igneous Complex (KIC) 6

1.2.3 Swartbooisdrift and Epembe carbonatites 7

1.3 Geology of the study area 8

1.4 Methodology 10

2 CHAPTER 2: GENERAL OVERVIEW OF CARBONATITES AND RARE EARTH ELEMENTS 12

2.1 Carbonatites overview 12

2.1.1 Tectonic setting of carbonatites 12

2.1.2 Origin of carbonatite magmas 13

2.1.3 Carbonatites and REE concentration 14

2.2 Overview of Rare Earth Elements (REE) 15

2.2.1 Definition and characteristic of REE 15

2.2.2 Properties and Uses of REE 16

2.2.3 REE mineralogy 17

2.2.4 Economic importance of REE 18

3 CHAPTER 3: FIELD WORK AND PETROGRAPHY 21

3.1 Introduction 21

3.2 Geological field visit and sampling 21
3.3 Field Observations 21
3.3.1 Carbonatite 21
3.3.2 Associated country rocks 22
3.4 Petrography 22
3.4.1 Hand Specimen Petrography 22
3.4.2 Microscopy Petrography 28
3.4.3 X-Ray Diffraction analysis 30
4 CHAPTER 4: GEOCHEMISTRY 32
4.1 Geochemistry of major elements 32
4.2 Geochemistry of trace and REE elements 32
4.2.1 Trace element 33
4.2.2 Rare Earth Element 34
4.3 Radiometry maps and REEs 43
5 CHAPTER 5: DISCUSSION AND CONCLUSION 47
5.1 Carbonatite type and petrography 47
5.2 Major and Trace element geochemistry 49
5.3 REE Geochemistry 50
5.4 REE distribution in Epembe carbonatite 52
5.5 Conclusions 53
6 REFERENCES 54
7 APPENDICES 61
Appendix A: Sample preparation: 61
Appendix B: Geological map 63
Appendix C: Ortho-ASTER 3ALevel1 64
Appendix D: List of collected field samples from Epembe carbonatite 65
Appendix E: Description of field samples 65
Appendix F: Mineralogy and textural characteristic of Epembe carbonatite from thin section analysis 67
Appendix G: XRD results 72
Appendix H: Analytical Results 85

List of Figures

Figure 1-1 *Satellite image (Landsat 8 sharpened) showing the location of the study area and the EPL 3299 boundary which incorporates the Epembe Carbonatite dyke (data source for satellite image: National Aeronautics and Space Administration (NASA) and Directorate.* 3
Figure 1-2 *Simplified regional map, showing the distribution of mobile belts (inset map) and pre-Pan-African basement rocks on the northern Namibia (Figure adapted from Simon, 2017 modified after Miller et al. 1983) and southern Angola (Modified after Carvalho et al. 2009).* 5
Figure 1-3 *Geological overview map of the southern part of the Kunene Intrusive Complex and the Epupa Metamorphic Complex. The Intrusion of the late Epembe Alkaline suite is seen on the southern margin of EMC (syenites and nepheline syenites). The Epembe dyke is shown in blue. Map adapted and modified after Menge (1996).* 7
Figure 1-4 *Local geological map of the Epembe-syenite Complex showing the Epembe carbonatite dyke and the surrounding rocks (Data source: GS*..... 9
Figure 1-5 *Regional and Local geological maps. a) Simplified regional map of part of the Kunene Intrusive/igneous Complex (KIC) showing the extent of the study area marked with a black rectangle, b) local area sketch map of the study area showing the Epembe carbonatite dyke. (Modified from Simon et al. (2007) after Becker et al. (2006)).* 11
Figure 2-1 *Carbonatite classification diagram based on their dominant modal mineral and on their corresponding major geochemistry. Redrawn after (Woolley and Kempe 1989)*..... 13
Figure 2-2 *The geochemical periodic table of elements, group of elements in their chemical behaviour. REEs are shown at the bottom of the main table (White, 2005).* 16
Figure 2-3 *Different uses and proportions of the REE and the relevant production figures for different countries in 2015 (Zhou et al. 2017).* 19
Figure 2-4 The distribution of global rare earth production by country (Barakos et al. 2016 20
Figure 2-5 *World map showing the global distribution of rare earth element deposits producing mines and exploration targets. (Mountain Pass is currently in maintenance mode) (Source: Barakos et al. 2016)* 20
Figure 3-1*: Google Earth image (Landsat 8, sharpened) of the Epembe carbonatite dyke showing the sampling locations.* 23
Figure 3-2 *Carbonatite outcrop (photo taken facing southeast). The topographic high is dominated by carbonatite and minor syenite whilst the low lying plains on either side are underlain by gneisses of the Epupa Metamorphic Complex.* 24
Figure 3-3 *Field outcrop photographs demonstrating differences in outcrop exposures. A) Topographic high massive carbonatite outcrop (sample No: EPB02, GPS: S 17 ° 30' 44''; E 13° 25' 41.7''), B) Cliff-like fenitised outcrop on the north east side of the carbonatite of the carbonatite intrusion (GPS: S 17° 31' 25.9"; E 13° 26' 41.7"), this granitic gneiss is pink-grey and displays a weak gneissose banding which is dominated by mafic layers. C) Low lying carbonatite outcrops partially covered by sand and gravel located about 100m (west of the dyke) away from the main carbonatite body (sample No: EPB13, GPS: S 17° 30' 34.5"; E 13° 24' 40.7"). D) Partially buried low lying and discontinuous carbonatite outcrops (sample No: EPB06, GPS S 17° 31' 27.3"; E 13° 25' 54.1")*. 24

Figure 3-4 *Schematic representations of the different carbonatite profiles or phases observed at Epembe carbonatite dyke. The lower profile (margins), the middle profile and the upper profile. The lower and middle profiles show a gradational change to massive, coarse crystalline calcite in the upper profiles. The contacts between the profiles are not very well established and therefore are largely inferred.* 25
Figure 3-5 *Epembe Carbonatite outcrops with multiple structures and lithologies. a) Carbonatite with local calcite lenses b) carbonatite showing some cleavages highlighted in red, c) highly fractured granitic gneiss, d) carbonatite characterised by textural pattern that is probably related to magmatic flow, e) massive and non-textured carbonatite, f & g) carbonatite showing weathering, h) massive and mineralised carbonatite with disseminated apatite grains. Scale: hammer =35 cm, pencil = 15cm.* 26
Figure 3-6 *The local country rocks around the Epembe carbonatite dyke. a) Highly fractured fenitised granitic gneiss, fine- to medium-grained, grey to reddish in colour; b) Massive syenite outcrop, typically light-dark grey, medium to coarse grained. Scale: Hammer = 60cm.* 27
Figure 3-7 *Photographs of hand specimens of the carbonatites. A) In outcrop phenocryst of biotite (up to 50mm) characterises this heavily weathered carbonatite that does not contain any feldspar. It is cross cut by late hydrothermal calcite veining; B) White coarse-grained calcite crystals up to 5.0 mm; C) Carbonatite sample displaying equigranular holocrystalline grains of sugary calcite with a pinkish colour due to the presence of feldspar and darker minerals including pyrochlore and aegirine; D) carbonatite samples characterised by dark brown pyrochlore crystals; E) a section of fresh carbonatite displaying calcite and late stage veins stained with iron oxides; F) medium-grained pinkish-brown carbonatite with dark-greenish phlogopite (Mg-biotite) phenocryst. Scale: pencil = 15cm, coin diameter = 25mm.* 27
Figure 3-8 *Thin section photomicrographs of selected representative carbonatite samples in cross polarised light (XPL) and plane polarised light (PPL), showing mineralogical characteristics of the Epembe carbonatites. A) EPB03: Coarse-grained calcite with mica fills in the cracks and fractures (XPL,) B) EPB02: ovoid apatite grains and feldspars embedded in calcite matrix (XPL); C) EPB03: Photomicrograph of coarse-grained calcite, and an ovoid apatite grain hosting pyrochlore grain - arrowed (PPL,); D) EPB08: elongated and aligned apatite grains and calcite grains (PPL,). EPB13: E) medium to fine-grained granular groundmass (gm) of anhedral feldspars, interstitial calcite and minor amount of quartz forming equigranular texture (XPL,) seen also as un-oriented grains; F) coarse grained aegirine in the calcite matrix (XPL). Abbreviations: Aegirine (Aeg), Apatite, (Ap), Pyrochlore (Plc), Calcite (Ca), Microcline (Mc), Plagioclase (Plg).* 29
Figure 4-1 *Ternary diagram (MgO-CaO-FeOt {+MnO) for carbonatites with Epembe carbonatite samples plotting in the field of calcio-carbonatite (≥80%). Field boundaries of ferro-, calcio-, and magnesio-carbonatite after Woolley & Kempe (1989).* 34
Figure 4-2 *Graph of major elements (TiO_2, MnO; Fe_2O_3; SiO_2; P_2O_5; Al_2O_3) plotted against MgO for Epembe carbonatite samples. All oxides with an exemption of MnO exhibit a positive trend.* 35
Figure 4-3 *Major Elements vs. CaO of the investigated Epembe carbonatite samples. Fe_2O_3, MgO, Al_2O_3, Na_2O+K_2O, SiO_2, and FeO show a negative correlation with an increasing CaO. MnO show an increase with increasing CaO content. P_2O_5 does not exhibit a strong variation.* 36
Figure 4-4 *Major element (Al_2O_3, TiO_2, P_2O_5, FeO, $K_2O + Na_2O$, MgO, CaO against SiO_2). All oxides with an exception of CaO exhibit a positive Trend.* 37
Figure 4-5 *Correlation between phosphorus (ppm) and niobium + tantalum (ppm) of the Epembe carbonatite. The general trend shows a positive correlation.* 40

Figure 4-6 *Graph of total REE+Y Vs Nb + Ta. Shows weak correlation (R^2 = 0.1458)*.....40
Figure 4-7 *Binary plot of REE total (ppm) versus selected trace element (ppm). Elements Zr, P, Nb show a weak correlation with the total REE while U and Ti displays insignificant relationship with total REE.*.....41
Figure 4-8 *REE pattern for carbonatite, fenite and syenite samples from the Epembe carbonatite dyke and surrounding rocks. Chondrite normalised using data from McDonough and Sun (1995).* 43
Figure 4-9 *Airborne radiometric data showing the distribution of potassium (ppm) in the study area, the deep blue to light blue colours indicates area with the lowest radioactive rocks, while the green-orange-red range of colours show the intermediate radioactive rocks and the pink colour represents areas with high radioactive rocks. The inferred Epembe carbonatite dyke is delineated by a black outline (Data source: GSN)*.....44
Figure 4-10 *Airborne radiometric data showing the distribution of uranium (ppm) in the study area, the deep blue to light blue colours indicates area with the lowest radioactive rocks, while the green-orange-red range of colours show the intermediate radioactive rocks and the pink colour represents areas with high radioactive rocks. The inferred Epembe carbonatite dyke is delineated by a black outline (Data source: GSN)*.....45
Figure 4-11 *Airborne radiometric data showing the distribution of thorium (ppm) in the study area, the deep blue to light blue colours indicates area with the lowest radioactive rocks, while the green-orange-red range of colours show the intermediate radioactive rocks and the pink colour represents areas with high radioactive rocks. The inferred Epembe carbonatite dyke is delineated by a black outline (Data source: GSN)*.....46
Figure 5-1 *Bocks of syenites (xenoliths) that have been incorporated into the intruding carbonatite. A) Syenite xenoliths with flow banding oriented in a north-west to south-east direction; B)* carbonatite *containing xenoliths of Syenites and aegirine. Scale: Hammer (35 cm), pencil (15 cm).*.....47
Figure 5-2 *Thin section photographs of two carbonatite samples displaying the vein/fractures cutting through the carbonatite. The veins are observed to be filled with opaque iron-oxide minerals.* 48
Figure 5-3 *Phase diagram of aluminous lherzolites with melting interval (gray area), sub-solidus reactions and geothermal gradient. The diagram demonstrates the pressure and temperature effect on mineral formation where by it can be deduced that plagioclase is favoured a shallower (<30 km) depth as opposed to garnet (80 – 400 km) (Figure adapted from Wyllie, 1981).* 51
Figure 5-4 *Chondrite normalised rare earth elements (REEs) composition in Epembe carbonatite. The comparative data for global average calcio-carbonatite composition is shown (after Woolley and Kempe, 1989). Chondrite normalising data from Sun and McDonough (1995).* 52
Figure 7-1 *Crushing processes. A) A researcher is crushing samples using a Geo-crusher in the GSN laboratory; B) Sample sizes after crushing that were sending to the milling machine.*.....61
Figure 7-2 *Milling process. A) Samples were milled using a pulveriser machine (RS 200) at GSN laboratory; B) pulp samples (-64 microns) that were send for ICP-MS and X-RF study.*.....62
Figure 7-3 *Geological map of 1:250k maps of the study are*.....63
Figure 7-4 *Processed Ortho-Aster 3ALevel 1 RGB_321 of the study area*.....64

List of Tables

Table 1-1 *Stratigraphy of the different rock unit in the study area together with ages (modified from Menge, 1986 & 1996; Seth et al., 2003).* 4
Table 2-1 A selection of REE bearing minerals (Walters et al. 2011)..... 17
Table 3-1 Summary of the optical characteristics of the mineralogy of Epembe carbonatite..... 30
Table 3-2 *Mineralogical composition of Epembe minerals*..... 31
Table 4-1 *Whole rock major-elements analyses (wt. %) of Epembe carbonatite. Average calcio-carbonatite compositions are after Woolley and Kempe (1989).* 38
Table 4-2 *Trace element analyses results (ppm) for Epembe carbonatite samples. Global average calcio-carbonatite compositions are from Woolley and Kempe (1989).* 39
Table 4-3 *REE chondrite normalised data for sixteen samples of carbonatite, fenite and syenites from Epembe-Syenite complex. Chondrite values after McDonough and Sun (1995).*..... 42
Table 7-1 *List of collected field samples from Epembe carbonatite* 65
Table 7-2 *Description of field samples* 65
Table 7-3 *Mineralogy and textural characteristic of Epembe carbonatite from thin section analysis*..... 67

List of Acronyms

ECSC - Epembe Carbonatite-Syenite Complex
EMC - Epupa Metamorphic Complex
ESAP Epembe-Swartbooisdrift Alkaline Province
KIC - Kunene Igneous Complex
EC - Epupa Complex
REEs - Rare Earth Elements
LREE - Light Rare Earth Element
HREE - Heavy Rare Earth Element
EPL - Exclusive Prospecting License
XRD - X-Ray Diffraction
XRF - X-Ray Fluorescence
MME - Ministry of Mines and Energy
GSN - Geological Survey of Namibia
Ma - Millions years
Ga - Billion years
ICP-MS - Inductively Coupled Plasma Mass Spectrometry
ASTER - Advanced Spaceborne Thermal Emission and Reflection Radiometer.
ENVI - Environment for Visualizing Images
Ppm - parts per million
wt. % - percentage by weight
NASA - National Aeronautics and Space Administration

CHAPTER 1: INTRODUCTION AND PROJECT DETAILS

1.1 General introduction

Following the banning of China's export of rare earth elements (REE) to Japan and reduced export quotas of REE, a significant spike in REE prices occurred between 2006 and 2012 (Morrison and Tang, 2012). However, it is noted that those reports were disputed by China who denied such statements. These actions caused the demand for REE to increase and the exploration for more REE deposits accelerated. In addition, China's decision to stockpile its REE resources (Lottermoser, 1992) also resulted in a noticeable global increase in the search for REE.

During recent years, REE have attracted the attention of different exploration companies and researchers alike to examine the potential host rocks for REE which includes monazite ± apatite veins, carbonatites, pegmatites, peralkaline igneous rocks, ion adsorption clays, placers, and some deep-ocean sediments (Kanawaza and Kamitani, 2006). Currently, most light rare earths (LREE) are extracted from carbonatite-related deposits while heavy rare earths (HREE) are mostly derived from REE-bearing ion-adsorption clays (Wall, 2014).

According to Pell (1996), mineralised carbonatite systems are multi-commodity exploration targets which are highly attractive, however, not well understood. Carbonatites have become popular exploration targets for junior mining firms across the globe as they are the principal suppliers of REE and niobium which are considered essential metals for some main economic sectors (European Commission, 2014).

Apart from their importance in the high-technology industries (Xie *et al.* 2014), REE if combined with petrology and geochemical analyses are considered valuable tools for petrogenetic studies of igneous rocks, which includes determining the history of the source of melts, the mineralogical and chemical composition of the source during melting, the condition of melting, extent of the melting processes involved and how the melt is modified by assimilation, metasomatism, differentiation and by fluids (Hensen, 1980). This research report will focus on the analysis of rare earth elements (REE) of the Epembe carbonatite dyke within the Epembe Carbonatite-Syenite Complex (ECSC), in the Kunene region, Namibia, with the aim of establishing and understanding the distribution of REE within the Epembe carbonatite.

In Namibia, materials produced from carbonatite or related deposits include iron and fluorite from Okorusu, and sodalite from Swartbooisdrift for use as a semi-precious stone, as well as for dimension stone and ornamental purposes (Menge, 1986). Some carbonatites, such as Lofdal (located at Lofdal village northwest of Khorixas, in the Kunene region) and Dicker Wilhelm (located 20 km west of Aus in the Karas region of Namibia) potentially represent large resources of REE. These are being evaluated for future development. Other carbonatite occurrences such as the Epembe carbonatite dyke are being explored for niobium (Nb) and tantalum (Ta) by Kunene Resource Holdings (Pty).

Several geological studies have been undertaken on the Epembe Carbonatite-Syenite Complex (ECSC) which has been focused mainly on in-depth geological mapping, petrological studies of the Nb-Ta ± U mineralisation as well as rare metal metallogenesis (Falshaw, 2012; Simon, 2017),as well as in-depth mineralogical study of apatite and pyrochlore minerals (Mariano and Mariano, 2013; Unger *et al*. 2018). The current project provides a significant opportunity for investigation of the REE characteristics of the carbonatite dyke of the same complex which has not been done to date.

1.1.1 Rationale

According to Kanawaza and Kamitani (2006), the past 30 years has seen a significant increase in the demand for REE. This demand is driven by the emergence of technology for green and low carbon economies, aimed at mitigating global climate change. REE have a huge impact in our everyday lives due to their use in many technological applications especially concerning the growth of sustainable energy technologies such as high strength magnets, permanent magnets, batteries for e-mobility and energy-efficient lighting (Kuhn and Gevers, 2015). Without REE, modern technology would be different and many applications impossible. In addition, REE are vital for the defense manufacture and are contained in cruise missiles, precision guide munitions, radar systems and reactive armor. They are also important to new green technology such as wind-powered turbines and plug-in hybrid vehicles, as well as oil refineries, where they are used as a catalyst (Hurst, 2010). In spite of their wide application and increasing demand, REE come from very few sources. 95% of the worldwide production comes from China (Hatch, 2012) and China has used its competitive advantage to increase the price of REE by limiting export of these elements. Consequently, security of supply has become a concern for many manufacturing countries (Verplanck and Gosen, 2011). As a result, understanding the distribution and origin of REE, as well as identifying and quantifying our nation's REE resources have become a priority. In that light, carbonatites are now one of the principal sources of REE and as such an increased understanding has a direct impact on the exploration industry.

1.1.2 Problem statement

In Namibia, most carbonatites have been studied for niobium (Nb) and tantalum (Ta) mineralisation and only a few carbonatites have been studied for their potential REE concentration (Falshaw, 2012 and Do Cabo, 2014). Despite being the largest carbonatite dyke in Namibia, the Epembe carbonatite dyke, remains understudied, probably due to the notorious harsh terrain, inaccessibility and remoteness. But the initial research work by Ferguson *et al.* (1975) and Menge (1986, 1998) within the Kunene Alkaline Complex has paved ways to the discovery of a niobium-tantalum deposit at Epembe. Also the work conducted by Miller (2008), has contributed to the broad understanding of the regional geology of the Epembe carbonatite. However, none of the previous studies fully investigated the REE content and their distribution within the dyke, and as a result the mineral assemblage and distribution of the REE of the Epembe carbonatite dyke are unknown. Therefore, the focus of this study is to investigate the distribution of the REE in this dyke.

1.1.3 Location of the study area

The carbonatite dyke within the ECSC is situated in the Kunene region of Namibia about 800 km north of the Namibian capital city Windhoek and roughly 95 km NW from the township of Opuwo. More specifically, the dyke is situated between the two small villages of Ohamaremba and Epembe on the north-western border of Namibia (Fig.1.1) The ECSC is within the Exclusive Prospecting Licence (EPL) number 3299 jointly owned by Kunene Resource Holdings (Pty) and Craton Mining and Exploration Pty) Ltd. The EPL 3299 covers a total surface area of approximately 29,050 ha.

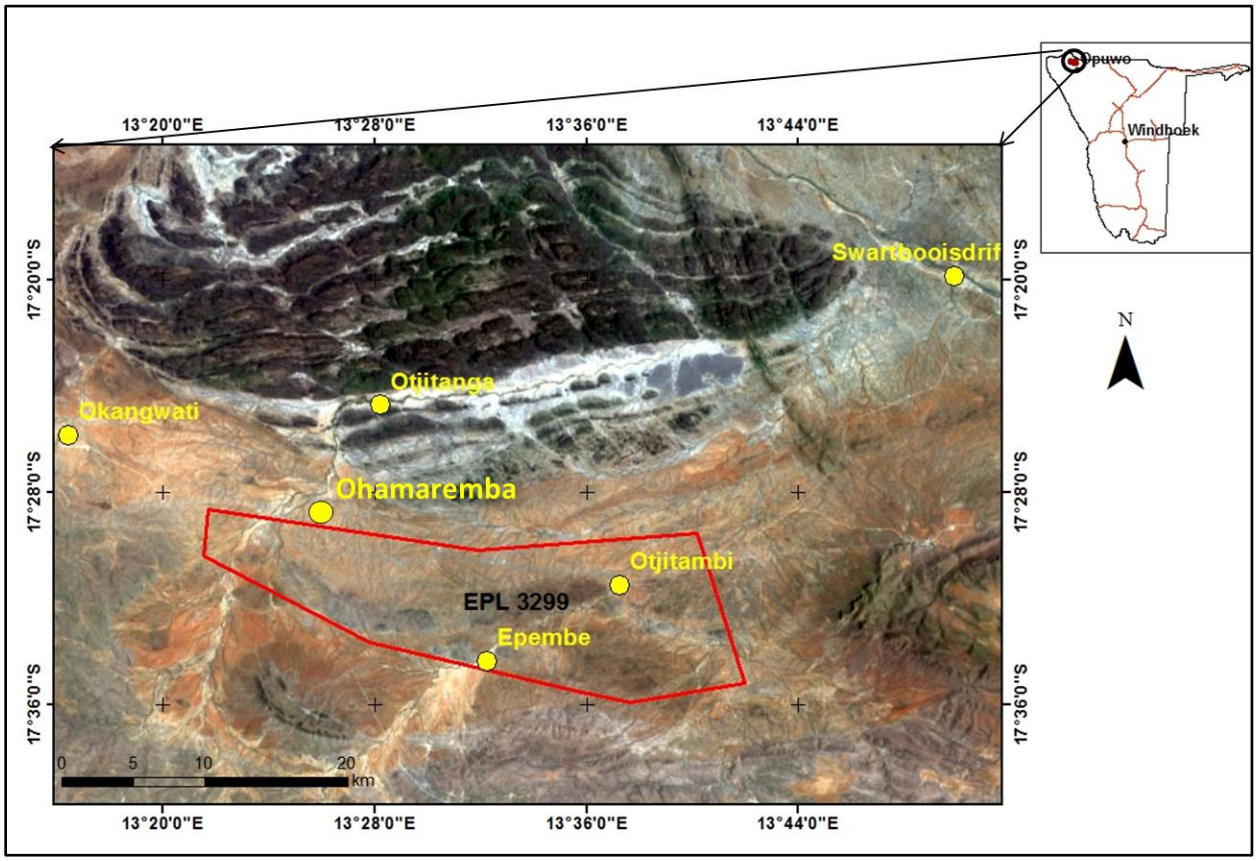


Figure 1-1 *Satellite image (Landsat 8 sharpened) showing the location of the study area and the EPL 3299 boundary which incorporates the Epembe Carbonatite dyke (data source for satellite image: National Aeronautics and Space Administration (NASA) and Directorate.*

1.1.4 Objectives of the study

The main objectives of the study are:

- To identify and characterize the types of carbonatites at the Epembe Carbonatite-Syenite Complex based on their geology, geochemistry and petrography.
- To examine the geochemical variation of the Epembe carbonatite with an emphasis on the rare earth element concentrations.
- To investigate the relationship between the distribution of REEs and radiometric elements.

1.2 Regional geology of the study area

The regional geology of the area is characterized by gneisses of the Epupa Metamorphic Complex (EMC), intruded by two different igneous alkaline suites: The Mesoproterozoic anorthositic rocks of the Kunene Igneous Complex (KIC) with a concordant U-Pb single zircon age of 1370 Ma (Mayer *et al.* 2000) and the Epembe –Swartbooisdrift Alkaline Complex with a minimum age of 1100 Ma on the basis of U-Pb (zircon) and K-Ar (biotite) data of Menge (1986), the latter hosting the Epembe carbonatite dyke. These metamorphic/ igneous complexes are partly underlain by sedimentary rocks of the Damara and Karoo Super groups, but these only occur in the research area as isolated, transported scree boulders and not as a continuous lithological cover (Falshaw, 2012). A brief geological stratigraphy of the area is presented in Table 1.1.

Table 1-1 *Stratigraphy of the different rock unit in the study area together with ages (modified from Menge, 1986 & 1996; Seth et al., 2003).*

<table>
<tr><th>Lithology</th><th>Intrusive unit</th><th>Sub-Unit</th><th>Complex</th><th>Age</th></tr>
<tr><td>Carbonatite</td><td>Epembe carbonatite Swartbooisdrift carbonatite</td><td rowspan="3"></td><td rowspan="2">Epembe-Swartbooisdrift Alkaline complex</td><td rowspan="2">± 1100 Ma</td></tr>
<tr><td>Syenite</td><td></td></tr>
<tr><td>Nepheline syenite</td><td>Otjitanga-Epembe Nepheline Suite</td><td></td><td>± 1250 Ma</td></tr>
<tr><td>Serpentinite, hornblendite , anorthosite, troctolite</td><td>Otjitambi Hyperite</td><td rowspan="4">Satellite Suite</td><td rowspan="4">Kunene Igneous Complex</td><td rowspan="4">± 1370 Ma</td></tr>
<tr><td>Anorthosite</td><td>Marginal Zone</td></tr>
<tr><td>Anorthosite (subordinate Olivine anorthosite)</td><td>Upper Zone</td></tr>
<tr><td>Troctolite (subordinate anorthosite)</td><td>Lower Zone</td></tr>
<tr><td>Granite gneiss amphibolite</td><td colspan="2"></td><td>Epupa Metamorphic Complex</td><td>± 1470 Ma</td></tr>
</table>

1.2.1 Epupa Metamorphic Complex (EMC) (also Epupa Complex [EC])

The Mesoproterozoic Epupa Metamorphic Complex (EMC) is located at the southwestern border of the Archean to Proterozoic Congo Craton of Central Africa and is bounded towards the east by the Mesoproterozoic 1250 Ma Kibaran fold belt (Brandt, 2003) (Fig. 1.2).

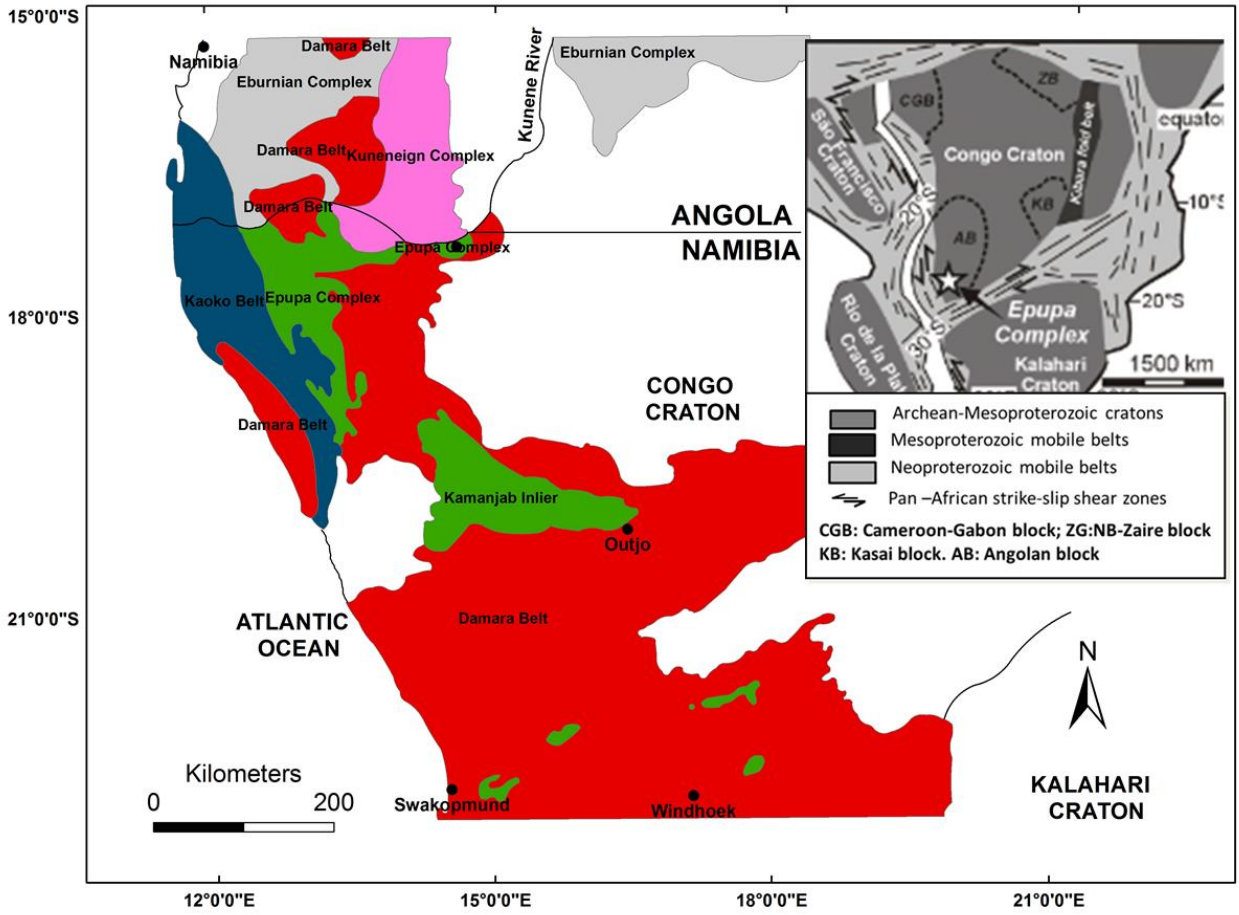


Figure 1-2 *Simplified regional map, showing the distribution of mobile belts (inset map) and pre-Pan-African basement rocks on the northern Namibia (Figure adapted from Simon, 2017 modified after Miller et al. 1983) and southern Angola (Modified after Carvalho et al. 2009).*

There are three pre-Pan-African complexes: The Epupa Metamorphic Complex (EMC), Kunene Igneous Complex (KIC) and the Epembe-Swartbooisdrift Alkaline Province (ESAP). The EMC is the largest of the three pre-Pan African complexes, and is a combination of metamorphic and igneous rocks which represent the oldest basement (Paleo-Mesoproterozoic) units below younger anorthosite rocks of the Kunene Igneous Complex (KIC) (Maier *et al.* 2002). The EMC is poorly mapped and understood, it includes highly deformed rocks which are difficult to distinguish because of the intensity of both pre- and post-Damaran deformation.

The EMC is described by Brandt (2003), to be composed of upper amphibolite facies and ultrahigh-temperature (UHT) granulite facies rocks. The EMC of the studied area has been subdivided into two

distinctive metamorphic units by Brandt et al. (1999, 2003) based upon petrological investigation and field relationships. These are termed the Orue Unit and the Epembe Unit (Fig.1.3).

Based on the work of Martin (1965) as well as Kostlin (1967), the Orue unit mainly consists of a widely migmatised volcano-sedimentary sequence, which was intruded by large masses of granites which were later metamorphosed and became metagranitoids. They exhibit uniform upper amphibolite facies, metamorphic grade as well as structural similarities, therefore the volcano-sedimentary sequence and the metagranitoids have been grouped together by Brandt *et al.* (2003) as the 'Orue Unit' (1334 ± 21 Ma Seth *et al.* 2003).

The Epembe Unit with a protolith age of up to 1810 Ma (Drüppel *et al.* 2001; Seth *et al.* 2003) is a generally E-W trending, well defined terrane of UHT granulite facies, of ortho- and paragneisses. The central part of this unit comprises volcano-sedimentary successions of interlayered mafic and felsic granulites, intercalated with subordinate migmatitic metasedimentary granulite. This E-W trending unit is approximately 50 km in length and up to 10 km in width (Brandt *et al.* 2000; 2003; 2007).

Both of these volcano-sedimentary sequences have undergone substantial burial to mid-crustal levels (Brandt, 2003) but are separated by a sub-vertical E-W trending fault known as the Otjitambi-Ehomba fault. The Epembe unit was later intruded by the Epembe Intrusive suite (Part of the ESAP) and consists mainly of the small stocks of the carbonatite dykes, nepheline syenite and lamprophyre (Maier *et al.* 2002).

1.2.2 Kunene Igneous Complex (KIC)

The EMC rocks are intruded by a large anorthosite massif of Mesoproterozoic age known as the Kunene intrusive/igneous Complex (KIC). This is noted by Drüppel (1999), to form the largest massif-type anorthosite complex of the world measuring up to 20 000 km^2 in size. The southern part of the KIC was first described by Beetz (1933), establishing the presence of gabbro, norite, anorthosite and pyroxenite in the complex. These were then divided into three distinct igneous successions by other researchers (e.g. Menge, 1996): the massive, light-coloured anorthosite in the NW in sharp contact with layered dark leucotroctolite-anorthosite in the Zebra Mountains, together with a small unit of anorthosite and subordinate olivine.

The emplacement age of KIC is now well constrained. Recent radiogenic age determinations yielded a Mesoproterozoic emplacement age for the KIC (McCourt *et al.* 2013). An almost concordant U-Pb single zircon age of 1370 ± 4 Ma was obtained for a co-genetic mangerite vein from the Angolan part of the KIC (Mayer *et al.* 2004), consistent with an almost concordant U-Pb single zircon age of 1385 ± 25 obtained by Drüppel *et al.* (2007) for a pegmatitic dark anorthosite sample from the Namibian part of KIC which is also coherent with a U-Pb upper interception zircon age of 1370 ± 2 Ma from a syeno-diorite dyke that are related to the anorthosite (Drüppel *et al.* 2007).
Likewise, Maier *et al*. (2013) obtained an age of 1363 ± 17 Ma in their U – Pb baddeleyite dating, largely in agreement with the U – Pb zircon age of 1385 ± 7.6 attained by McCourt *et al.* (2013) from mangerite

dyke and gneiss. This is largely in accordance with the newly obtained U – Pb zircon and baddeleyite range of ages (1376 Ma and 1438 Ma) for anorthosite rocks from across the KIC *(*Bybee *et al.* 2019).

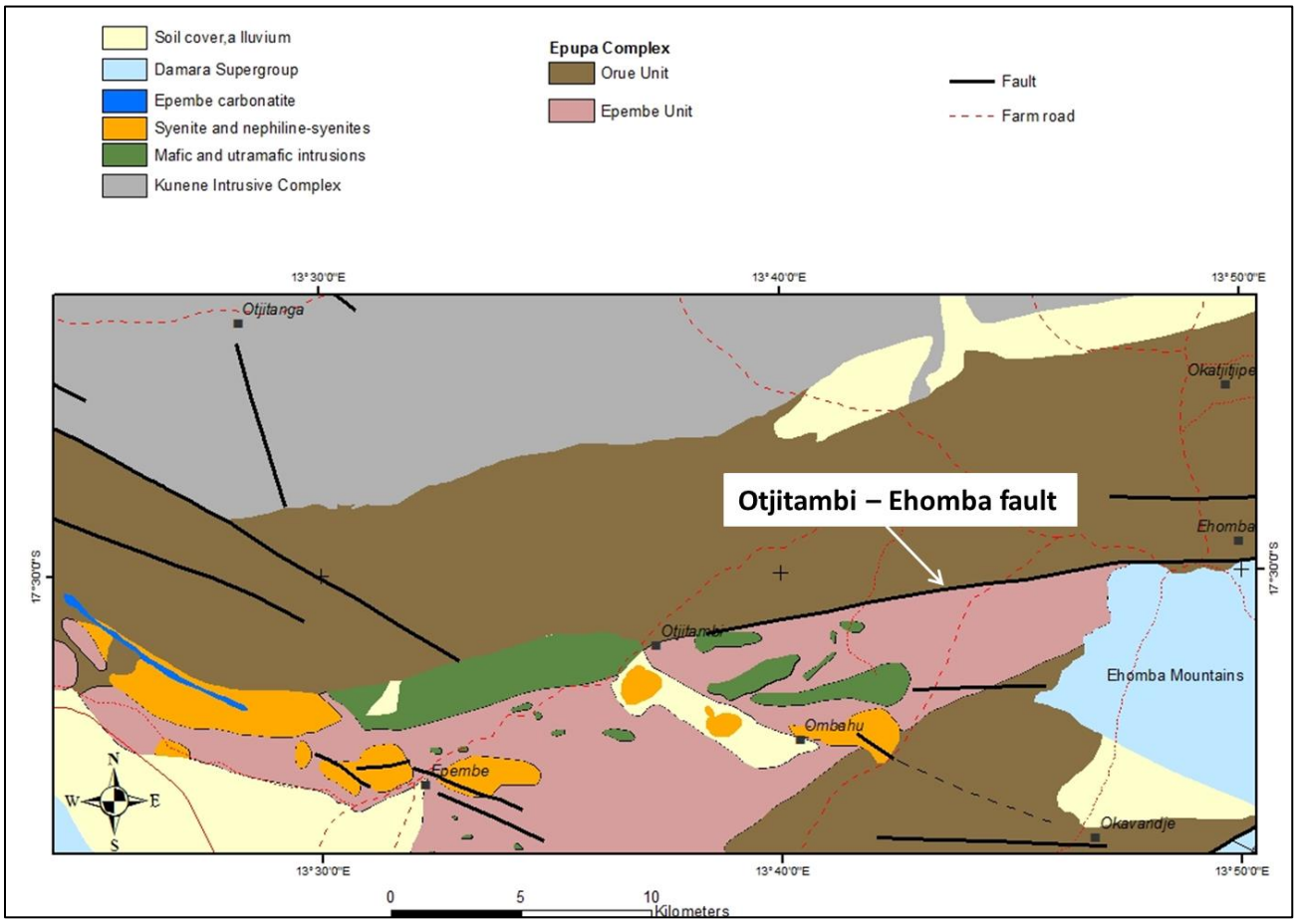


Figure 1-3 *Geological overview map of the southern part of the Kunene Intrusive Complex and the Epupa Metamorphic Complex. The Intrusion of the late Epembe Alkaline suite is seen on the southern margin of EMC (syenites and nepheline syenites). The Epembe dyke is shown in blue. Map adapted and modified after Menge (1996).*

1.2.3 Swartbooisdrift and Epembe carbonatites

A group of sodalite-rich carbonatite dykes occur near Swartbooisdrift on the Namibia/Angola border (Menge, 1986). Swartbooisdrift carbonatite dykes consist of banded sodalite, analcite, ankerite, cancrinite, albite and magnetite and they intruded pre-existing lamprophyres and syenite dykes. The sodalite dykes have been exploited as a source of semi-precious stone and dimension stone. The Epembe carbonatite (located about 40 km southwest of Swartbooisdrift) are distinctly younger than both the anorthosite and the syenite as suggested by the recently obtained concordant U-Pb ages of 1184 ± 10 Ma (Simon *et al.* 2017) which is slightly older than Swartbooisdrift carbonatite which has an age obtained from pyrochlore of 1140 – 1120 Ma (Drüpel *et al.* 2005).

1.3 Geology of the study area

The geology of the study area is dominated by granulite, amphibolite facies and ortho- and paragneissic rocks of the Epupa Complex (EC) and a variety of syenites and carbonatites (Menge, 1996). The Epembe Alkaline Suite, which intrudes the EMC, consists mainly of nepheline syenite plugs, the Epembe carbonatite dyke, marginal syenite, and minor syenite and lamprophyre dykes (Fig. 1.4). The Swartbooisdrift Subsuite comprises sodalite-ankerite ferro-carbonatite dykes, syenite dykes, a calcite carbonatite dyke, composite syenite-lamprophyre-carbonatite dykes and biotite-albite dykes, which occur mostly within Kunene anorthosite. Dolerite and quartz dolerite dykes of unknown age occur in the same area and generally follow the same regional trends. Nepheline syenites yielded U-Pb ages of 1216 ± 2.4 Ma and 1213 ± 2.5 Ma from single zircons (*Seth et al.* 2003) while the maximum age of Swartbooisdrift is provided by the pyrochlore age of 1140 – 1120 Ma (Drüppel *et al.* 2005). The Epembe carbonatite however is slightly younger than both the syenites and Swartbooisdrift carbonatite as suggested by concordant U-Pb age of 1184 ± 10 Ma from the zircon megacrysts from Epembe carbonatite dyke (Simon, 2017).
The Epembe carbonatite dyke is described as a linear feature (6.5 km) in length, but Ferguson *et al.* (1975) also mentioned narrow veins outside/around the main intrusion zone of the dyke particularly in the west and northeast portions of KIC and numerous smaller intrusions away from the contact with the syenites within the country gneiss.

According to Menge (1996), the Epembe carbonatite dyke has been emplaced along a northwest trending fault zone, into syenite and nepheline syenites and extends for 6.5 km in a northwest to southeast direction and dips steeply (70° to 80°) towards the southwest (Fig.1. 4 and Fig. 1.5). The Epembe carbonatite is described as having a maximum outcrop width of approximately 200 - 400 m and this partially soil covered dyke is proposed to pinch out towards the east-southeast in the form of several impersistent veins. The dyke is flanked by fenitised metamorphic rock and by alkaline igneous intrusive bodies of shonkinite and nepheline syenite (light pinkish grey in Fig.1 4). The degree of fenitisation varies throughout the area but is generally concentrated in shattered and jointed rocks adjoining both intrusions, developing more erratically further away from the dyke.

According to a recent study of the Epembe carbonatite by Mariano and Mariano (2013) the mineralogy of the carbonatite is unusually simple (comprising calcite, apatite, pyrochlore, microcline, magnetite, biotite, albite, zircon and monazite,) compared to other carbonatites. According to technical reports of Kunene Resource Holdings (Pty), the Epembe carbonatite deposit is likely to represent a single major (once off dominant magmatic event or single episode of intrusion with successive magmatic pulses) magmatic event; it shows a layered internal structure and successions of magmatic pulses. A few other minor carbonatites dykes (about 1m wide) are reported to have been observed in the area, with few dykes occurring in the Epupa gneisses. The dyke is plunging and is likely to be open at depth.

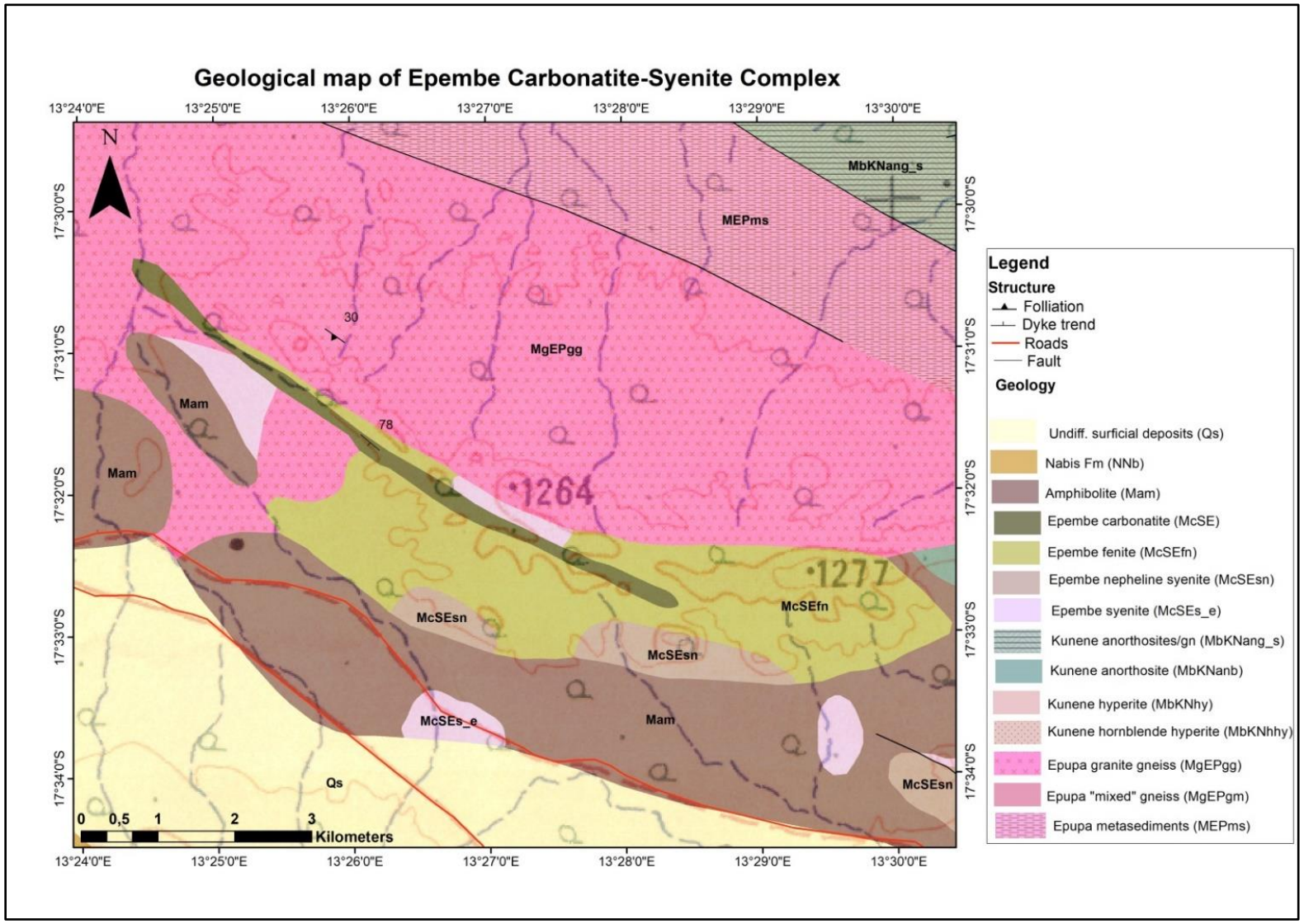


Figure 1-4 *Local geological map of the Epembe-syenite Complex showing the Epembe carbonatite dyke and the surrounding rocks (Data source: GS*

1.4 Methodology

The methodology used in this study is divided into four parts; (1) field work procedure which involved geological field sampling, (2) geochemical analysis, (3) data processing and (4) interpretation. Field sampling was preceded by a desk top study, involving a review of existing publications, maps and miscellaneous documents (e.g. exploration reports). A total of sixteen (EPB01 –EPB16) grab samples were collected from the carbonatites and surrounding rocks. Geological field visits and sampling were done over five days, from 14th -18th November 2017 at theEpembe Carbonatite-Syenite Complex.

Microscopic study was done on ten (10) selected carbonatite thin sections investigated under both plane and crossed polarized light in order to identify mineralogical phases within the carbonatite.

For analytical analysis, sample preparations were done at the GSN laboratories. Whole rock samples were crushed to about 0.5 – 15 mm then milled in a vibrating disc to a powder finer than 64 microns. A barren quartz flush was pulverised between each sample to minimize any possible contamination. Batches of sixteen (16) pulp samples were sent for analysis to the Wits University Earth Lab. Control and duplicate samples were not undertaken due to the cost involved.

Concentrations of major-element oxides as well as trace elements were determined using the Norrish Fusion technique using in-house correction procedures and a Panalytical (Philips PW2404) X-ray fluorescence spectrometer. Major elements were fused using Johnson Matthey Spectrol flux 105 at 1100°C and raw data corrected using in-house software. Standard calibrations were made up using synthetic oxide mixtures and international standard rocks as well as in-house controls. Sample mass used was 035 gm and flux mass 2.5 gm. Precision is taken as 1% for elements in abundance of greater than 5% by mass, and 5% for elements in abundance less than 5% by mass.

Trace elements were determined on pressed pellets using a Moviol solution binder. Standardisation was carried out using International Reference Materials USGS series (USA) and NIM series (South Africa). Precision was determined on the basis of counting time and is taken as 5% for elements in abundance greater than 100 ppm and 10% for elements in abundance between 10 and 100 ppm.

Rare Earth Elements were examined by inductively coupled plasma-mass spectrometry (ICP-MS) techniques using the Perkin Elmer DRC-e and analysed against certified primary solution standards. International reference materials AGV-2, BCR-1 and BR-1 were analysed with every run. Agreement to accepted values of the standards was better than 10% for all elements and in many cases better than 5%. Dissolution of 50 mg of sample was carried out with high purity HF-HNO3 using a MARS microwave digester.

Mineral identifications were done at Geological Survey of Namibia using Bruker AXS D8 Advance X-ray Diffraction (XRD) connected to a desktop computer. Portions of the milled rock sample were uploaded into the machine through a sample holder. With the help of Eva computer software, characteristic peaks of each mineral were produced and the data was exported in a PDF format.

Radiometric maps of thorium (Th), potassium (K) and uranium (U) were produced (data provided by the GSN) in order to study the relationship between REE concentration and radiometric elements.

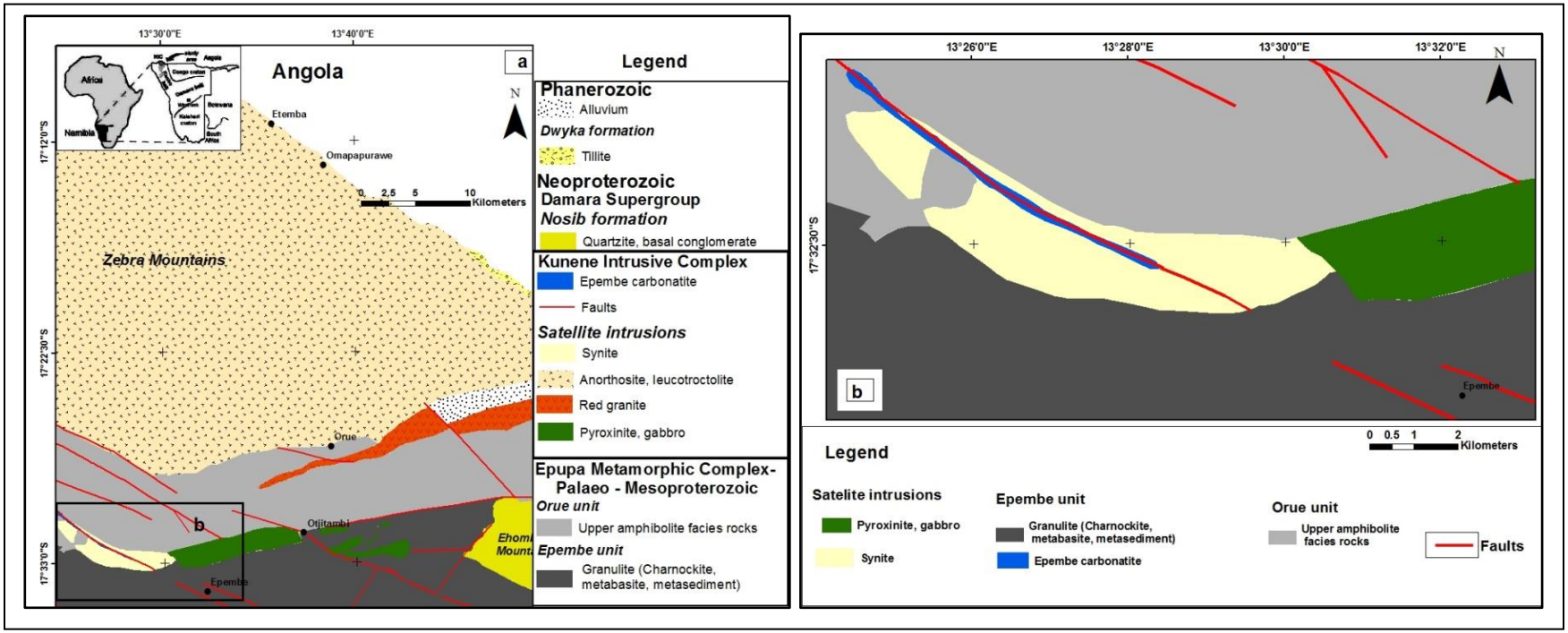


Figure 1-5 *Regional and Local geological maps. a) Simplified regional map of part of the Kunene Intrusive/igneous Complex (KIC) showing the extent of the study area marked with a black rectangle, b) local area sketch map of the study area showing the Epembe carbonatite dyke. (Modified from Simon et al. (2007) after Becker et al. (2006)).*

CHAPTER 2: GENERAL OVERVIEW OF CARBONATITES AND RARE EARTH ELEMENTS

2.1 Carbonatites overview

Carbonatites are described as igneous rocks containing a high percentage of carbonate minerals (>50 %) and containing less than 20 % SiO_2 (Nelson *et al.* 1988). These rocks can be either plutonic or volcanic, many of which contain apatite, magnetite, barite, and fluorite as well as significant concentrations of REE, phosphorus, niobium, uranium, thorium, barium, copper, zirconium and other incompatible or rare elements (Peter *et al.* 1986). Many known carbonatite bodies are typically zoned in association with alkali complexes although only few a deposits may consist of dykes, sills, breccias and veins (Shelley, 1993).

Carbonatites have been divided based on the abundance of their carbonate mineral, calcite, or dolomite-carbonatites (Fig. 2.1) as well as their corresponding major element geochemistry (Le Bas 1987; Woolley and Kempe 1989; Woolley., 1982). Alternatively, a process-related classification would divide them into two groups: *primary carbonatites* and *carbothermal residua* (Mitchell, 2005).

The IUGS (International Union of Geological Sciences) classification of carbonatites is established on the relative abundances (in wt. %) of calcium (CaO), magnesium (MgO) and iron (FeO, Fe_2O_3 and MnO) and hence aimed to be used when the rock's mineralogy is unknown (Woolley and Kempe, 1989).The alkali-rich carbonatite (natrocarbonatite) have not been included in the general classification of carbonatite, because there is only one known example of their type, and hence only three carbonatite types are distinguished (Gittins and Harmer, 1997) (Fig.2.1.).

2.1.1 Tectonic setting of carbonatites

According to Jones *et al.* (2013), the majority of carbonatites and alkaline igneous complexes are normally located in relatively stable, intra continental regions often within Precambrian shields and they span an age from Archean to recent. A significant proportion of known carbonatites are reported to be associated with extensional environments (esp. the East African Rift Valley). However, Ernst and Bell 2009, noted other carbonatites that are associated with faults and domal swells.

Where rifting and faulting occur in response to doming, for example in the East African Rift system and Kola alkaline province, carbonatites and alkaline complexes may be located on high topographic elevations, which have been interpreted as the outcome of crustal doming (Woolley, 1989). In addition, rifted continental margins such as those found in Brazil and Namibia contain carbonatite and alkaline complexes and these are related to rising asthenospheric mantle and plumes (Pirajno, 2004a).

Some carbonatites may develop near plate margins or be associated with incipiently rifted continental plates and in areas of partially melted oceanic crust such as the Cape Verde and Canary Islands (Le Bas, 1987).

According to Mitchell (2005), carbonatites are typically spatially associated with wide a variety of feldspathic silicate rocks such as ijolite, nepheline syenite, melilitite, nephelinite, ailikite and the

kimberlite clans. The association both locally and regionally of carbonatites with alkali-rich, silica-poor igneous rocks suggests a strong genetic relationship. Syn-tectonic carbonatites are also known from the accreted terrains of the Western Cordillera of British Columbia and the frontal nappe complex of the 1000 Ma Natal Metamorphic Province at the Bull's Run Complex (Pell and Hey, 1989).

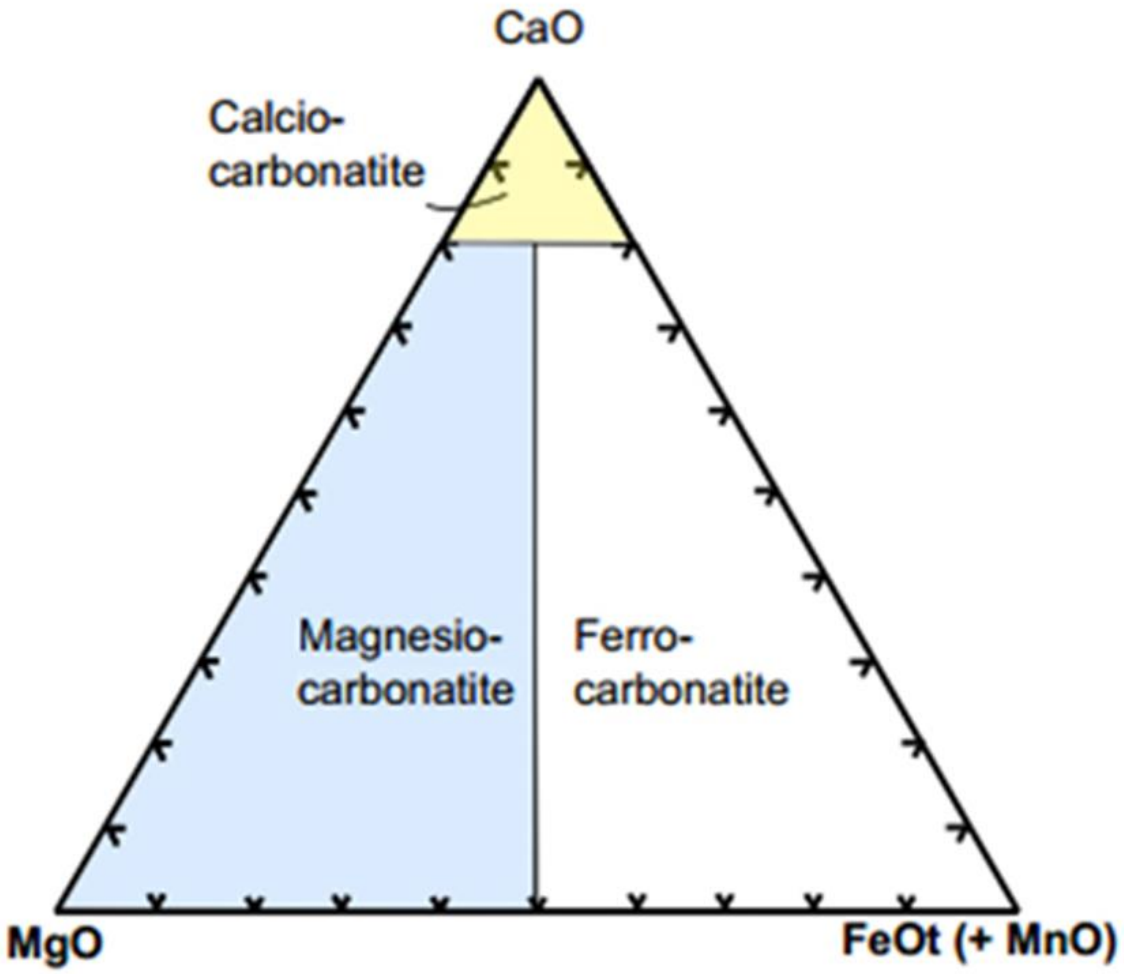


Figure 2-1 *Carbonatite classification diagram based on their dominant modal mineral and on their corresponding major geochemistry. Redrawn after (Woolley and Kempe 1989)*

2.1.2 Origin of carbonatite magmas

One of the most important aspects in determining the carbonatite source is by characterizing the parental magma from which the carbonatite was derived. Carbonatite-forming magmas may originate through various processes. These include: as a primary product of partial melting of mantle containing carbonate minerals (Gittins, 1989; Harmer & Gittins, 1998, Gittins & Harmer, 2003), the final product of

segregated silicate melt containing carbothermal residual or dissolved carbonate or melt as a result of broad crystal fractionation (Veksler *et al.* 1998, Mitchell, 2005) and liquid immiscibility from an early homogeneous silicate-rich carbonate melt (Le Bas, 1977; Kjarsgaad & Hamilton, 1989; Lee and Wyllie, 1998).
Petrological and geochemical evidence has been presented for the eruption of primary carbonatite magmas directly from the mantle e.g. (Bailey, 1993), for the extrusion of calcio-carbonatite magma e.g. Keller, (1981, 1989). The mantle origin is evident from isotope and trace element chemistry. Low degrees of partial melting are indicated by trace element chemistry. However the location of partial melting, and the nature of and relationship with parental magma (if any are involved)are still debated.

Although carbonatites produced by fractional crystalisation may exist (e.g. Veksler *et al.* 1998), the process is unlikely to produce all carbonatites, because the process will not produce the concentrations of Nb, REE and other incompatible elements characteristic of carbonatites and the required concentration of CO_2 (for the volume of carbonatites observed) are not present in the proposed parental melts (Gittins, 1989). Another observation that does not support fractional crystalisation is the bimodal distribution of Ca and Mg content in carbonatite, which are almost always dominated by either calcite or dolomite; this is referred to as the compositional dichotomy (Bailey, 1993). Although not disproven, the hypothesis of carbonatite genesis by fractional crystalisation is usually paid little attention, as there is a lack of supporting experimental data.

Even though Hammer and Gittins (1998) do not exclude the possibility of a model involving liquid immiscibility in the mantle, the experimental data and relevant model only supports liquid immiscibility producing carbonatite in the crust. Lee and Wyllie (1998) argued that the formation of immiscible carbonate-rich and silicate magmas in the mantle is unlikely due to a large separation of silicate-carbonate immiscibility volume and liquidus field boundaries.

Based on isotopic evidence, Bell *et al.* (1999) consider parental melts of carbonatite to be derived from asthenosphere-lithosphere interactions. The cause of such interaction is unknown, but may be mantle plumes or lithospheric delamination. More recent work favours a sub-lithospheric location for the generation of carbonatite melt as argued by Bell and Simonetti (2009).

2.1.3 Carbonatites and REE concentration

Rare earth element deposits are primarily hosted in carbonatites and alkaline igneous rocks even though rare contents of REE minerals are also reported to occur in other magmatic rocks such as granites and pegmatites (Goodenough *et al.* 2017). Carbonatites represent the main source of global REE with producing mines at Bayan Obo and Maoniuping in China, and Mt Weld in Australia, and also in the Mountain Pass mine in California, (USA), which was recently closed. These are all in weathered or fresh carbonatites; a lot of carbonatites have been studied (Smith *et al.* 2016; Verplanck *et al.* 2016). After carbonatites, alkaline silicate igneous rocks are the second type of igneous rocks with high abundances of REE although it is highlighted that they are highly variable.
The majority of carbonatite and alkaline igneous rocks are found in the form of ring complexes or concentrically sited intrusions into the country rock in a pipe- or funnel-shaped structure (Kynicky *et al*.

2012). Many carbonatite-hosted deposits have been altered by hydrothermal fluids and metasomatic processes which introduce ions (those ions are collected during the reactions between solutions and the rocks they encounter) such as niobium, uranium, phosphorus, strontium, barium, lanthanum, fluorine and thorium into the system resulting into the development of new minerals (Thompson *et al.* 2011).

2.2 Overview of Rare Earth Elements (REE)

This section presents a brief description of rare-earth elements (REE) with emphasis on their properties, mineralogy, occurrence, economic importance and production, supply and demand and use.

2.2.1 Definition and characteristic of REE

In the periodic table, the rare earth elements comprise of seventeen (17) chemical elements (Fig. 2.2), namely the fifteen (15) lanthanides plus scandium and yttrium which have similar geochemical behaviours (IUPAC). The rare earth elements comprise a series of elements with atomic numbers from 57 to 71 from lanthanum to lutetium. The elements from lanthanum to gadolinium are referred to as light REE (LREE); and from terbium to lutetium as heavy REE (HREE). Yttrium has ionic radii similar to holmium and it only occurs in 3^+ states; thus yttrium is grouped with the HREEs (Verplanck and Gosen, 2011). Scandium though trivalent is not sufficiently similar to classify it as either a LREE or HREE.

The unique characteristic of REE arises from the common 3+ ion they form over a wide range of oxygen fugacity (fO_2) (Rollinson, 1993). The exception is cerium (Ce) and europium (Eu) which can exist in other oxidation states (2+). The ionic size of these elements decreases with increasing atomic number (White, 2005). In general, REE have high ionic charges and large radii, a character which makes these elements incompatible. Highly charged rare earths and the lighter elements are more incompatible as opposed to these with low charges and heavier rare earths with smaller ionic radius (White, 2005).

According to Walters and Lusty (2010), the relative abundance of REE in natural material differs significantly and relate to two main factors. Rare earth elements with odd atomic numbers have lower abundance than their even numbered neighbours. Secondly, the LREE are more strongly concentrated in the continental crust than the HREE with higher atomic numbers.

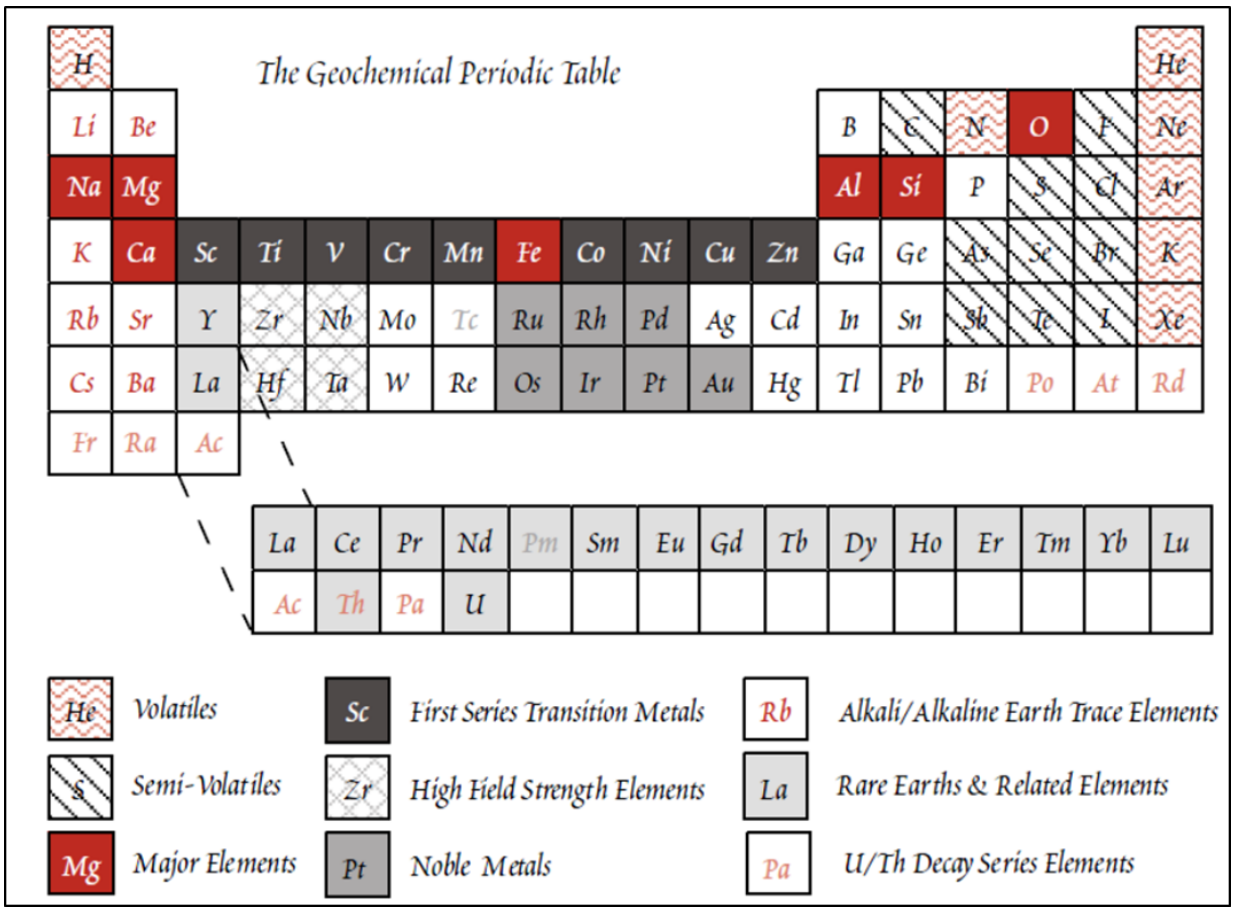


Figure 2-2 *The geochemical periodic table of elements, group of elements in their chemical behaviour. REE are shown at the bottom of the main table (White, 2005).*

Even though the geochemical properties of REE are comparable; their chemical, electrical, metallurgical, catalytic, magnetic as well as their optical properties differ, and these unique properties and differences have led to their prominences in a variety of emerging technologies.

2.2.2 Properties and Uses of REE

REE share many common properties that make them difficult to separate or even distinguish from each other. These common properties of REE as summarized by Charalampides *et al.* (2015) include high density, high thermal conductance, and high melting point, as well as high conductivity. In addition, REE are silver, silvery-white, or grey metals; they have a high luster but tarnish readily in air; they occur naturally together in minerals (e.g., monazite is a mixed rare earth phosphate). Due to their unusual physical and chemical properties, such as unique magnetic and optical properties, REE have diverse uses that touch many aspects of modern life and culture. Specific REEs are used individually or in combinations (BGS, 2010).

REE are used in the components of many devices used daily in our modern society, such as: the screens of smart phones, computers, and flat panel televisions; the motors of computer drives; batteries of hybrid and electric cars; and new generation light bulbs (King, 2019). Lanthanum-based catalysts are

employed in petroleum refining. Large wind turbines use generators that contain strong permanent magnets composed of neodymium-iron-boron.

2.2.3 REE mineralogy

Unlike other elements, REE occurs in a wide range of mineral types including halides, oxides, phosphates, carbonates and silicates (Table: 2.1), but they do not occur as metallic elements (Walters *et al.* 2011). The most abundant REE-bearing minerals in carbonatites include bastnäsite, monazite, allanite, apatite, loparite and xenotine while in alkaline igneous rocks eudialyte together with apatite, and loparite are the most common minerals. Other important minerals are the carbonates synchysite and parIsite. The complex silicates which include eudialyite and steenstrupine also contain significant amounts of REE, as do the phosphate churchite and the carbonate ancylite (Mehmood, 2018). A number of rare earth-minerals contain uranium and thorium in variable amounts but uranium and thorium do not constitute essential components in the composition of these minerals (Kanazawa and Kamitani, 2006 in Do Cabo, 2014).

Table 2-1 A selection of REE bearing minerals (Walters et al. 2011)

Mineral	**Formula**	**Approximate REO %**
Aeschynite - (Ce)	$(Ce, Ca,Fe,Th)(Ti,Nb)_2(O,OH)_6$.	32
Allanite - (Ce)	$(Ce,Ca,Y)_2(Al,Fe^{3+})_3(SiO_4)_3OH$.	38
Apatite	$Ca_5(PO_4)_3(F,Cl,OH)$	19
Bastnasite - (Ce)	$(Ce,La)(CO_3)F$	75
Brannerite	$(U,Ca,Y,Ce)(Ti,Fe)_2O_6$	9
Britholite -(Ce)	$(Ce,Ca)_5(SiO_4,PO_4)_3(OH,F)$	32
Eudialyte	$Na_4(Ca,Ce)_2(Fe^{2+},Mn,Y)ZrSi_8O_{22}(OH.Cl)_2(?)$.	9
Euxenite - (Y)	$(Y.Ca.Ce,U,Th)(Nb,Ta,Ti)_2O_6$	24
Fergusonite -(Ce)	$(Ce,La,Nd)NbO_4$	53
Gadolinite -(Ce)	$(Ce,La,Nd,Y)_2Fe^{2+}Be_2Si_2O_{10}$	60
Kainosite - (Y)	$Ca_2(Y,Ce)_2Si_4O_{12}CO_3.H_2O$.	38
Loparite	$(Ce,La,Na,Ca,Sr)(Ti,Nb)O_3$	30
Monazite - (Ce)	$(Ce,La,Nd,Th)PO_4$	65
Parisite - (Ce)	$Ca(Ce,La)_2(CO_3)_3F_2$.	61
Xenotime	YPO_4.	61
Yttrocerite	$(Ca,Ce,Yla)F_3.nH_2O$.	53
Huanghorite -(Ce)	$BaCe(CO_3)_2F$.	39
Cebaite -(Ce0	$Ba_3Ce_2\ (CO_3)_5F_2$.	32
Florencite -(Ce)	$CeAl_3\ (PO_4)_2(OH)_6$.	32
Synchysite -(Ce)	$Ca\ (Ce,La)(CO_3)_2F$.	51
Samarskite -(Y)	$(Y, Ce, U, Fe3^{+})_3(Nb,Ta,Ti)_5O_{16}$.	24
Knopite	$(CaTi,Ce_2)O_3$	NA

2.2.4 Economic importance of REE

REEs are well known for their exceptional optic, magnetic, electronic and catalytic properties that solve challenges related to modern technology and hence make them valuable for a variety of applications. They are regarded as highly valuable elements for innovation, especially regarding the development of technologies and sustainable energy (Kuhn and Gevers, 2015).

The REE trades are categorised into nine (9) main sectors: catalysts, polishing, glass, phosphors and pigments, metallurgy, batteries, magnets, ceramics, and others (USGS, 2011) (Fig 2.3). More specifically, they play a vital and increasing role in a wide range of consumer electronics, in military applications as well as in environmental technologies (Walters *et al.* 2013). Several of these technologies support sustainable development, for instance through increased energy efficiency and renewable energy production (Walters *et al.* 2013). Specifically, REEs are used as components in high technology devices, including computer hard disks, smart phones, computer monitors, digital cameras, fluorescent and light-emitting-diode (LED) lights, electronic displays and flat screen televisions (USGS., 2014).

Given the range of REE applications, the world-wide demand is expected to grow by 8 to 11% each year (Walters *et al.* 2013). The increase in demand is intertwined with environmental implications of production and existing supply risks due to an intricate and complex market. This has led to the identification of REEs as materials critical to evolving technologies, such as clean-energy applications, high-tech military components, and electronics (Long *et al.* 2010)

In 2015, the worldwide REE use was projected at 119,650 metric tons of REO (Fig 2.3), where catalysts were the biggest sector, followed by magnets, polishing, and others. The market analysis by Zhou *et al.* (2017) also shows that by 2020, the worldwide REE demand is projected to increase by 5% annually. Furthermore, the global REE demand would remain high for a long time together with the growing market of clean energy. The increasing demand of REE will create pressure as well as challenges to the world supply chain of REE. However, the two lightest rare earths, La and Ce are projected to have a surplus supply which is expected raise the demand over the next 10-years and therefore lowering the prices of La and Ce. Moreover, efforts are being made to come up with new applications for REE mostly in China (Goodenough *et al.* 2017).

2.2.5 Rare Earth Production

Global REE production in 2015 was recorded at 126 000 metric tons of REO (Fig. 2.3) whereby China and Australia are the main producers with the rest of production coming from USA, , India, Russia, Thailand and Malaysia. Of the total production, about 20% is estimated to come from illegal production which is mainly from southern China, primarily extracted from ion adsorption clay deposits. Presently, over 200 REE-bearing minerals have been documented (Kanazawa and Kamitani, 2006); however, it is reported that many of the world's REE are being produced from four minerals: bastnäsite, xenotime, monazite, and loparite. In China, the biggest percentage of global REE production comes from mineral bastnäsite followed by monazite in Australia and India, and then loparite in Russia, and xenotime in Malaysia. These rare earth minerals are largely related to igneous rocks (alkaline and carbonatite rocks). In addition, other important REE minerals can be found in placer deposits, iron-oxide copper, pegmatites, -

gold (IOCG), marine phosphates, and residual deposits from deep weathering of igneous rock (Long et al. 2017).

Currently, REEs are mined from carbonatite bodies in China (Bayan Obo, Maoniuping, and Weisan Lake). The Bayan Obo deposit, Inner Mongolia, China, is the world's primary source of light rare earths. Fig 2.4 and 2.5 shows the distribution of global rare earth element resources and mineralised carbonatites respectively.

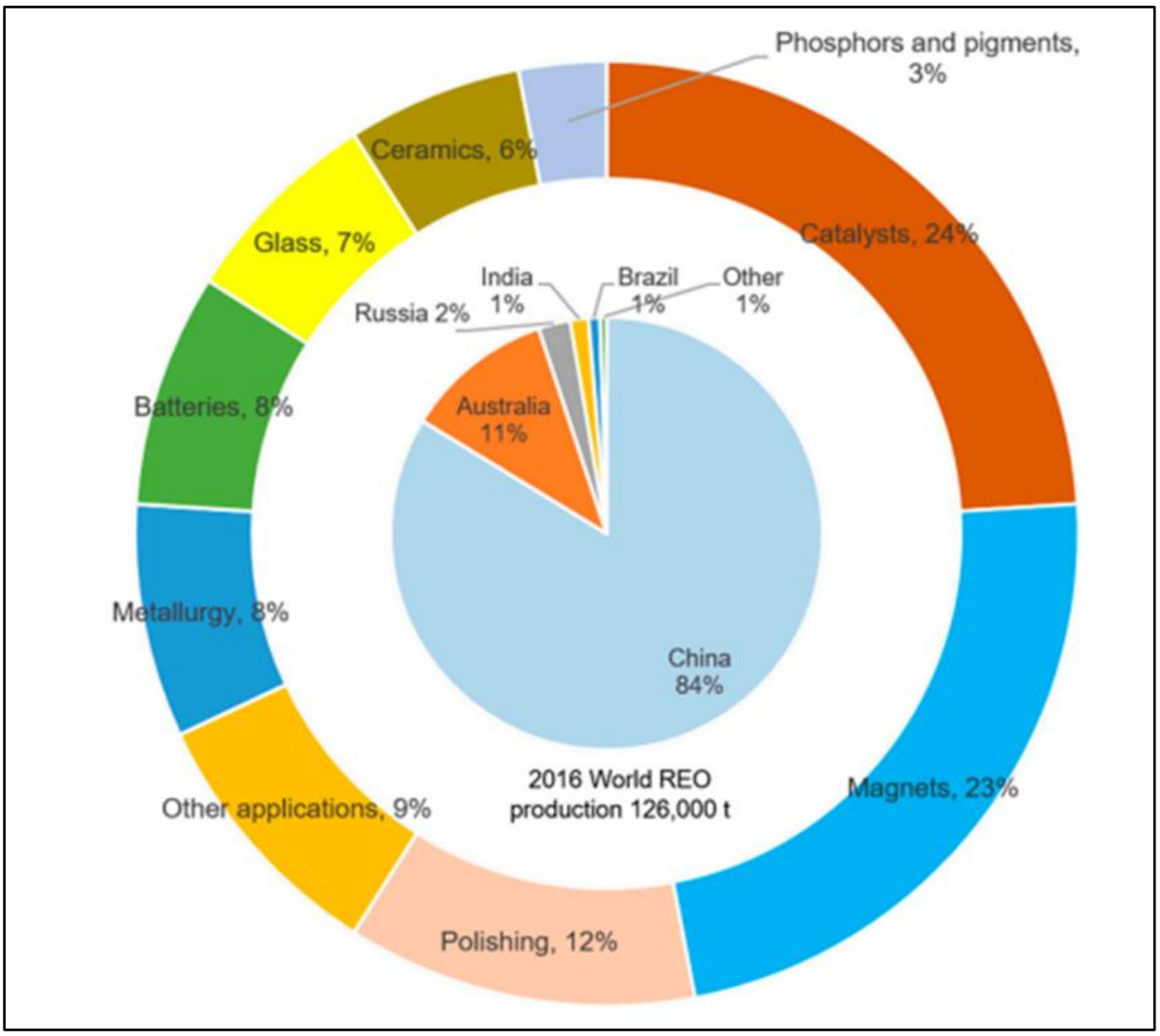


Figure 2-3 *Different uses and proportions of the REE and the relevant production figures for different countries in 2015 (Zhou et al. 2017).*

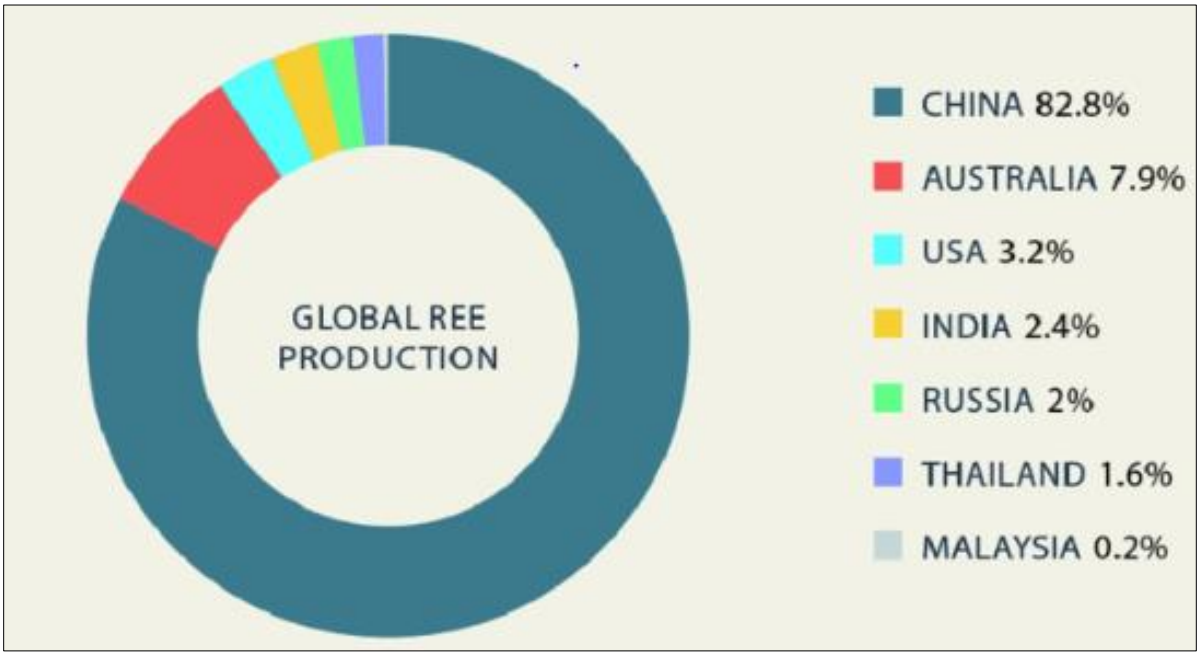


Figure 2-4 The distribution of global rare earth production by country (Barakos et al. 2016

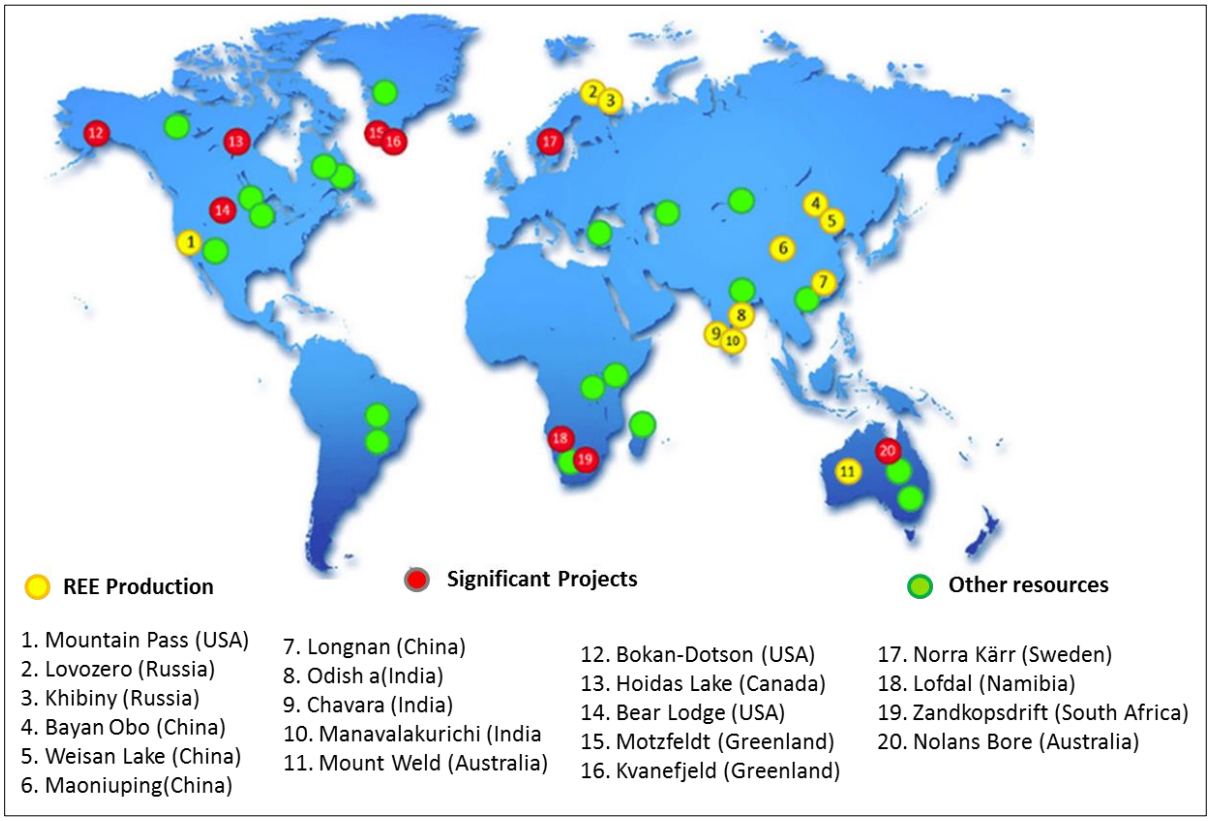


Figure 2-5 *World map showing the global distribution of rare earth element deposits producing mines and exploration targets. (Mountain Pass is currently in maintenance mode) (Source: Barakos et al. 2016)*

CHAPTER 3: FIELD WORK AND PETROGRAPHY

3.1 Introduction

This chapter aims to present the main findings from field work as well as petrographic observations. Field work was aimed at the collection of representative samples for geochemical analysis, and studying the relationship between the carbonatites and their host rocks. Prior to the field visit, the preparation phase involved collecting and organising existing geological maps, remote sensing data, and a literature review. A geological map at a scale of 1:250,000 were used to produce base maps of the study area (see Appendix B.)

An advanced spaceborne thermal emission and reflection radiometer (ASTER) image was processed using ArcMap and Environment for Visualising Images (ENVI 4.8) software to discriminate between rock types. A band combination of 3:2:1, R: G: B: was processed on an ortho-ASTER 3ALevel1 (3AL1) (see Appendix C) to produce a "true colour" image. Another band combination 4:6:8, R: G: B was performed on the same ASTER image for alteration analysis.

3.2 Geological field visit and sampling

A geological field visit and sampling campaign was carried out from 14th -18th November 2017. A total of sixteen (EPB1 –EPB16) fresh rock samples were collected along the carbonatite dyke and also from the surrounding syenites and fenites (Fig. 3.1). The list of the collected samples is given in Appendix D. The collected samples were described based on the mineralogy, colour, and texture and is given in Appendix E.

3.3 Field Observations

The study area is covered by scree and vegetation, although the intrusive carbonatite rocks outcrop well. They form ridges roughly 45 m above the surrounding area and 200 – 400 m in width which is partially covered by sand. Rocky exposure ranges in size from small low lying outcrops to continuous ridges over 100 m in length (Fig. 3.2 & Fig. 3.3). The flat, gravel-covered country surrounding the prominent ridges is underlain by syenites and carbonatite proximal to the main intrusion of carbonatite dyke and weathered rocks of the metamorphic Epupa Complex.

3.3.1 Carbonatite

The Epembe carbonatite dyke was emplaced during one major magmatic event along a shear zone within nepheline syenites of EMC. It is slightly heterogeneous, both texturally and mineralogically. Based on these textural and mineralogical variations, it can be divided into three different categories representing distinct magmatic pulses i.e. the lower (the margins), the middle profile) and the upper profile (centre) of the dyke (Fig. 3.4).These magmatic profiles are distinguished based on differences in colour and mineral characteristics. The lower and middle profiles are defined by a reddish brown colour whilst the upper profile is light grey. Also the lower and middle profiles are composed of elongated calcite grains that show gradational changes to massive, coarse crystalline calcite in the centre of the dyke. The red-brown coloration observed in the lower and middle profile (Fig. 3.5a) could be caused by

many factors, including alteration of secondary feldspars (K-feldspar/nepheline) by late hydrothermal or weathering events; the presence of partly oxidized magnetite grains or most probably the creation of radioactive halos into the surrounding carbonatite matrix from uraniferous minerals. Despite the changes, the entire dyke is observed to be primarily made up of coarse-grained calcite (~92%) thus referenced as a calcite-carbonatite.

In some places, the carbonatite is characterized by hilly outcrops of disseminated apatite grains in a calcite matrix exhibiting a resistant weathering pattern (flow bands)(Fig. 3.5d), a texture that can be related to magmatic flow or crystallisation, while elsewhere the carbonatites appear massive, unmineralised and dominated by dolomite (Fig.3.5e). Major minerals observed in this carbonatite include calcite, K-feldspar, dolomite and mica (mainly phlogopite and biotite) while accessory minerals comprise ankerite, aegirine, apatite, pyrochlore, quartz, iron-bearing minerals (hematite and magnetite) and epidote. At outcrop scale, the carbonatite displays a rough surface texture.

Late-stage calcite veins are observed cross-cutting the carbonatite throughout the dyke. The veins appear as unorientated, anastomosing veinlets, typically hairline in size but up to 2 cm wide, exploiting any planes of weakness in the carbonatite host. Apatite can occur both as dense clusters of prismatic crystals, but more commonly in the form of large, isolated, rounded crystals.

3.3.2 Associated country rocks

The country rocks hosting the Epembe carbonatite are syenites and fenitised granitic gneisses of the EMC. The fenitised granitic gneiss is pink to red in colour; medium-grained (average grain size ≈ 0.5 – 1mm) and in some places appears highly fractured (Fig. 3.6a). It contains quartz, plagioclase, biotite, chlorite and feldspar. The rock is foliated in places and it exhibits a gneissic texture. Outcrops are characterized by carbonatite veins cutting through the granite-gneiss thus indicating a later intrusion of carbonatite. The syenites occur as massive, very hard, fine- to medium-grained (average grain size <1mm) rocks, grey to reddish in colour (Fig. 3.6b) (probably due to hematitisation) as small isolated bodies and locally as xenoliths within the carbonatites. They consist of orthoclase feldspar, aegirine-augite, and nepheline and minor calcite.

3.4 Petrography

For the purpose of this study, only carbonatite samples were selected for in-depth petrographic studies. This section presents and discusses the mineral assemblage of the Epembe carbonatites based on hand specimens and optical microscope observation. Hand specimen images (Fig 3.7), and thin section photographs are presented in Fig. 3.8 to illustrate mineralogy and texture. Detailed descriptions are presented in Table 3.1.

3.4.1 Hand Specimen Petrography

Collected samples were photographed and described. Mineralogy, colour and texture of the studied samples are presented in Appendix E. Generally speaking, the mineralogy of the Epembe Carbonatite-Syenite Complex is fairly simple. Major minerals observed are apatite, biotite, K-feldspar, plagioclase, magnetite and aegirine.

At outcrop and in hand specimen carbonatite surfaces are brown, while fresh exposed surfaces are a light tan colour. The brown coloration is inferred to be due to ferruginous staining as an oxidation product during weathering. In hand specimen, reddish-brown to white-grey carbonatites show slight variations in both grain size and mineralogy, ranging from fine- to coarse-grained (0.5 – 5.0 mm) and massive; locally they are intruded by late-stage hydrothermal calcite veins (Fig. 3.7A), which are also observed at the outcrop level. In all studied carbonatite samples, calcite is the dominant carbonate mineral with the carbonatite varying in composition from almost monomineralic pure calcite (Fig. 3.7B) to varieties with accessory minerals such as apatite, pyrochlore, K-feldspar and, locally, aegirine forming interlocking and hypidiomorphic textures. Yellowish-green apatite is found consistently throughout the Epembe carbonatite dyke (between 3 - 7 wt. %) as 0.1-2.5 cm of both rounded crystals, well-shaped hexagonal crystals, which may be prismatic, and disseminated in the calcite matrix (Fig. 3.7C). In hand specimen, pyrochlore crystals are observed as dark-brown, glassy octahedral crystals and irregular masses (Fig. 3.7 D). Typically, the pyrochlore is coarse-grained and ranges in size from tenths of a millimetre to greater than 2 mm.

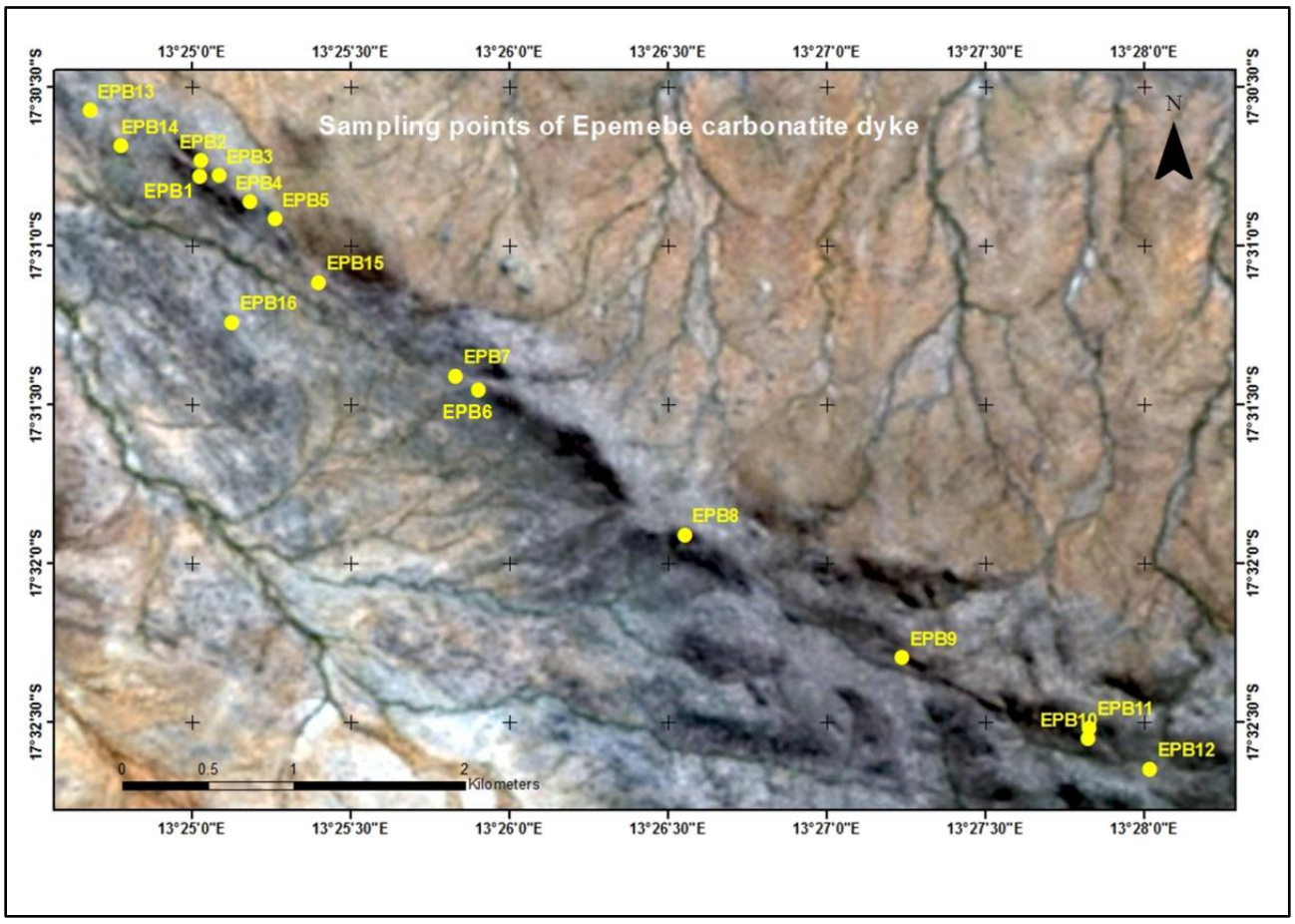


Figure 3-1 *Google Earth image (Landsat 8, sharpened) of the Epembe carbonatite dyke showing the sampling locations.*



Figure 3-2 *Carbonatite outcrop (photo taken facing southeast). The topographic high is dominated by carbonatite and minor syenite whilst the low lying plains on either side are underlain by gneisses of the Epupa Metamorphic Complex.*

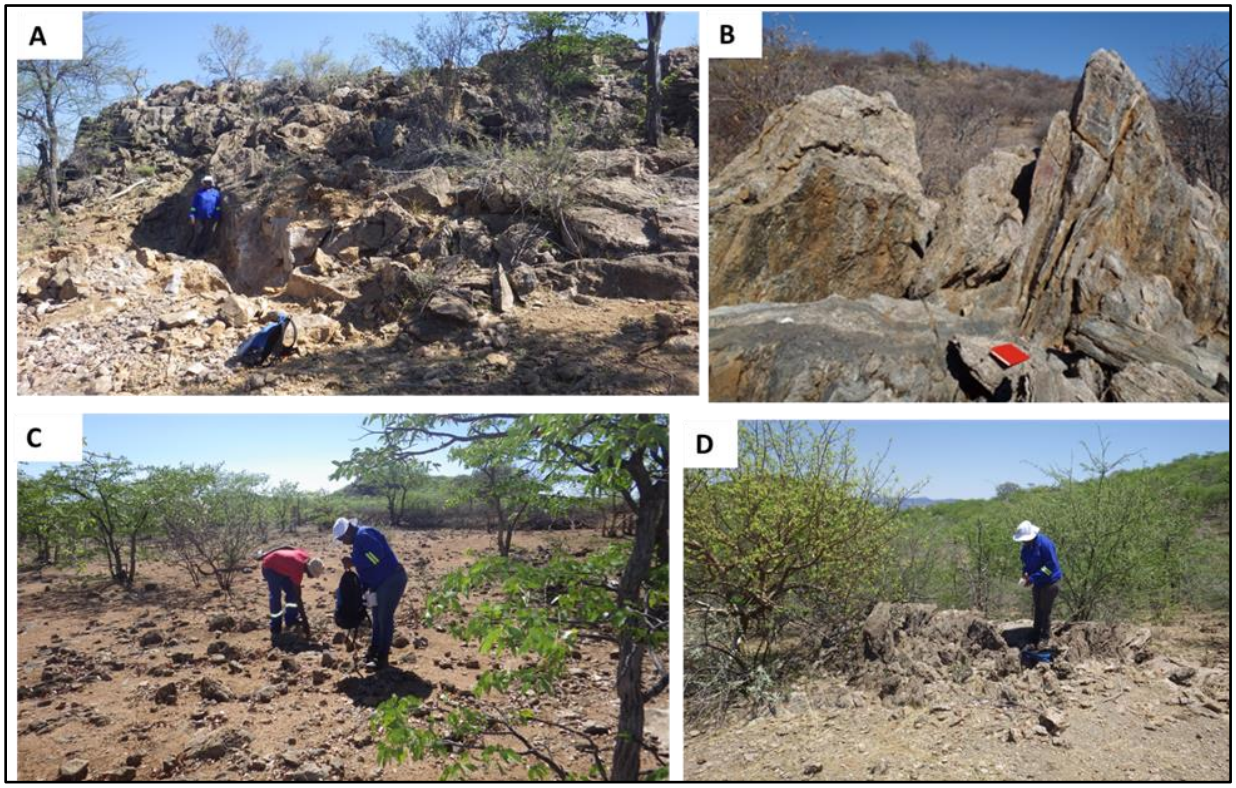


Figure 3-3 *Field outcrop photographs demonstrating differences in outcrop exposures. A) Topographic high massive carbonatite outcrop (sample No: EPB02, GPS: S 17 ° 30' 44''; E 13° 25' 41.7''), B) Cliff-like fenitised outcrop on the north east side of the carbonatite of the carbonatite intrusion (GPS: S 17° 31' 25.9"; E 13° 26' 41.7"), this granitic gneiss is pink-grey and displays a weak gneissose banding which is dominated by mafic layers. C) Low lying carbonatite outcrops partially covered by sand and gravel located about 100m (west of the dyke) away from the main carbonatite body (sample No: EPB13, GPS: S 17° 30' 34.5"; E 13° 24' 40.7"). D) Partially buried low lying and discontinuous carbonatite outcrops (sample No: EPB06, GPS S 17° 31' 27.3"; E 13° 25' 54.1").*

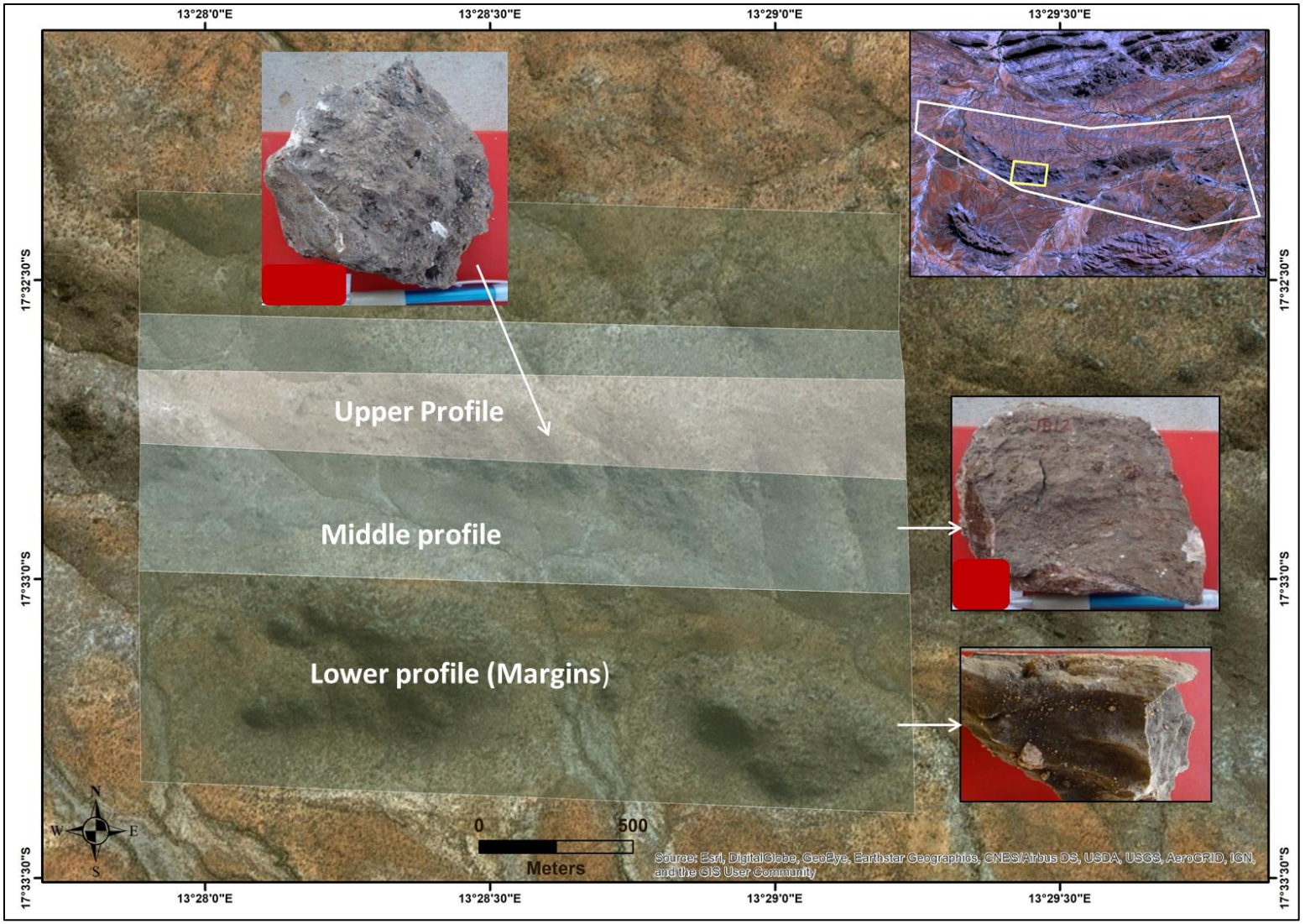


Figure 3-4 *Schematic representations of the different carbonatite profiles or phases observed at Epembe carbonatite dyke. The lower profile (margins), the middle profile and the upper profile. The lower and middle profiles show a gradational change to massive, coarse crystalline calcite in the upper profiles. The contacts between the profiles are not very well established and therefore are largely inferred.*

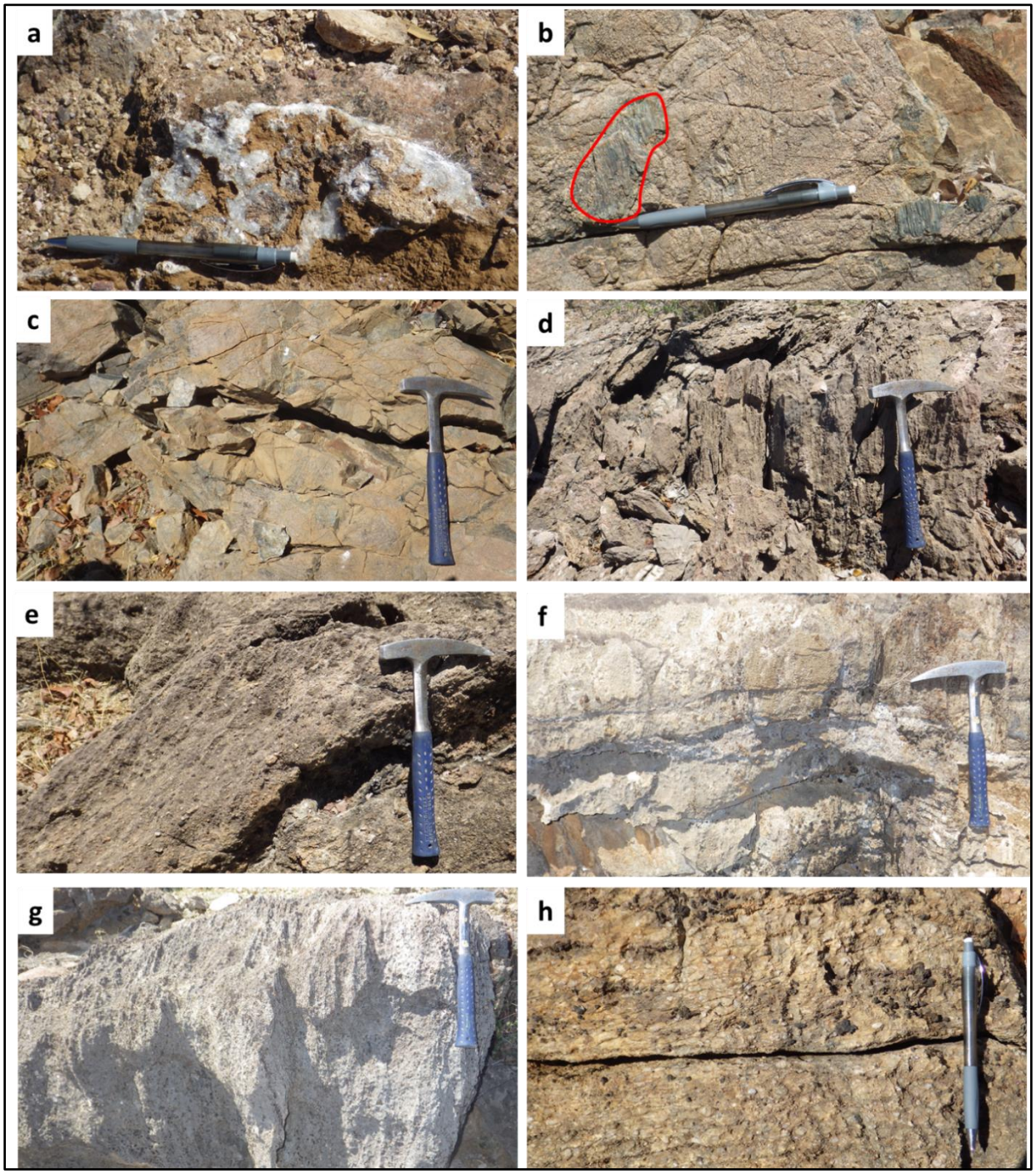


Figure 3-5 *Epembe Carbonatite outcrops with multiple structures and lithologies. a) Carbonatite with local calcite lenses b) carbonatite showing some cleavages highlighted in red, c) highly fractured granitic gneiss, d) carbonatite characterised by textural pattern that is probably related to magmatic flow, e) massive and non-textured carbonatite, f & g) carbonatite showing weathering, h) massive and mineralised carbonatite with disseminated apatite grains. Scale: hammer =35 cm, pencil = 15cm.*

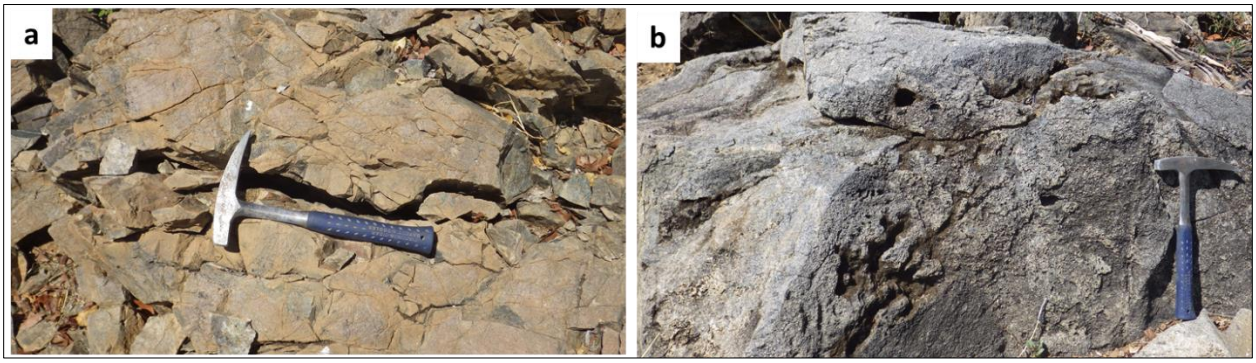


Figure 3-6 *The local country rocks around the Epembe carbonatite dyke. a) Highly fractured fenitised granitic gneiss, fine- to medium-grained, grey to reddish in colour; b) Massive syenite outcrop, typically light-dark grey, medium to coarse grained. Scale: Hammer = 60cm.*

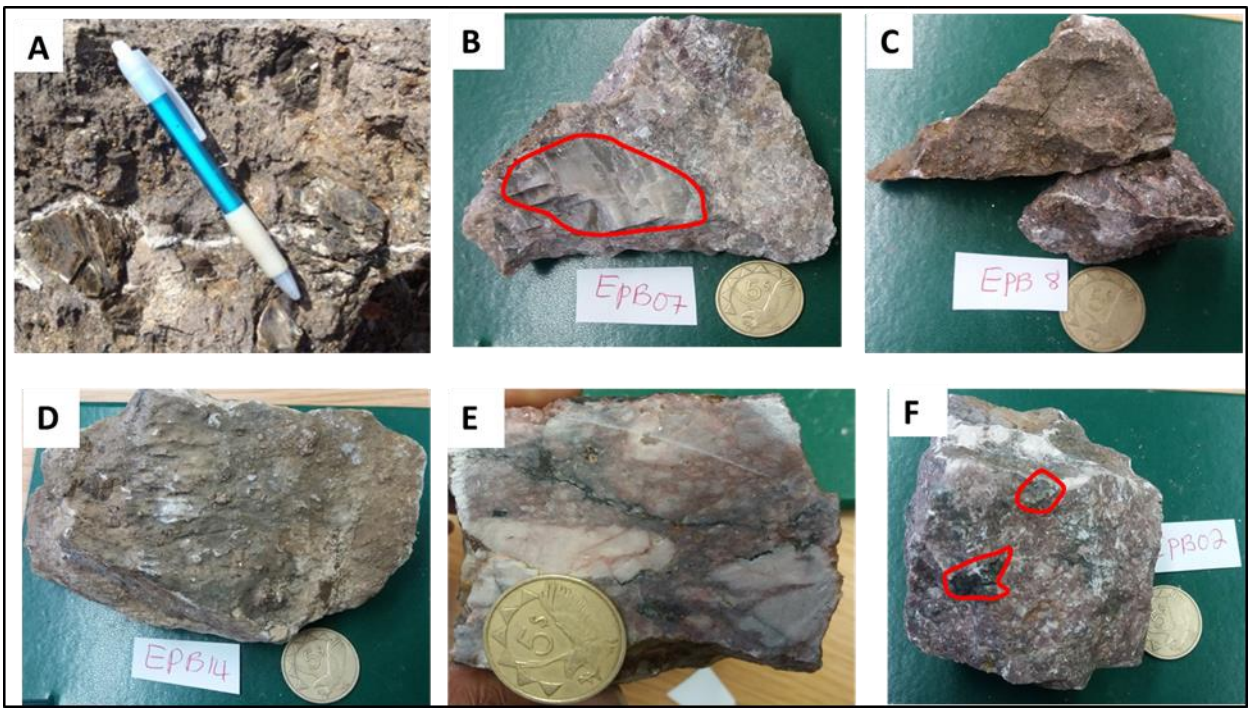


Figure 3-7 *Photographs of hand specimens of the carbonatites. A) In outcrop phenocryst of biotite (up to 50mm) characterises this heavily weathered carbonatite that does not contain any feldspar. It is cross cut by late hydrothermal calcite veining; B) White coarse-grained calcite crystals up to 5.0 mm; C) Carbonatite sample displaying equigranular holocrystalline grains of sugary calcite with a pinkish colour due to the presence of feldspar and darker minerals including pyrochlore and aegirine; D) carbonatite samples characterised by dark brown pyrochlore crystals; E) a section of fresh carbonatite displaying calcite and late stage veins stained with iron oxides; F) medium-grained pinkish-brown carbonatite with dark-greenish phlogopite (Mg-biotite) phenocryst. Scale: pencil = 15cm, coin diameter = 25mm.*

3.4.2 Microscopy Petrography

Ten thin sections were studied with a polarizing Carl Zeiss Axiolab microscope connected to a computer and investigated under polarized and crossed light in order to establish mineral textures and identify mineralogical compositions of the main carbonatite minerals and REE accessory phases. Thin sections were prepared at the Geological Survey of Namibia and photomicrographs were taken using a camera attached to the microscope.

Based on both hand specimen observations and optical microscopy, the most common mineral in the Epembe carbonatite is calcite (~90%). Two generations of calcite are observed. In some samples calcite appears as large euhedral grains with well-developed cleavages (Fig. 3.8A) while in others it is found as medium- to fine-grained crystals (Fig. 3.8B), perhaps indicating different crystallisation histories.

The second most commonly occurring mineral is apatite, which has been observed in all the studied carbonatite samples. Apatite grains appear sub-rounded to oval in shape and are associated with pyrochlore but also with feldspars, calcite and aegirine (Fig. 3.8C & D). Some apatite grains appear elongate and typically aligned.

Another principal accessory mineral is pyrochlore. It is observed as a honey brown to pale yellow mineral and sometimes as opaque crystals with its grain size varying from fine to medium (1µm -0.5m) grain especially in the veins. Pyrochlore is mostly found in intricate intergrowths with apatite as well as calcite. Some pyrochlore crystals exhibit zonation which may be indicative of a long lasting crystallisation within carbonatite magma chamber (Wyllie and Biggar, 1996), a characteristic only restricted to late stage carbonatite magmatism.

Researchers such as Knudsen (1989) and Chakhmouradian and Williams, (2004) have described the development of pyrochlore composition throughout magmatic evolution. It has been observed that during the initial stage of carbonatite magmatism, Ta and Nb are possibly transported as fluoride and phosphate complexes which explain the common association of apatite with pyrochlore. In some instances, pyrochlore is found as an inclusion (Fig. 3.8C) within the apatite crystals suggesting that apatite formed first before pyrochlore.

Other minerals observed are those belonging to the mica (mainly biotite and phlogopite) and feldspar (plagioclase – albite, microcline) groups, which are found in affiliation with magnetite, hematite and chlorite forming groundmass (Fig.3.8E). They primarily occur in clusters of discrete grains, sometimes coating the grain margins of adjacent minerals such as pyrochlore, identifying them as late stage crystallisation products. Mineral aegirine is observed coarse grained (up to 1cm) in the calcite matrix (Fig. 3.8F).

Dolomite occurs in minor amounts as fine-grained crystals in veinlets or replacing calcite. Some dolomite replaces the grain boundaries of pyrochlore and apatite. Detailed mineralogical descriptions and additional photomicrographs are presented in Appendix F, while the optical characteristics of observed mineral are summarized in Table 3.1.

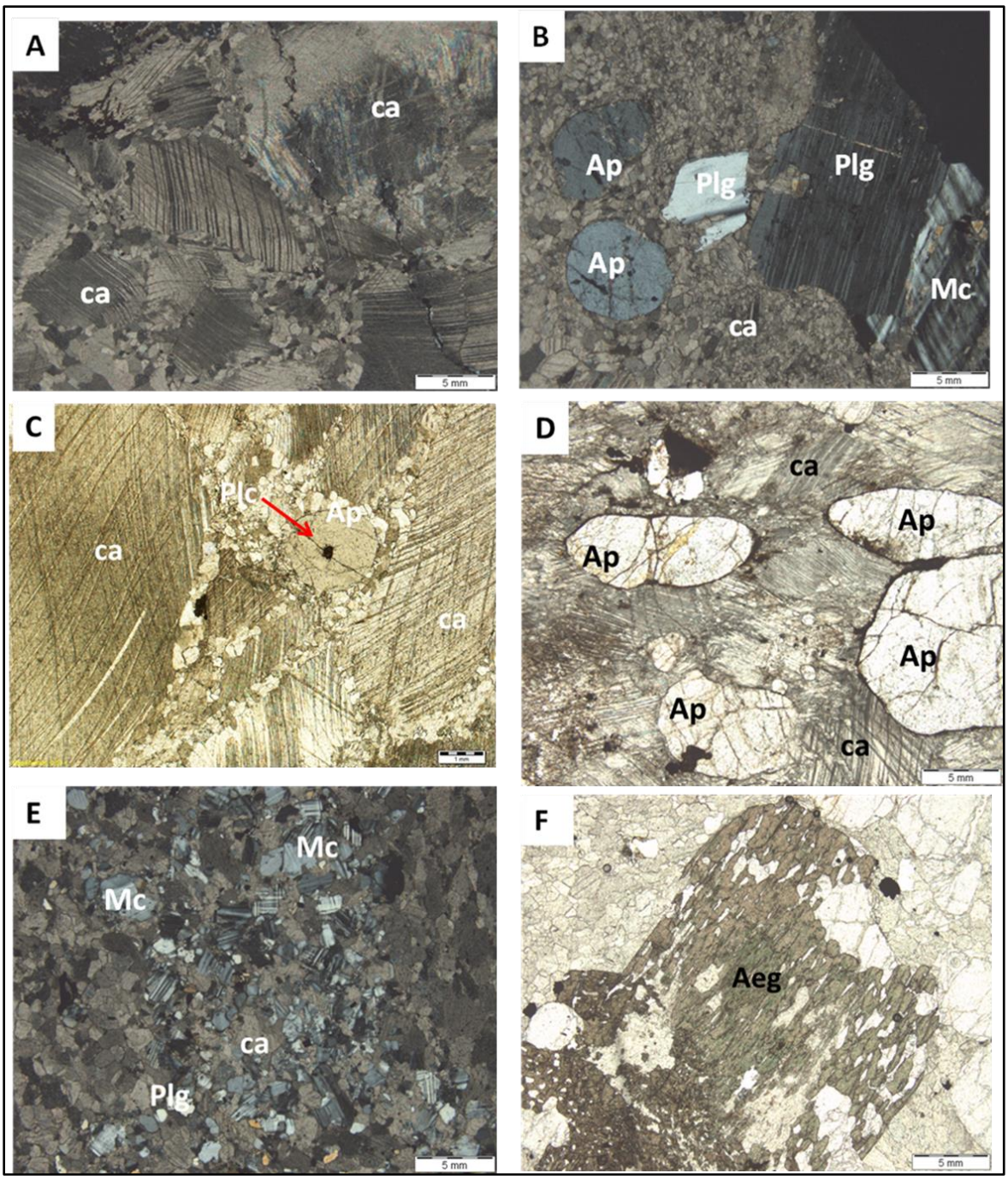


Figure 3-8 *Thin section photomicrographs of selected representative carbonatite samples in cross polarised light (XPL) and plane polarised light (PPL), showing mineralogical characteristics of the Epembe carbonatites. A) EPB03: Coarse-grained calcite with mica fills in the cracks and fractures (XPL,) B) EPB02: ovoid apatite grains and feldspars embedded in calcite matrix (XPL); C) EPB03: Photomicrograph of coarse-grained calcite, and an ovoid apatite grain hosting pyrochlore grain - arrowed (PPL,); D) EPB08: elongated and aligned apatite grains and calcite grains (PPL,). EPB13: E) medium to fine-grained granular groundmass (gm) of anhedral feldspars, interstitial calcite and minor amount of quartz forming equigranular texture (XPL,) seen also as un-oriented grains; F) coarse grained aegirine in the calcite matrix (XPL). Abbreviations: Aegirine (Aeg), Apatite, (Ap), Pyrochlore (Plc), Calcite (Ca), Microcline (Mc), Plagioclase (Plg).*

3.4.3 X-Ray Diffraction analysis

In order to complement the petrographic results and better investigate the REE mineralogy, carbonatite samples were submitted for mineralogical assessment using the X-Ray Diffraction (XRD) technique for the identification of minerals. Samples were taken to the GSN, Ministry of Mine and Energy for mineral analysis using a Bruker AXS XRD machine connected to a desktop computer. Portions of the milled rock sample were uploaded into the machine through a sample holder. With the help of Eva computer software, characteristic peaks of each mineral were produced and the data were exported in a PDF format (Appendix G).

The results indicate that calcite (specifically magnesian calcite [Ca, Mg]) is the major minerals at Epembe carbonatite together with accessories of albite, microcline, quartz, cancrinite and phlogopite Most minerals observed in both thin section and hand specimen (e.g. apatite, pyrochlore, magnetite etc.) were undetectable by XRD. The difference between XRD and thin section mineral analyses results could partly be due to a couple of reasons: (1) XRD is a semi-quantitative technique that has a detection limit in the range of 1 -5%, therefore minerals occurring in trace amounts will not be detected and/or 2) a representative problem of the tested samples (even though there is no evidence of the latter).

The observed carbonatite minerals (based on both hand specimen, optical microscopy and XRD analysis are tabulated in Table 3.2, including their estimated modal abundances by averages.

Table 3-1 *Summary of the optical characteristics of the mineralogy of Epembe carbonatite*

Minerals	Texture and Characteristics
Calcite	Calcite is the dominant minerals~90%. The calcite appears as coarse-grained and shows good, well developed cleavages (multiple twinning) with high birefringence.
Apatite	Apatite appears white-light grey to colourless crystals with spherical to sub-rounded shape .Apatite is scattered throughout the coarse-grained calcite matrix forming a porphyritic (up to 2.5mm) texture.
Pyrochlore	Reddish-brown in colour with well-developed crystal faces (euhedral to sub-hedral). Occurs as large isolated grains suspended in a calcite matrix. Pyrochlore shows a strong association as inclusions within apatite. Grain size is less than 0.2 mm (Fig. 3.6c).
Feldspar	Feldspar is one of the common minerals represented by colourless Plagioclase (albite?) located in the fine-grained matrix it ranges in size from fine grains in veins to medium grained.
	K-feldspar (microcline) – holocrystalline, inequigranular groundmass of sub-hedral, medium to coarse-grained alkali feldspar.
Mica	Biotite (phlogopite?) is recognised as pale to deep brown and sometimes as greenish brown tabular crystals found as interstitial grains between aggregates of other mineral
Hematite Magnetite	Rectangular, opaque and cubic grains of iron minerals are observed either interstitial to the coarse grains of calcite or in the fine-grained matrix.
Aegirine	Where present, aegirine is typically brownish green in colour, appearing as large aligned phenocrysts (up to 4 mm) either disseminated throughout the matrix or

	as cumulate concentrations.
Quartz	Quartz occurs scarcely as either inclusions within other minerals or part of the ground mass associated with Fe-bearing minerals and mica.
Biotite Chlorite	Where present, biotite and chlorite are found in clusters or appear to be exploiting fractures.
Dolomite	Coexists with calcite and is dominant on the edges of opaque minerals.

Table 3-2 *Mineralogical composition of Epembe minerals*

Mineral	**Chemical formula**	**Estimated modal abundances (vol.% range)**
Major minerals		
Calcite (Magnesian Calcite)	$(Ca, Mg)CaO_3$	80 -90 %
Dolomite	$CaMg(CO_3)_2$	2 – 3 %
Albite	$Na(Al\ Si_3O_8)$	3 - 5 %
Microcline	$K(AlSi_3O_8)$	3 - 5 %
Biotite(Phlogopite)	$K(Mg,Fe^{2+})_3(A;,Fe^{3+})Si_3O_{10}(OH,F)_2$	1 – 2 %
Accessory minerals		
Apatite	$Ca_5(PO_4)_3(F,OH)$	15 -20 %
Pyrochlore	$(Na, Ca, Sr,\ Pb, U)_2(Nb, Ta,Ti)_2O_6(OH,F)$	2 - 10 %
Iron Oxide	Fe_2O_3	0.5 - 1%
Magnetite	Fe_3O_4	0.5 - 1%
Zircon	$ZrSiO_4$	2 – 3 %
Monazite	$(REE)PO_4$	0.5 – 1 %
Epidote	$Ca_2(Al,Fe)_2(SiO_4)_3(OH)$	1 – 2 %
Quartz	SiO_2	4 – 5 %
Cancrinite	$Na6Ca_2[(CO_3)_2\|\ Al6Si6O24] \cdot {}_2H_2O$	0.5 – 1 %
Ankerite	$Ca(Fe,Mg,Mn)(CO_3)_2$	0.5 – 1 %

CHAPTER 4: GEOCHEMISTRY

Sixteen representative samples of the Epembe carbonatite were analysed for major and trace elements including rare earth elements. Major elements were analysed by X-Ray Fluorescence (XRF) and trace elements by inductively coupled plasma mass spectrometry (ICP-MS). The geochemical analyses were carried out at the Earth Lab of the University of Witwatersrand**.**

4.1 Geochemistry of major elements

Major element compositions of the sixteen samples are presented in Appendix H. They show comparatively high concentrations of calcium (CaO: 38.01 - 55.31 wt. %), while iron (FeO: 0.87 - 9.29 wt. %), magnesium (MgO: 0.19 – 1.33 wt. %) and silica (SiO2: 1.30 – 10.89 wt. %) are low. Total alkalis (K_2O + Na_2O < 2.0 wt. %) are also low, but aluminium (Al_2O_3: 0.35 - 4.45 wt. %) shows moderate concentrations. Phosphorus (P_2O_5) is low ranging from 0.23 to 3.43 wt. %, and nickel (NiO) and chromium (Cr_2O_3) are present in very insignificant amounts of 0.00 and < 0.025 wt. %, respectively. Furthermore, the carbonatite is characterised by a significant proportion of volatiles as shown by the high values of loss on ignition (LOI: 28.18 – 41.56 wt. %); by comparison, fenite and syenite samples only show a LOI of 0.67 Wt. % and 3.03 wt. % respectively. The high volatile content in the analysed carbonatites is associated with a loss of carbon dioxide (CO_2).

The major element data show that the carbonatites are all calcio-carbonatites when plotted on an MgO-CaO-FeO+MnO ternary diagram (Woolley and Kempe, 1989), with all samples plotting above the 80% reference line with a single exception, which lies below that value but still above 50% CaO (Fig. 4.1). The calcio-carbonatite is the type of carbonatites as a rock based on the modal abundances of calcite as a carbonate mineral. In the case of Epembe carbonatite, the calcite is specifically magnesian calcite ([Ca, Mg] CO_3), which is a type of calcite consisting of randomly substituted magnesium carbonate in a disordered calcite lattice.
Ratios between Al_2O_3, SiO_2, Fe_2O_3 and TiO_2 with MgO (Fig. 4.2) indicate a positive linear trend, while P_2O_5: MgO and MnO: MgO plots show a scattered distribution of data points. The same behaviour is observed when plotting these oxides against the MgO/CaO ratios. Conversely, when plotted against calcium oxide (CaO), all major elements with the exception of MnO show a negative trend (Fig. 4.3), i.e. they decrease with increasing CaO; while P_2O_5 does not exhibit a strong variation.

Major elements of Al_2O_3, TiO_2, P_2O_5, FeO, K_2O + Na_2O, MgO, CaO when plotted against SiO_2, exhibit a positive trend which could relate to contamination of carbonatite by silicate rocks (Fig. 4.4).

In comparison with global averages of calcio-carbonatite (Wooley and Kempe, 1989), the Epembe carbonatite (Table 4.1), shows slightly elevated SiO_2, Al_2O_3, FeO and Fe_2O_3 while MgO and P_2O_5 are just below the average; other elements fall within the same ranges as that of average calcio-carbonatite.

4.2 Geochemistry of trace and REE elements

Contrary to major elements, trace elements are not rock-forming elements and therefore tend to concentrate in a few minerals such that they are excluded from most common minerals e.g. strontium (Sr) is excluded from most common minerals except plagioclase. Similarly barium (Ba) is not found in

most minerals except in alkali feldspar. As such, trace elements are very useful in determining magma source as well as in formulating models for magmatic differentiation. The most common trace elements used in petrogenetic interpretations of igneous rocks are Nb, Ba, Sc, Ni, Cr, V, Rb, Sr, Zr, Y and REE (La to Lu).

4.2.1 Trace element

Trace element results are presented in Table 4.2. with analyses showing high concentrations of phosphorus (P) (up to 18076 ppm sample EPB01), titanium (Ti) (up to 5122 ppm sample EPB03), strontium (Sr) (highest in sample EPB02 12315 ppm) and niobium (Nb) (highest value 2022 ppm in sample EPB03). Barium (Ba), cerium (Ce), and niobium (Nb) exceeded the detection limits by ICP-MS in sample EPB 12. Cesium (Cs) and tungsten (W) are low in the carbonatite samples, with concentrations of < 3 ppm and 1 ppm, respectively, while the other trace elements show moderate concentrations. The high content of those elements in the Epembe carbonatite provides information on the types and quantity of trace minerals in the Epembe carbonatite dyke. The high content of phosphorus in sample EPB01 is indicative of an apatite ($Ca_5[PO_4]_3[F, OH]$) rich sample while the sample rich in Ta and Nb implies the abundance of pyrochlore ($[Na,Ca, Sr, Pb, U]_2(Nb, Ta,Ti)_2O_6(OH,F)$ minerals in those specific samples. The good correlation observed between Ta + Nb and P (Fig. 4.5), is an indication that most samples that are rich in pyrochlore are also rich in apatite hence supporting the thin section evidence of close associations occurring of the two minerals.

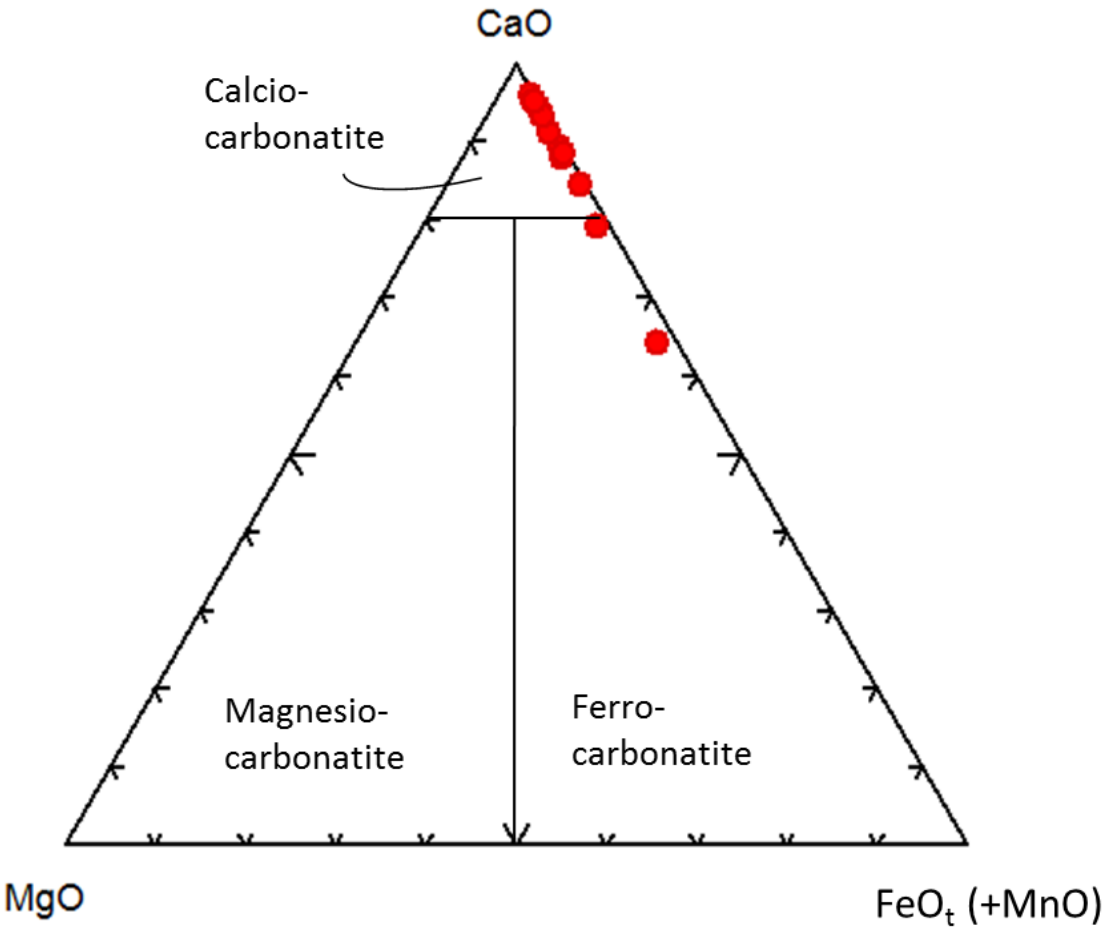


Figure 4-1 *Ternary diagram (MgO-CaO-FeOt {+MnO) for carbonatites with Epembe carbonatite samples plotting in the field of calcio-carbonatite (≥80%). Field boundaries of ferro-, calcio-, and magnesio-carbonatite after Woolley & Kempe (1989).*

In order to compare the element constituents of each mineral, geochemical diagram of total REE against selected trace elements were constructed. Nb+Ta shows a weak correlation (R^2 = 0.1458) with total REE+Y (Fig. 4.6); while element Zr, Nb and P also showing minor correlation with total REE (with R^2 = 0.129, 0.114 and 0.006 respectively trends) (Fig. 4.7).

4.2.2 Rare Earth Element

The main purpose of this study is to establish the geochemical variation and distribution of REEs in the Epembe carbonatite. For ease of interpretation and comparison with previous work, analytical results (Appendix H) have been normalised to chondrite values by dividing REE concentrations by the chondrite values (Rock, 1987) of the specific element. The normalised results are presented in Table 4.3 and REE patterns are illustrated in Fig. 4.8. In this study, the chondrite REE values from Sun and McDonough (1995) were used.

Rare Earth content of Epembe carbonatites are high, with some rare earth element content above the detection limit of ICP-MS (in sample EPB 12, high concentrations of Ce and Nd are reported from the laboratory as 'saturated'). Despite this, the lowest total rare earth (REEt + Y) concentration is observed

in sample EPB 12 with only 406 ppm, while the maximum concentration in a carbonatite sample is 912 ppm (EPB01). The total REE content in fenite (EPB05) is moderately higher than that of syenites (EPB10 & EPB16) but significantly lower than that in the sampled carbonatite. The elevated REE content of fenites relative to syenites (Fig.4.8.) can be attributed to metasomatic process whereby REE constituents were introduced into the fenites by carbonatitic hydrothermal fluids during the carbonatite intrusions.

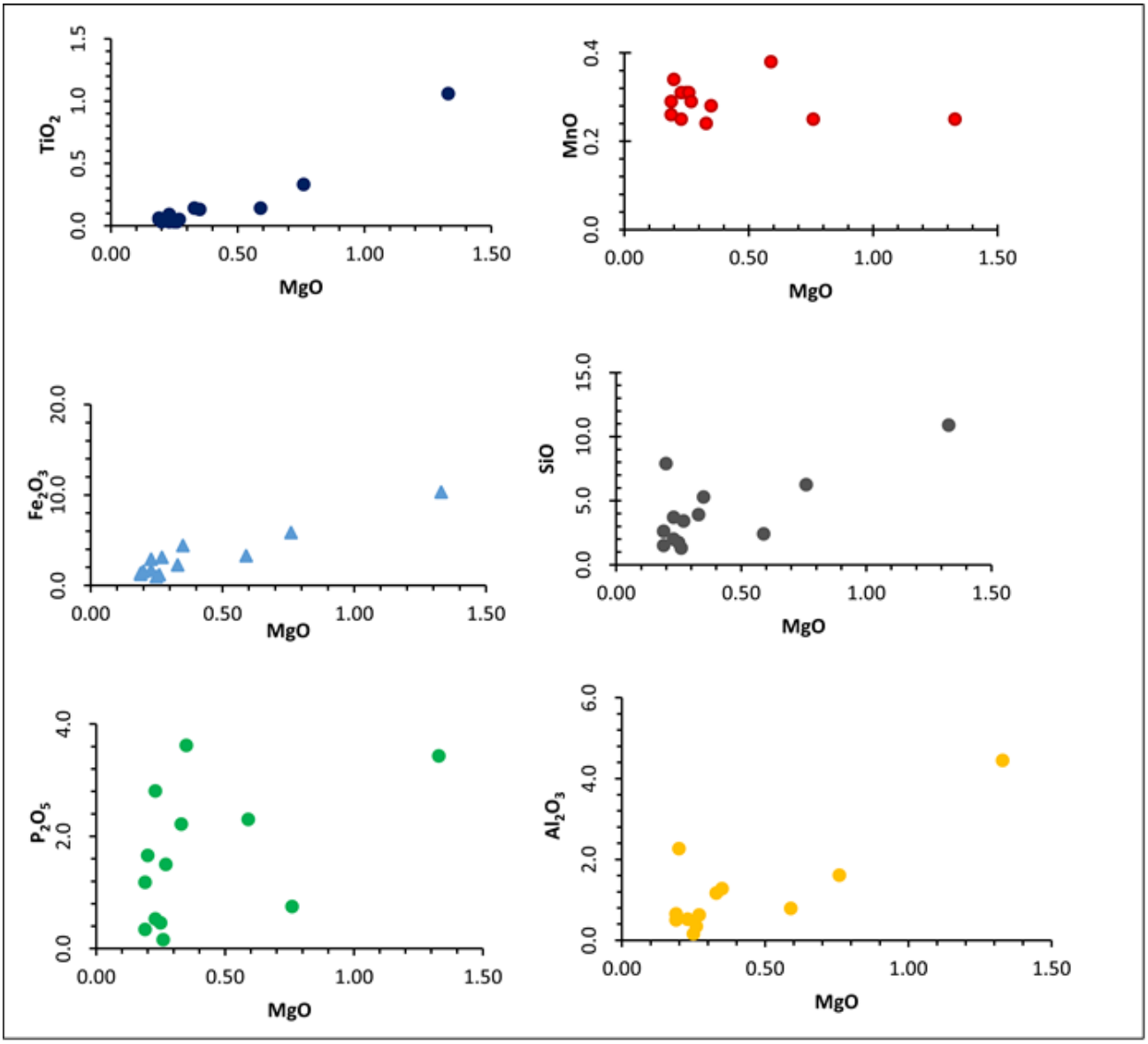


Figure 4-2 *Graph of major elements (TiO_2, MnO; Fe_2O_3; SiO_2; P_2O_5; Al_2O_3) plotted against MgO for Epembe carbonatite samples. All oxides with an exemption of MnO exhibit a positive trend.*

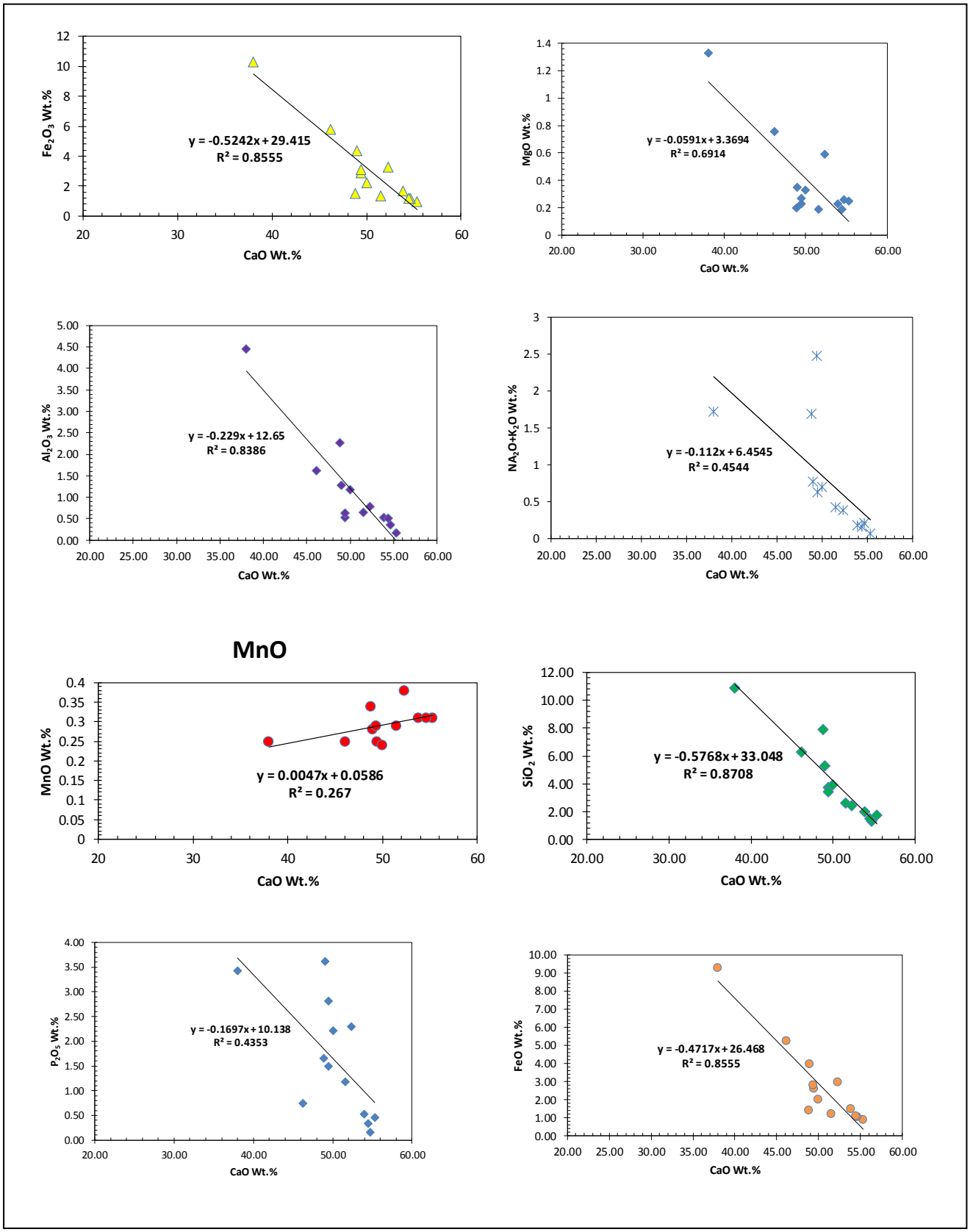


Figure 4-3 *Major Elements vs. CaO of the investigated Epembe carbonatite samples. Fe_2O_3, MgO, Al_2O_3, Na_2O+K_2O, SiO_2, and FeO show a negative correlation with an increasing CaO. MnO show an increase with increasing CaO content. P_2O_5 does not exhibit a strong variation.*

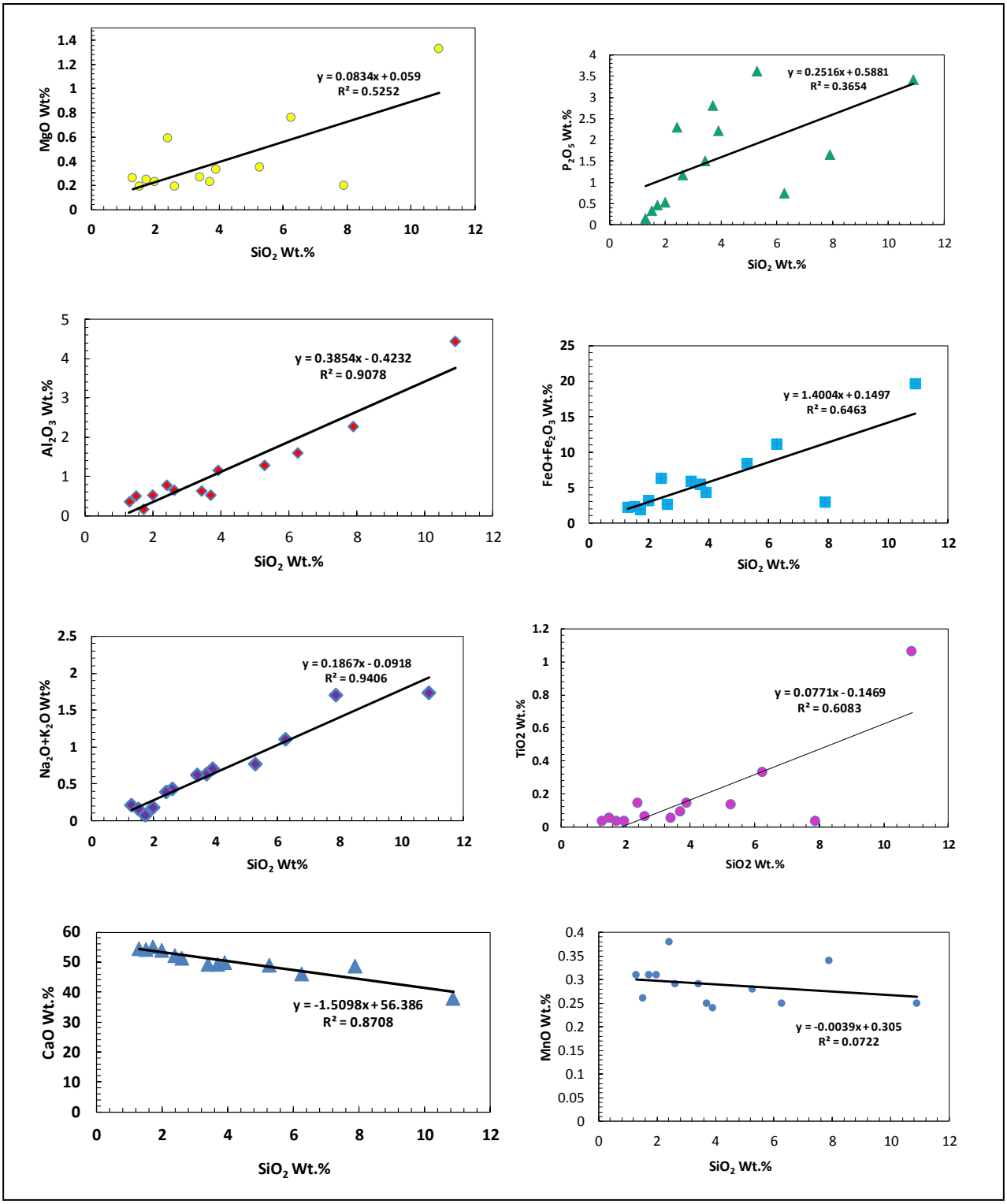


Figure 4-4 *Major element (Al_2O_3, TiO_2, P_2O_5, FeO, K_2O + Na_2O, MgO, CaO against SiO_2). All oxides with an exception of CaO exhibit a positive Trend.*

Table 4-1 *Whole rock major-elements analyses (wt. %) of Epembe carbonatite. Average calcio-carbonatite compositions are after Woolley and Kempe (1989)*

Sample	SiO_2	Al_2O_3	Fe_2O_3	FeO	MnO	MgO	CaO	Na_2O	K_2O	TiO_2	P_2O_5	Cr_2O_3	NiO	LOI	Total
EPB01	5.28	1.28	4.41	3.97	0.28	0.35	48.98	0.22	0.55	0.13	3.62	0.02	0.00	34.71	99.82
EPB02	3.71	0.52	2.89	2.60	0.25	0.23	49.47	0.44	0.19	0.09	2.81	0.02	0.00	36.78	97.41
EPB03	10.89	4.45	10.33	9.29	0.25	1.33	38.01	0.21	1.52	1.06	3.43	0.02	0.00	28.18	99.66
EPB04	3.91	1.17	2.25	2.02	0.24	0.33	50.00	0.11	0.59	0.14	2.22	0.03	0.00	37.14	98.13
EPB06	1.73	0.16	0.97	0.87	0.31	0.25	55.31	0.05	0.02	0.03	0.46	0.02	0.00	40.83	100.14
EPB07	1.99	0.52	1.67	1.50	0.31	0.23	53.90	0.03	0.15	0.03	0.53	0.02	0.00	40.29	99.66
EPB08	2.62	0.65	1.36	1.22	0.29	0.19	51.54	0.01	0.42	0.06	1.18	0.02	0.00	39.88	98.23
EPB09	1.30	0.35	1.18	1.06	0.31	0.26	54.69	0.04	0.17	0.03	0.16	0.02	0.00	41.56	100.08
EPB11	6.26	1.61	5.83	5.25	0.25	0.76	46.18	0.19	0.91	0.33	0.75	0.02	0.00	36.08	99.17
EPB12	2.41	0.79	3.29	2.96	0.38	0.59	52.33	0.03	0.36	0.14	2.30	0.03	0.00	37.53	100.18
EPB13	3.42	0.63	3.10	2.79	0.29	0.27	49.41	0.34	0.28	0.05	1.50	0.03	0.00	38.11	97.43
EPB14	7.90	2.27	1.55	1.39	0.34	0.20	48.83	0.26	1.44	0.03	1.66	0.02	0.00	34.41	98.92
EPB15	1.51	0.50	1.22	1.10	0.26	0.19	54.45	0.01	0.15	0.05	0.34	0.02	0.00	41.04	99.74
Average Epembe carbonatite	**4.07**	**1.15**	**3.08**	**2.77**	**0.29**	**0.40**	**50.24**	**0.15**	**0.52**	**0.17**	**1.61**	**0.02**	**N/A**	**37.43**	**99.12**
Average Calcio carbonatites (*Woolley and Kempe ,1989*)	**2.72**	**1.06**	**2.25**	**1.01**	**0.52**	**1.80**	**49.12**	**0.29**	**0.26**	**0.15**	**2.10**	**N/A**	**N/A**	**37.40**	**N/A**

NB: Major analysis results obtained from XRF are not able to provide both Fe_2O_3 and FeO, therefore the FeO values were obtained by calculation and assuming Fe_2O_3 * 0.8998 of the total iron oxides. Stoichiometry calculations adapted after Gaillard *et al*. (2003).

Table 4-2 *Trace element analyses results (ppm) for Epembe carbonatite samples. Global average calcio-carbonatite compositions are from Woolley and Kempe (1989).* Please note: N/A means data not available. It should be noted that many of the data compiled by Woolley & Kempe (1989) came from carbonatite samples that are treated as representing a carbonatite class using wt.% CaO, MgO, and (FeO + Fe_2O_3 + MnO) as the classification criteria. Therefore, as shown with this table, 'calciocarbonatite' represents samples in which the proportion of CaO/ (CaO + MgO +FeO + Fe_2O_3 + MnO) is greater than 80%.

Sample	EPB01	EPB02	EPB03	EPB04	EPB06	EPB07	EPB08	EPB09	EPB11	EPB12	EPB13	EPB14	EPB15	Epembe carbonatite		Global Carciocarbonatite	
														Avearge	Range	Average	Range
Li	1.86	0.49	4.53	1.37	0.49	1.21	0.75	0.34	2.01	1.71	0.51	0.77	0.73	1.29	0.34 - 2.01	0.10	N/A
P	18076.91	11637.61	12778.69	8314.23	2024.97	2546.25	5109.31	751.43	3516.50	11330.12	7512.34	7694.05	1491.79	7137.25	751 - 1807.91	N/A	
Sc	4.38	7.03	3.96	3.66	1.19	0.78	1.77	0.45	1.86	2.36	6.38	1.51	1.07	2.80	0.78 - 7.03	7.00	0.6 - 18
Ti	674.36	381.25	5122.76	644.72	43.60	137.70	217.33	69.00	1535.99	600.21	184.22	113.75	144.34	759.17	43.60 - 1535.99	N/A	N/A
V	161.81	89.28	116.55	33.90	2.72	8.25	17.29	5.45	47.35	28.60	148.95	3.72	19.43	52.56	2.72 -161.81	80.00	0 - 300
Cr	12.13	9.57	8.32	6.05	4.62	13.25	3.82	3.96	8.62	8.45	23.91	10.36	5.34	9.11	3.82 - 23.91	13.00	2 - 479
Co	7.55	3.25	11.47	4.39	2.64	2.20	4.06	2.19	7.92	10.62	5.67	4.27	3.44	5.36	2.20 - 11.47	11.00	2 - 26
Ni	19.65	17.75	11.88	17.32	19.84	21.22	16.59	19.30	24.07	31.68	21.52	27.21	30.22	21.40	16.59 - 30.22	18.00	5 - 30
Cu	9.27	7.89	7.43	4.55	9.73	6.29	9.38	3.51	17.73	19.23	6.88	5.98	4.49	8.64	3.51 - 19.23	24.00	4 - 80
Zn	13.75	12.87	99.36	15.10	6.71	6.37	518.03	10.57	59.37	27.73	8.97	54.41	5.99	64.55	5.99 - 518.03	188.00	20 - 1120
Ga	12.47	7.06	16.12	8.22	3.29	3.71	4.66	4.97	15.18	8.22	6.33	6.63	3.79	7.74	3.29 - 16.12	<5	N/A
Rb	17.99	6.35	20.90	20.86	0.99	3.41	7.24	9.58	77.38	13.53	7.19	21.39	3.72	16.19	0.99 - 77.38	14.00	4 - 35
Sr	4232.20	12315.44	7544.46	8641.79	5108.84	4538.52	8954.93	5381.32	8282.47	3354.48	9446.24	7502.44	4832.95	6933.54	4232.20 - 12315.44	N/A	N/A
Y	83.48	75.31	54.56	72.66	76.14	70.69	74.33	91.07	69.77	86.18	67.44	63.28	52.53	72.11	52.58 - 86.18	119.00	25 - 346
Zr	125.73	99.53	114.13	94.08	2.61	2.45	116.13	3.07	224.42	34.96	72.88	6.87	7.64	69.58	2.61 - 224.42	189	4 -2320
Nb	1532.57	1090.02	2022.64	159.58	7.69	40.05	280.70	45.17	150.53	225.13	64.15	51.78	24.80	438.06	7.69 - 2022.64	1204.00	1 - 15000
Ba	96.63	134.62	205.81	142.23	53.78	516.21	135.76	110.28	182.43	saturated	141.36	247.50	98.64	172.10	53.78 - 516	N/A	N/A
Sn	18.09	17.93	11.40	4.23	0.24	1.70	3.68	0.97	4.62	1.04	16.98	1.44	1.05	6.41	0.24 - 18.09	N/A	N/A
Cs	0.63	0.24	1.35	0.71	0.02	0.20	0.07	1.88	2.95	0.96	0.15	0.12	0.12	0.72	0.02 -1.35	20	
Hf	5.04	5.68	3.05	2.10	0.12	0.13	2.09	0.19	3.95	0.84	3.59	0.19	0.29	2.10	0.12 - 5.68	N/A	N/A
Ta	76.50	187.42	367.28	33.41	0.49	10.76	54.01	8.36	12.84	48.35	8.42	2.16	3.02	62.54	0.49 - 367.28	5.00	N/A
W	0.65	0.12	0.27	0.19	0.14	0.23	0.12	0.24	0.37	0.27	0.10	0.22	0.15	0.23	0.10 - 0.65	N/A	N/A
Pb	5.81	6.74	6.21	5.02	6.50	2.99	143.84	6.99	4.76	19.16	7.04	23.24	1.74	18.46	1.74 -143.84	56.00	30 -108
Th	21.90	6.37	8.06	2.08	0.40	0.34	3.22	3.28	3.05	2.26	0.41	0.76	0.96	4.08	0.34 - 21.90	52.00	5 - 168
U	26.74	331.90	480.06	25.15	2.18	6.19	67.62	10.67	6.00	50.28	9.09	1.92	2.10	78.45	1.92 -480.06	8.70	0.3 - 29

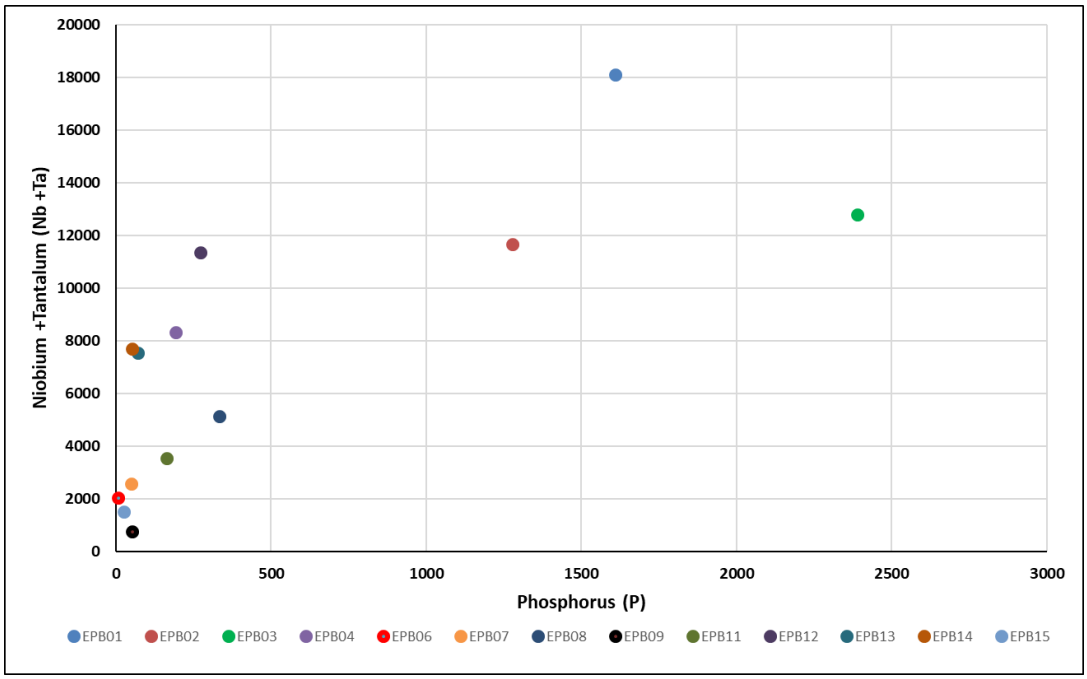


Figure 4-5 *Correlation between phosphorus (ppm) and niobium + tantalum (ppm) of the Epembe carbonatite. The general trend shows a positive correlation.*

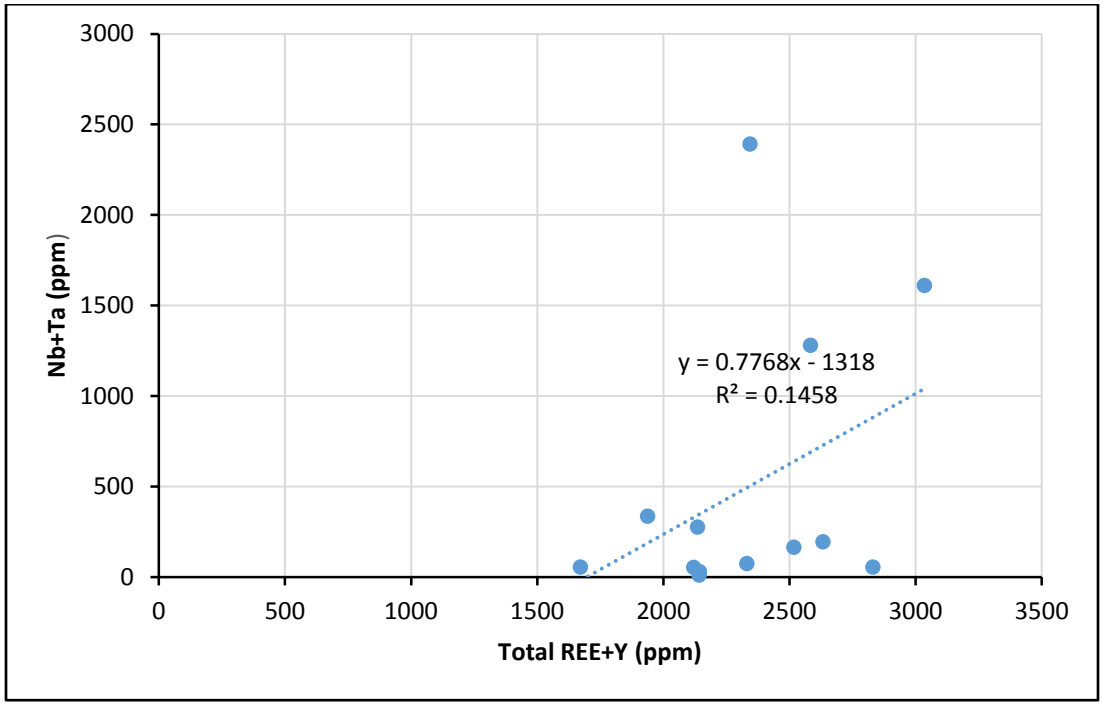


Figure 4-6 *Graph of total REE+Y Vs Nb + Ta. Shows weak correlation (R^2 = 0.1458).*

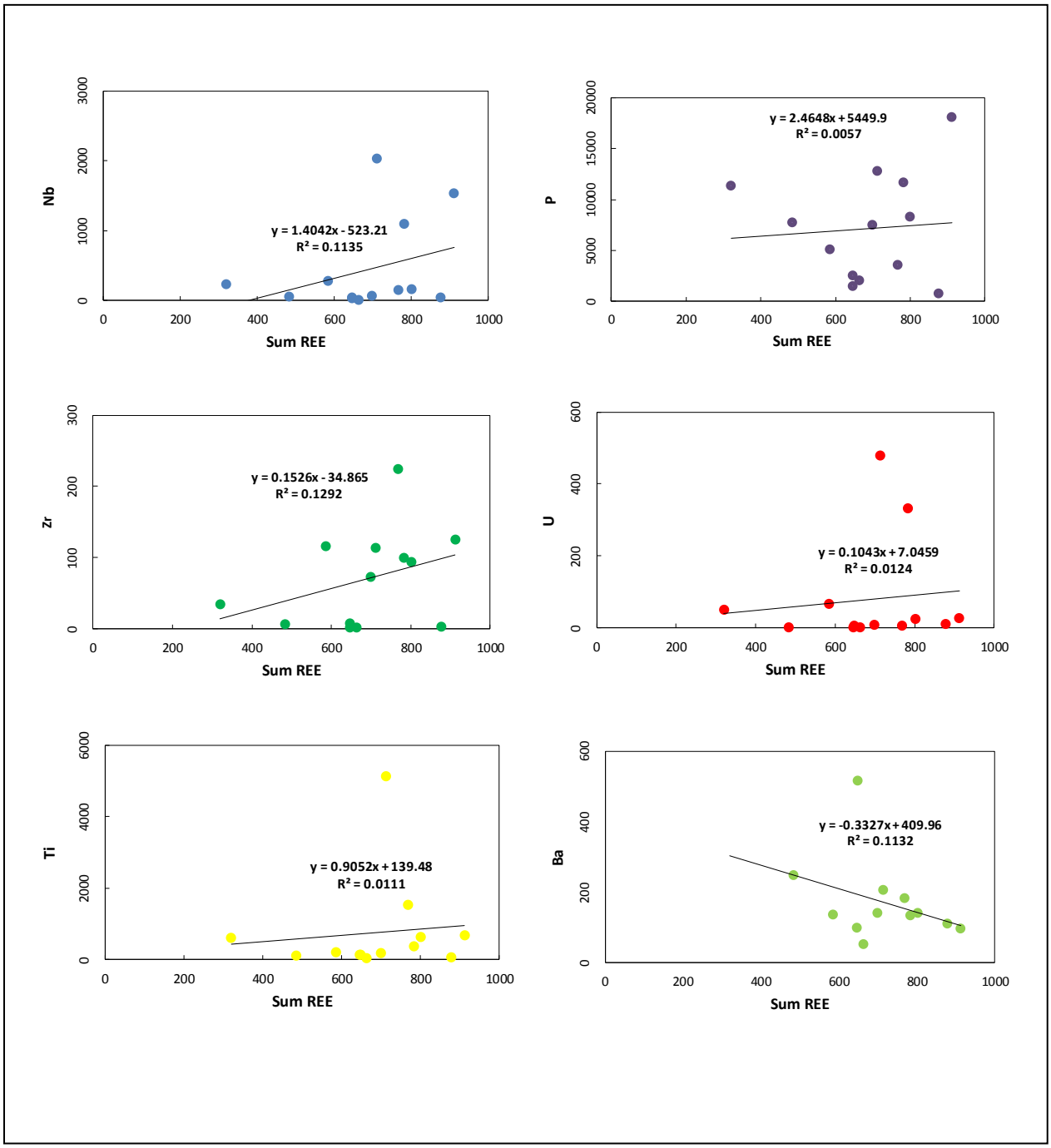


Figure 4-7 *Binary plot of REE total (ppm) versus selected trace element (ppm). Elements Zr, P, Nb show a weak correlation with the total REE while U and Ti displays insignificant relationship with total REE.*

Table 4-3 REE chondrite normalised data for sixteen samples of carbonatite, fenite and syenites from Epembe-Syenite complex. Chondrite values after McDonough and Sun (1995).

Sample	EPB01	EPB02	EPB03	EPB04	EPB05	EPB06	EPB07	EPB08	EPB09	EPB10	EPB11	EPB12	EPB13	EPB14	EPB15	EPB16	Chondrite normalizing factors(ppm)
Rock unit	carbonatite	carbonatite	carbonatite	carbonatite	fenite	carbonatite	carbonatite	carbonatite	carbonatite	syenite	carbonatite	carbonatite	carbonatite	carbonatite	carbonatite	syenite	
La	746.32	672.41	638.33	702.41	664.20	555.41	522.48	462.63	691.29	55.32	705.46	725.86	563.63	324.10	596.76	113.85	0.24
Ce	567.33	484.27	437.09	501.78	474.15	424.36	393.64	343.99	557.16	53.19	473.46		419.79	275.56	415.65	87.11	0.61
Pr	424.82	352.23	327.74	364.96	308.73	280.52	285.82	248.59	381.95	26.85	344.25	433.32	321.14	232.44	307.79	72.00	0.09
Nd	348.26	290.29	297.74	298.64	224.63	218.85	246.19	207.47	327.75	23.15	286.44		281.65	180.39	226.30	60.37	0.46
Sm	194.36	158.20	140.92	152.32	105.43	109.30	122.76	119.52	170.93	13.50	140.39	193.52	146.16	120.74	120.24	36.23	0.15
Eu	152.52	123.07	109.11	118.81	57.57	80.11	93.20	94.58	122.49	12.70	109.93	152.63	114.14	96.96	88.85	26.55	0.06
Gd	147.44	121.40	104.50	119.12	64.30	90.22	97.08	97.08	134.81	8.97	109.89	150.97	112.24	92.75	91.51	22.17	0.20
Tb	96.65	76.23	63.27	74.65	30.36	60.91	62.74	64.32	84.29	5.07	67.37	97.42	72.96	65.40	57.34	14.76	0.04
Dy	73.56	57.87	45.39	56.55	19.03	50.18	50.25	53.46	65.35	3.79	51.28	73.56	57.02	51.27	42.68	11.32	0.25
Ho	54.56	44.45	33.32	43.26	12.27	41.90	40.02	42.67	51.25	2.77	39.18	56.79	44.03	41.83	34.05	8.66	0.05
Er	42.38	35.75	27.09	35.64	10.91	37.26	34.30	34.56	42.61	2.29	33.47	46.43	36.01	33.64	29.24	7.63	0.16
Tm	37.69	32.43	23.56	32.02	8.14	38.38	34.29	33.24	38.46	2.02	30.16	42.19	33.48	32.71	27.61	7.49	0.02
Yb	35.18	31.74	22.40	31.49	7.93	40.31	34.96	32.33	37.83	1.89	29.68	40.43	32.04	31.81	27.14	7.83	0.16
Lu	31.26	28.33	20.12	29.11	6.95	39.31	33.01	29.88	34.96	1.67	27.80	37.15	29.88	29.80	26.18	7.60	0.02
Total REE	**2952.33**	**2508.66**	**2290.57**	**2560.76**	**1994.59**	**2067.03**	**2050.75**	**1864.34**	**2741.12**	**213.18**	**2448.74**	**2050.28**	**2264.17**	**1609.42**	**2091.34**	**483.58**	**2.51**
Chondrite normalised ratios																	
EuN/EuN*	0.89	0.89	0.90	0.88	0.70	0.81	0.85	0.88	0.81	1.15	0.89	0.89	0.89	0.92	0.85	0.94	
CeN/CeN*	1.01	1.00	0.96	0.99	1.05	1.08	1.02	1.01	1.08	0.37	0.96		0.99	1.00	0.97	0.96	
LaN/YbN	21.21	21.19	28.49	22.31	83.74	13.78	14.94	14.31	18.28	29.30	23.77	17.95	17.59	10.19	21.99	14.55	
LaN/SmN	3.84	4.25	4.53	4.61	6.30	5.08	4.26	3.87	4.04	4.10	5.03	3.75	3.86	2.68	4.96	3.14	
GdN/YbN	4.19	3.82	4.66	3.78	8.11	2.24	2.78	3.00	3.56	4.75	3.70	3.73	3.50	2.92	3.37	2.83	
LaN/LuN	23.87	23.73	31.72	34.91	95.55	14.13	15.83	15.48	19.77	33.19	25.37	19.54	18.86	10.88	22.80	14.98	

EuN/EuN* gives the amplitude of the Eu anomaly (=EuN/square root (SmN*GdN); where the ratios of all carbonatite sample showing less than (<1). CeN/CeN* gives the amplitude of the Ce anomaly (=CeN/square root (LaN*PrN) with seven (including one fenite sample) sample having a ratio above one and the rest are below but close to 1. LaN/YbN ratio (=La normalised to chondrite/Yb normalised to chondrite) gives the general steepness of the REE pattern which is ranging from 10.19 – 28.49 in the carbonatite sample and while in fenite(EPB05) the ratio is up to 83.74 which is the highest and hence steepest. The LaN/ SmN gives the steepness for LREEs (2.68 – 5.08 in carbonatites) and GdN/YbN gives the steepness for HREEs (2.24 – 4.66

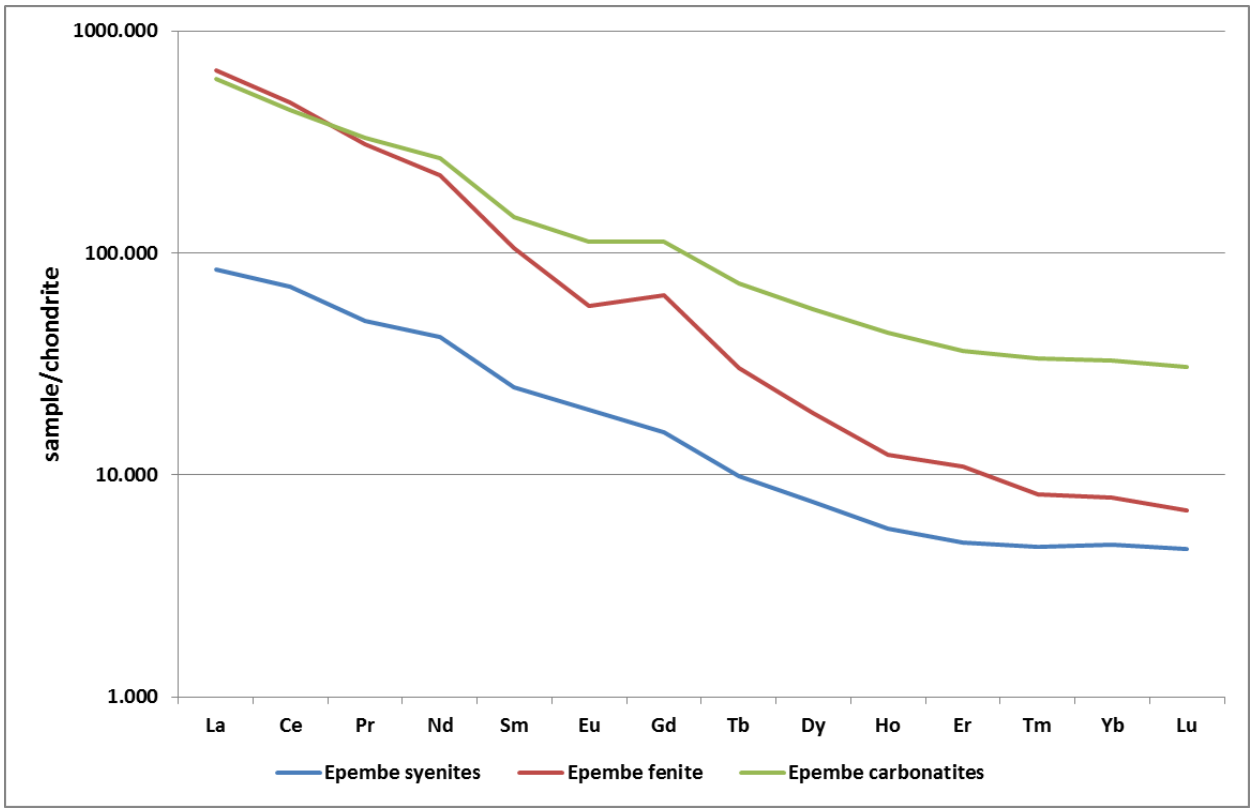


Figure 4-8 *REE pattern for carbonatite, fenite and syenite samples from the Epembe carbonatite dyke and surrounding rocks. Chondrite normalised using data from McDonough and Sun (1995).*

The REE distribution in the Epembe grab samples shows small variations both in total REE content and in the chondrite – normalised REE pattern (Table 4.3). The general chondrite-normalised trend shows a downward-sloping pattern, demonstrating a strong enrichment of light rare earth element (LaN/YbN = 10.19 – 28.49) compared to heavy rare earth element (GdN/YbN = 2.24 – 4.66) Fig.4.8), a feature common to most carbonatites because of the favorable geological context for LEE minerals formation (. All samples are characterized by a slight negative Eu anomaly and a positive Gd anomaly.

4.3 Radiometry maps and REE

Radiometric maps of the study area (Fig. 4.9 – 5.11.) show the presence of radioactive elements along and in the vicinity of the carbonatite dyke. Increased radioactivity corresponds to the Epembe carbonatite dyke, and confirms the geochemical data, which shows a variable to high content of uranium (2 – 480 ppm) and low content of thorium (0.34 – 21.00 ppm) REEs are hosted in the carbonatite together with the radioactive elements uranium, thorium and potassium, with which they share many chemical properties (e.g. both are incompatible and mobile). For this reason, radiometric surveys can be used as an indirect exploration method for REE.

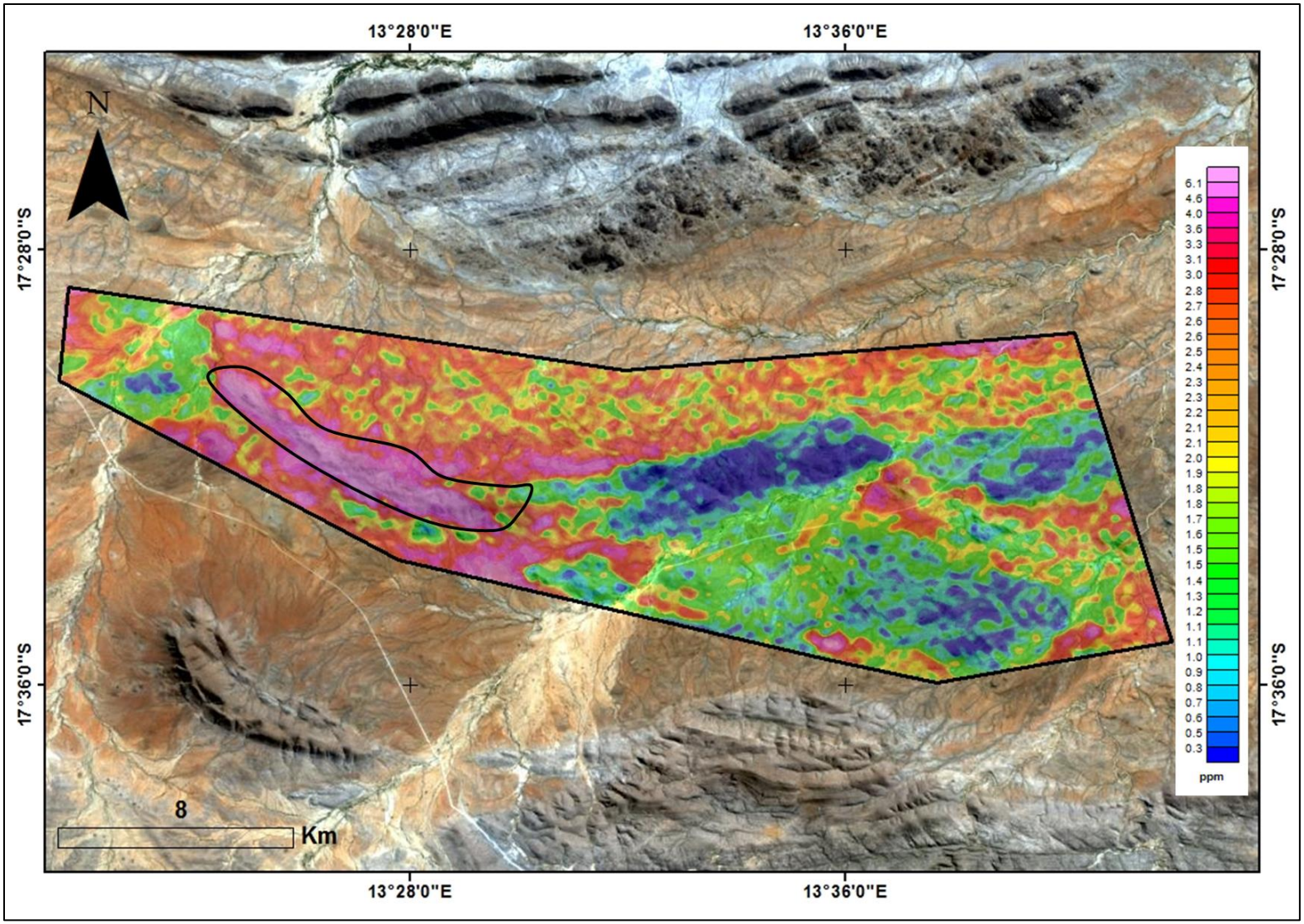


Figure 4-9 *Airborne radiometric data showing the distribution of potassium (ppm) in the study area, the deep blue to light blue colours indicates area with the lowest radioactive rocks, while the green-orange-red range of colours show the intermediate radioactive rocks and the pink colour represents areas with high radioactive rocks. The inferred Epembe carbonatite dyke is delineated by a black outline (Data source: GSN).*

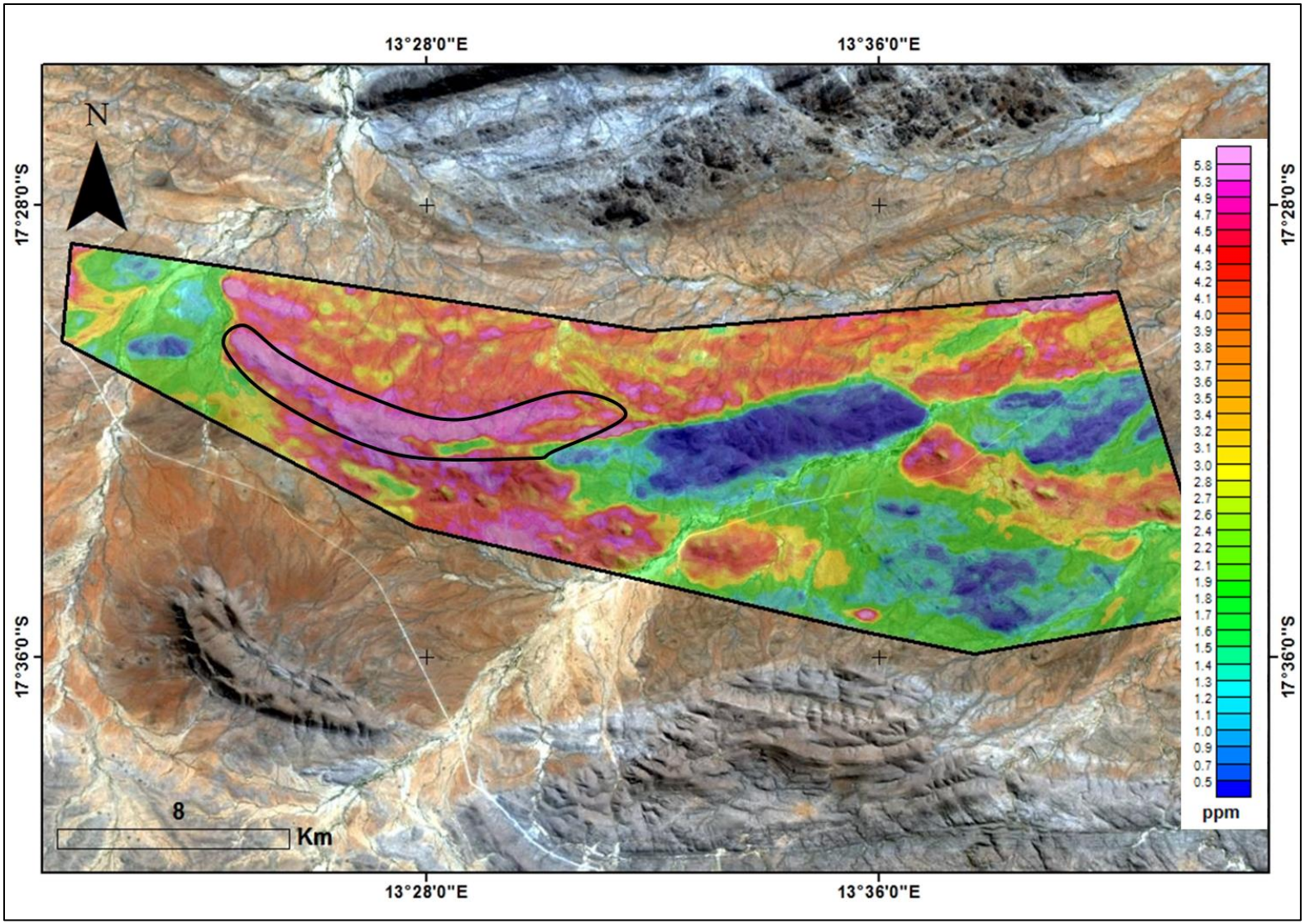


Figure 4-10 *Airborne radiometric data showing the distribution of uranium (ppm) in the study area, the deep blue to light blue colours indicates area with the lowest radioactive rocks, while the green-orange-red range of colours show the intermediate radioactive rocks and the pink colour represents areas with high radioactive rocks. The inferred Epembe carbonatite dyke is delineated by a black outline (Data source: GSN).*

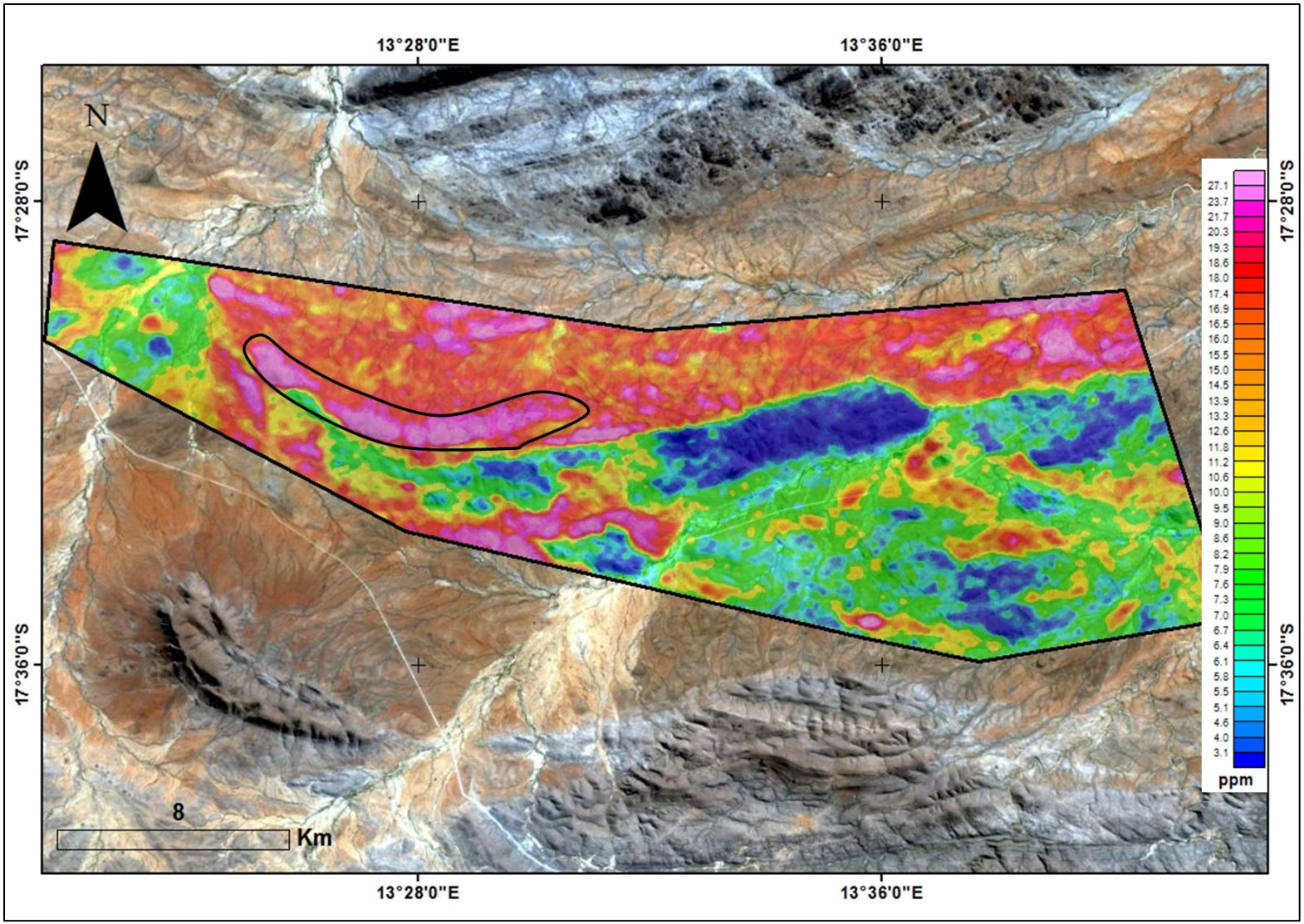


Figure 4-11 *Airborne radiometric data showing the distribution of thorium (ppm) in the study area, the deep blue to light blue colours indicates area with the lowest radioactive rocks, while the green-orange-red range of colours show the intermediate radioactive rocks and the pink colour represents areas with high radioactive rocks. The inferred Epembe carbonatite dyke is delineated by a black outline (Data source: GSN).*

CHAPTER 5: DISCUSSION AND CONCLUSION

In this section the results and data from the previous chapters are discussed and interpreted, as well as compared to those presented in the existing literature, in order to give a comprehensive overview of the REE mineralisation in the Epembe carbonatite dyke.

5.1 Carbonatite type and petrography

Field relationships indicate that the Epembe carbonatite intruded and fenitised the nepheline syenite of Epembe – Swartbooisdrift Intrusive Suite and is, therefore, younger. The main evidence for this is the blocks of this material (fenites) that have been veined, brecciated and incorporated into the intruding carbonatite as xenoliths (Fig.5.1). The contacts between the country rocks and the carbonatite show a very high degree of fenitisation, as evident in a prominent aureole, which may be a result of the high temperature of the carbonatite melt causing a change of minerals in the surrounding country rocks. These field relationships are supported by the respective geochronological data. While an emplacement age of 1184 ± 10 Ma (U-Pb single zircon; Simon *et al.* 2017) was determined for the carbonatite, the nepheline syenites were dated at 1216 ± 2.4 Ma and 1213 ±2.5 Ma (U-Pb single zircons; Seth *et al*. 2003).

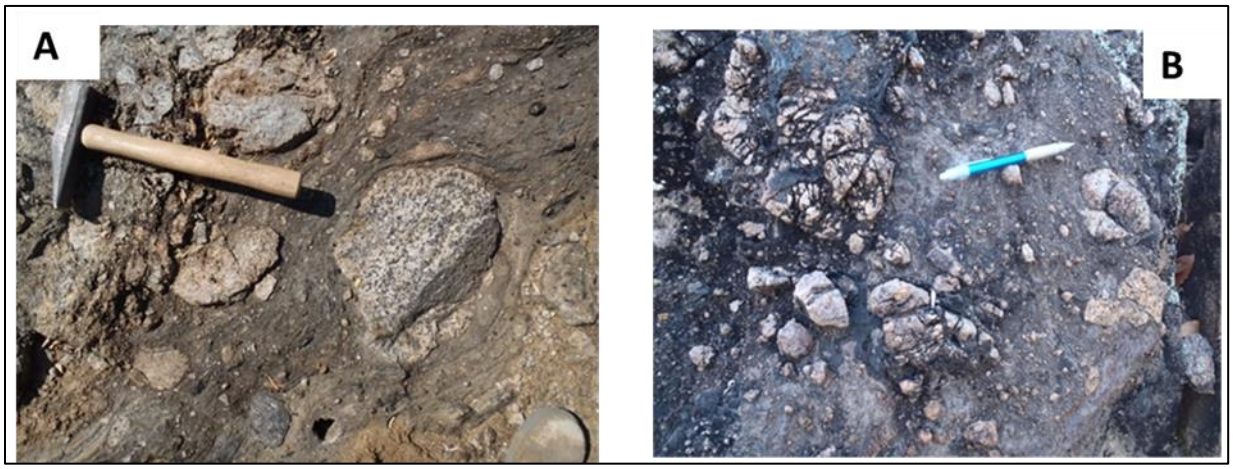


Figure 5-1 *Bocks of syenites (xenoliths) that have been incorporated into the intruding carbonatite. A) Syenite xenoliths with flow banding oriented in a north-west to south-east direction; B)* carbonatite *containing xenoliths of Syenites and aegirine. Scale: Hammer (35 cm), pencil (15 cm).*

The mineralogy of the Epembe carbonatites examined in this study consist predominantly of a calcitic matrix and enriched accessory minerals including but not limited to apatite, pyrochlore, feldspars, phlogopite, micas, magnetite, hematite, aegirine and zircon. The mineralogy of the Epembe carbonatite is thus relatively simple compared to other carbonatites. Textural characteristics and crystallisation order indicate the early formation of primary calcite which is observed as large euhedral crystals with well-developed cleavages. In the studied carbonatites calcite makes up as much as 50 and 90 Vol. % of the carbonatite, thus representing the main carbonate mineral. The calcite grains show a granular

texture in hand specimen with some individual grains exceeding 2 cm. In thin section the granular texture is also evident, with most calcite grains showing perfect rhombohedral cleavages. Calcite is often found in complex relationship with all other minerals, which suggests that they crystallised at the same time; they are also found as inclusions within either pyrochlore or apatite, which points to some of the calcite being formed earlier than pyrochlore and apatite. Secondary calcite however, is mostly associated with hydrothermal veins that are cutting across all other mineral constituents; the latter is evidence that they formed during a late-stage event. Also, the calcite grains in or around these veins are reduced in size indicating re-crystallisation. Most of the veins/fractures cutting across the carbonatite, as in samples EPB03 and EPB04 (Fig. 5.2), are filled with Fe-oxides, mainly dark to opaque hematite and some magnetite. The veins and fractures formed due to pressure of invading fluids and subsequently acted as conduits for hydrothermal fluids, in which they crystallised. The carbonatites also contain significant amounts of pyroxenes within these fractured areas. Hydrothermal processes injected fluids into the carbonatites along fractures, which upon cooling formed pyroxenes, Fe-oxides and feldspars now coating these fractures. Aegirine mainly occurs at the contacts between the calcite-apatite-feldspar minerals.

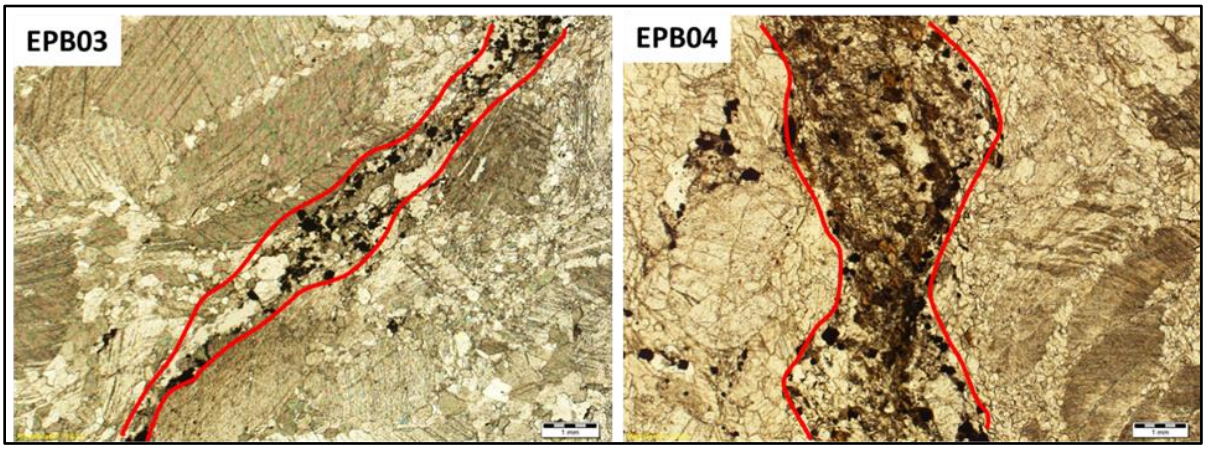


Figure 5-2 *Thin section photographs of two carbonatite samples displaying the vein/fractures cutting through the carbonatite. The veins are observed to be filled with opaque iron-oxide minerals.*

Even though field observations, mineralogy and texture of the Epembe carbonatites point to more than two pulses or generations of carbonatites, similar geochemical signatures show that all the observed carbonatite phases are sourced from the same magma and hence can be regarded as a single carbonatite dyke. Some carbonatites have a very variable chemical composition including REE , e.g. the Lofdal alkaline carbonatite complex (LACC) on the Bergville and Lofdal farms northwest of Khorixas, in the Kunene Region Namibia. The main calcite carbonatite at Lofdal shows a variable chemical composition with some generations of carbonatite showing enrichment in lighter REE while there is depletion in heavier REE, and some generations of the same carbonatite are characterised by a relatively higher concentration of heavy REE with respect to the other samples (Do Cabo, 2014). The relative enrichment in the heavy REE of in some Lofdal carbonatite could be due to the alteration of the rock by hydrothermal fluids rich in heavy REE, or those carbonatites could be from a carbonatite that formed from the residual magma composition which was enriched in heavy REE, giving a clear indication that

the different carbonatite at Lofdal are sourced from different magma unlike those at Epembe carbonatite.

5.2 Major and Trace element geochemistry

Apart from showing similar chemical compositions, the geochemistry of the Epembe carbonatites also is consistent with established normal values for carbonatite. Based on the classification system of Gittins (1997), which uses the dominant carbonate mineral to categorise carbonatites, the Epembe rocks classify as calcio-carbonatites. Similarity, the chemical classification system of Woolley and Kempe (1989) indicates that the Epembe carbonatites are calcio-carbonatite or calcite carbonatite. The Epembe carbonatites have CaO/ (CaO+MgO+Fe_2O_3+MnO) ratios of (50.24/50.24+0.4+3.08+0.29) =0.93 on average, which is in agreement with typical calcio-carbonatite with ratios of CaO/ (CaO+MgO+FeO+ Fe_2O_3 + MnO) > 0.8 These classifications are supported by thin section studies which show the rocks to be made up of more than 80% calcite, agreeing to the definition of carbonatite as a rock composed of more than 50% carbonate (Shelly, 1993; Streckeisen, 1979).

The whole rock major and trace element composition of the Epembe carbonatite is similar to the global average for calcio-carbonatites (Woolley and Kempe (1989; Tables 4.1 and 4.2). While the Epembe carbonatite is characterised by lower than average MnO, MgO, Na_2O, P_2O_5, V, Cr, Co, Cu, Zn, Y, Zr, Cs, Th, the values are still within the global ranges reported for these elements in the literature (e.g. Woolley and Kempe, 1989; Woolley and Church, 2005). Conversely, the Epembe carbonatite shows elevated contents of Li, P, Ti, Ta, and Nb in relation to other trace elements. Phosphorous, though abundant in average carbonatite (Woolley & Kempe, 1989) displays much higher values in the Epembe rocks, which is attributed to the ubiquitous presence of the phosphate mineral apatite. The unusual concentrations of tantalum (Ta), niobium (Nb) and uranium (U) at Epembe are due to the presence of pyrochlore as well as apatite. This agrees with exploration results by Kunene Resources, who found the economically interesting rare metals tantalum (Ta) and niobium (Nb), hosted in the mineral pyrochlore, thus characterising the Epembe dyke as a Ta-Nb-U deposit in 2012.

The slightly higher values of CaO and Al_2O_3, in the Epembe carbonatite in comparison to the global average can be explained by the presence of abundant calcite (CaO_3) and potassium aluminum silicate (microcline) and micas (biotite; phlogopite) in the Epembe carbonatites respectively. Elevated Fe_2O_3 in the Epembe carbonatite is supported by the occurrence of iron-bearing minerals (hematite, magnetite). Finally, the low concentration of K_2O and Na_2O is typical of carbonatite rocks. Even though the new geochemical data indicate that Epembe is similar to the other major carbonatite complexes in the world, the observed enrichment in critical metals of niobium (Nb) and Tantalum (Ta) which are commonly found together (they are geochemically very similar but have a very different genesis) is the main differentiating feature at the Epembe. It is reported that both of these elements are enriched in highly differentiated igneous rocks such as granites, in alkali granites and syenites, rare-metal granites and pegmatites and more importantly in carbonatites (Chakhmouradian, 2006). It can therefore be

interpreted that Epembe carbonatite is likely to be more fractionated compared to the most carbonatites studied for global average for calcio-carbonatites by Woolley and Kempe (1989).

The slightly elevated silica content of the Epembe carbonatite (~4 wt. %) compared to average compositions (cf. Woolley & Kempe 1989; 2.72 wt. %) (Table 4.1) can be related to contamination of the carbonatite by the silicate country rocks (fenites and syenites), which were found as xenoliths within the former. The degree of contamination is evident from Harker plots (Fig. 4.4), which show clear linear positive trends for all major oxides except CaO.

5.3 REE Geochemistry

Total REE concentrations in the Epembe carbonatite range from approximately 406 – 912 ppm. The REE patterns for all Epembe carbonatite samples are clearly the same with an overall trend exhibiting a strong steady decrease (negative slope) from LREE to HREE (Fig. 4.8 and 5.4), a feature common to most carbonatites (e.g. Jones *et al*. 2013). The Epembe carbonatites, nepheline syenites and fenites indicate a general enrichment in the incompatible elements over the compatible elements.

The elevated content of light REE (La-Ga) reflects an enrichment of incompatible elements in the dyke. The LREE are more incompatible than their counterparts of HREE and those tend to remain in melt and rather incorporated into late-stage forming minerals (more fractionated) minerals. These may be accumulated during the genesis of the carbonatitic melts and subsequent fractional crystalisation (Unger *et al.,* 2018). It can therefore be assumed that sample EPB01 is the most fractionated sample because it is characterised by the highest content of LREE (up to 789 ppm in total) while the less fractionated sample is probably EPB12 as it is characterised by the lowest content of total LREE (La –Gd) with a total of 308 ppm. These data are supported by the rock characteristics of the respective samples such that EPB01 sample is characterised by intergranular textures of low temperature minerals such as alkali feldspar and abundant apatite compared to sample EPB12 which is composed of more calcite and less feldspar and apatite, but those variances are noted to be insignificant.

According to Wyllie (1986), REE with the exception of Ce and Eu have a 3^+ valence in most cases. However, in some geological environments, Ce and Eu can have valences of 4^+ and 2^+, respectively, which may lead to anomalous behaviour of these elements relative to other REEs. Rollinson (1993) states that europium anomalies are mostly controlled by feldspar in contrast to the trivalent state REE which are incompatible. Therefore, the observed negative Eu anomalies in the Epembe carbonatite samples indicates the removal of feldspar (where it is incorporated in a divalent Eu into Ca-rich minerals, like calcic plagioclase from a melt by the partial melting of a rock (carbonatite) in which feldspar is retained. A europium anomaly is a characteristic of REE patterns of late magmatic carbonatite and it indicates that the source melt contains plagioclase, whereby Eu^{2+} ion had migrated into the plagioclase crystal to replace $Ca^{2+.}$ As Eu^{2+} has the same charge as Ca^{2+} and a similar radius (121 vs. 126 pm), it can readily substitute for $Ca^{2+.}$ The fact that plagioclase remained in the residue can also be explained by the depth at which partial melting has occurred. Shallow partial melts will retain plagioclase in the residue because that will be favourable conditions for plagioclase stability and deeper melts will keep plagioclase (Wyllie, 1995) (Fig.5.3).

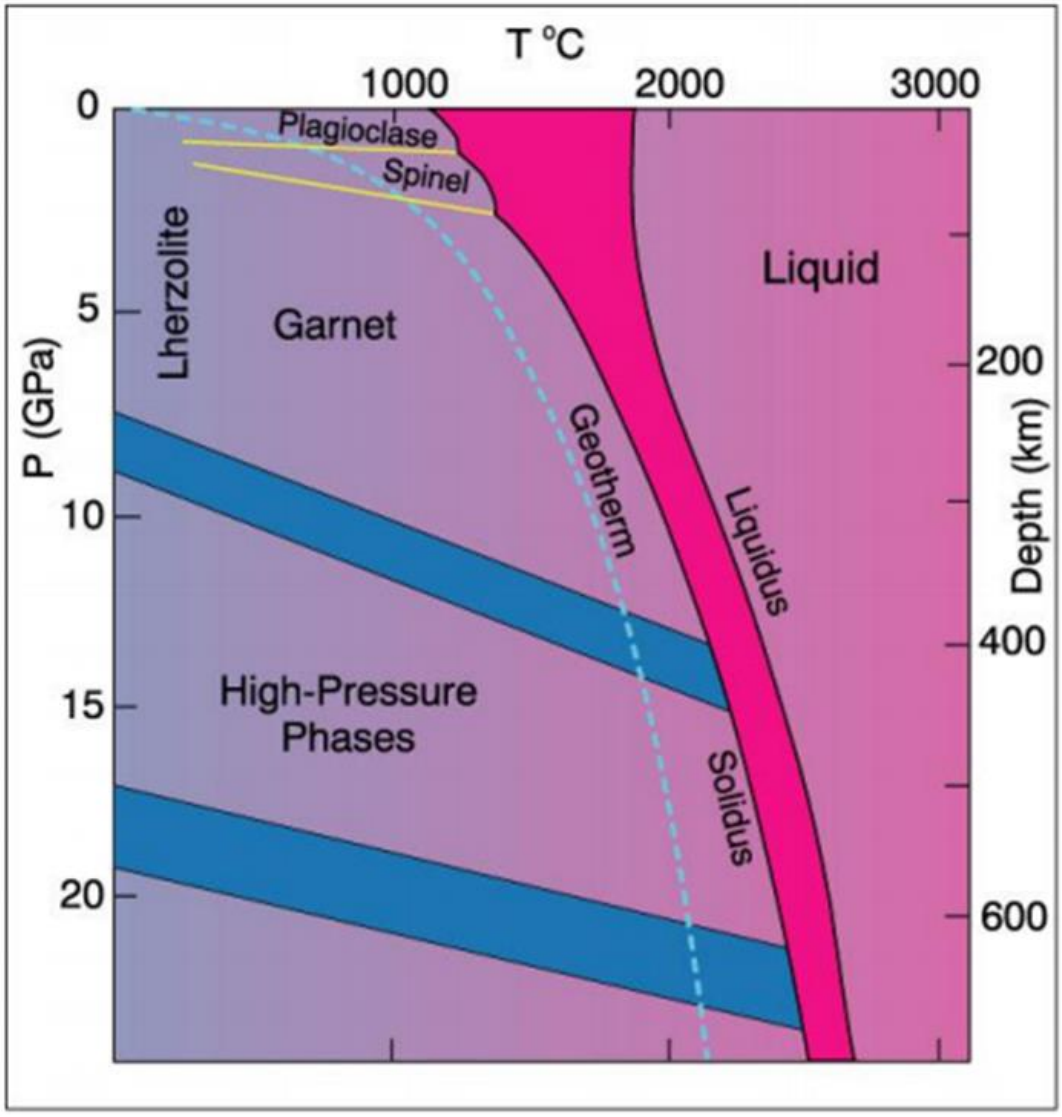


Figure 5-3 *Phase diagram of aluminous lherzolites with melting interval (gray area), sub-solidus reactions and geothermal gradient. The diagram demonstrates the pressure and temperature effect on mineral formation where by it can be deduced that plagioclase is favoured a shallower (<30 km) depth as opposed to garnet (80 – 400 km) (Figure adapted from Wyllie, 1981).*

The high values of (La/Yb) N ration (13 - 29) clearly demonstrates that the Epembe carbonatite is rich in LREE- which is a general aspect of global carbonatites and is often related to Sr and Ba enrichment (e.g. Tucker *et al.* 2012).

The chondrite-normalised REE patterns of the Epembe carbonatite are quite flat compared to average calcio-carbonatite (Fig.5.3). The Epembe carbonatites are enriched in LREE relative to HREE, a feature which is common for calcio-carbonatites. However, the total REE average of the Epembe carbonatites is slightly lower than that of global average calcio-carbonatite but comparable to that of global average calcio-carbonatite (Fig. 5.4) which can be related to the lack of REE-minerals in the Epembe carbonatites.

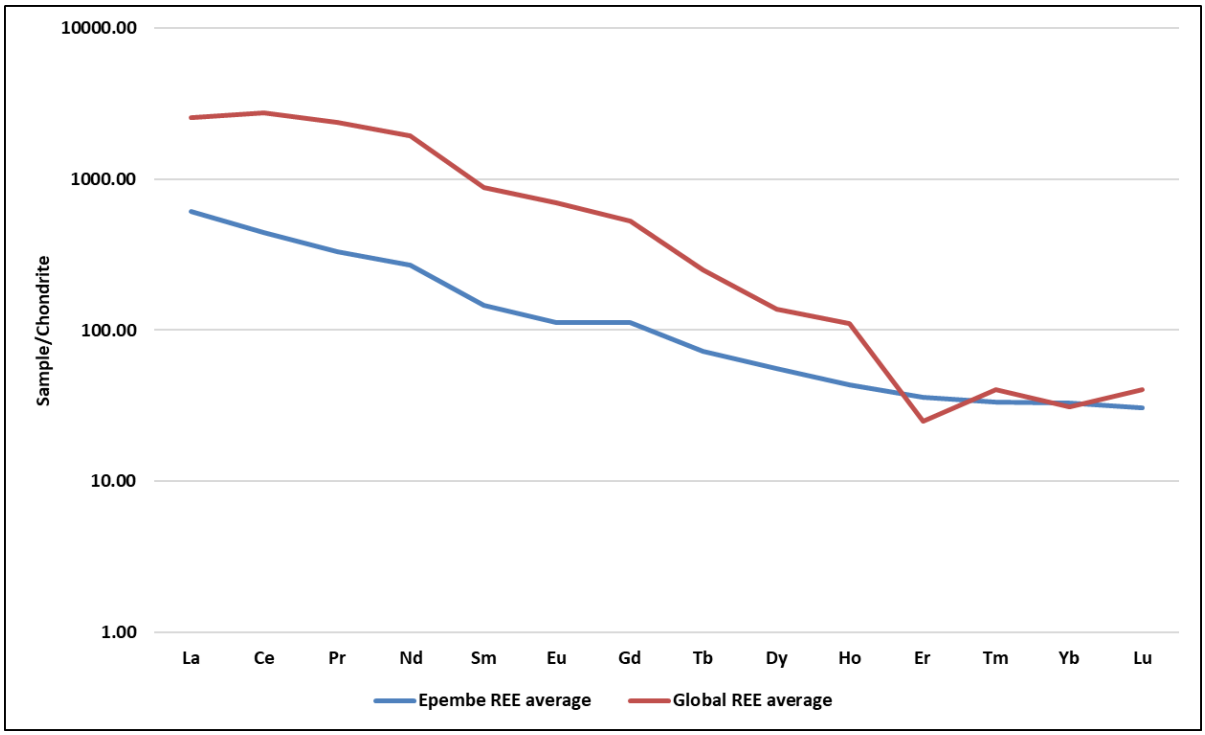


Figure 5-4 *Chondrite normalised rare earth elements (REEs) composition in Epembe carbonatite. The comparative data for global average calcio-carbonatite composition is shown (after Woolley and Kempe, 1989). Chondrite normalising data from Sun and McDonough (1995).*

5.4 REE distribution in Epembe carbonatite

It is known that of all igneous rocks carbonatite has the highest content of REE, but their affiliation with specific minerals is less well understood (Kjarsgaard, 1998). Earlier studies of REE distribution in carbonatite minerals and whole rock (e.g. Kapustin, 1966; Viladkar and Pawaskar, 1989) have established that REEs can be strongly enriched in both whole rock and in most primary minerals such as calcite, dolomite, pyrochlore, apatite and perovskite as well as in Ca-bearing phases i.e. carbonates, apatite, Nb-oxides and Ca-silicates. It is well established by Al Ani et al. (2011) that the REE reside mostly in the Ca-bearing phases such as apatite (Ca_5 $(PO_4)_3(F, OH)$, pyrochlore $(Na, Ca)_2Nb_2O_6$ (OH, F)] and carbonates (Calcite [$CaCO_3$], ankerite $Ca(Fe,Mg,Mn)(CO_3)_2$ where Ca^{2+}can be replaced by REE and/or with Sr^{2+} . Even though the Epembe carbonatite is enriched in REE, there were not many REE minerals found. The only REE-bearing mineral at the Epembe carbonatite is monazite (Ce, La, Y, Th) PO_4), but that is sparsely distributed. It can therefore be assumed that, the occurrence and distribution of REE at Epembe can be explained by the chemical substitution between REE and other cations of other minerals with similar ionic radii. With the exception of Ce (IV) and Eu (II), it is established that aqueous REE exist in a trivalent state and hence tend to be fractionated by other metallic elements (M^{3+}) and therefore can be easily complexed with inorganic and/or organic ligands such as carbonates, phosphates and organic matters (Edahbi *et al. 2018*).

In carbonatites, REE are mainly concentrated by fractional crystalisation (Chakhmouradian *et al. 2017*; Orris & Grauch., 2002 and Williams-Jones et al. 2012). In the Epembe carbonatite, it can be suggested that the main REE-bearing phases are phosphates and silicates which are common accessory phases throughout the Epembe carbonatite in which Ca^{2+} can be replaced by REEs. The whole rock geochemical results obtained from this study are in general agreement with earlier published analyses (by Mineral Liberation Analyzer [MLA]) on selected samples of apatite and pyrochlore from the Epembe carbonatite-syenite complex (Simon *et al. 2007*; Mariano and Mariano., 2013; Unger *et al. 2018*) who established that the REEs are mainly associated with apatite and other REE phosphates while Nb and Ta are hosted in pyrochlore. Specifically, Nb +Ta appear to be weakly correlating with REE+Y (Fig. 4.6). This could indicate that either the REE are hosted by pyrochlore or both the REE as well as Nb & Ta are enriched during the same process.

5.5 Conclusions

The geochemical study was conducted: (1) to identify and characterise the types of carbonatite at the Epembe Carbonatite-Syenite Complex based on geology, geochemistry and petrography; (2) to examine the geochemical variation of the Epembe carbonatite with an emphasis on the rare earth element concentrations; and (3) to investigate the relationship between the distribution of REEs and radiometric elements. The field relationships as well as the published geochronological data indicates that the Epembe carbonatite are younger than their host of fenites and nepheline syenites. The main mineralogical conclusions drawn from this study indicate that the Epembe carbonatite is calcio-carbonatites, with major minerals being calcite, with accessory minerals of apatite, pyrochlore, aegirine, feldspars and iron oxide minerals. Even though the total concentration of REEs are high (Total REE+Y=912ppm) there were no REE-bearing minerals observed at Epembe carbonatite except for monazite in trace amount. Geochemical results show that REE are either included in several accessory minerals such as apatite and pyrochlore and possibly in gangue minerals (i.e. silicates (include calcite and zircons) and carbonates). Epembe carbonatite is more enriched in LREE compared to HREE, a phenomenon attributed to fractional crystalisation enrichment process.

REFERENCES

Al Ani, T., Heikura, P. and Sarapää, O., 2011. REE-mineralogy and geochemistry of selected drillcores from Southern side of of Sokli Carbonatite Complex, NE-Finland. *Report.* Geological Survey of Finland.

Bailey, D. K., 1980. Volatile flux, geotherm and generation of the kimberlite-carbonatite-alkaline magma Spectrum. *Mineralogical Magazine*, 43,695 – 699

Barakos, G., Mischo, H. and Gutzmer, J., 2016. Rare earth underground mining approaches with Respect to radioactivity control and monitoring strategies, in I B De Lima & W Leal (eds), Rare Earths Industry: Technological, Economic, and Environmental Implications, Elsevier, Amsterdam, pp. 121-138.

Bull, J., 2013. Detailed Geological Mapping and Petrological Study of the Nb-Ta ± U Epembe Carbonatite-Syenite Complex, North-West Namibia. Msc Thesis, University of Exeter, unpublished

Bass, M. J., 1977. *Carbonatite - Nephelinite volcanisms.London*. Wiley and sons.

Bass, M. J., 1981. Carbonatite magmas. *Mineralogical Magazine*, 44, 133-140.

Beetz, P.F.W., 1933. Geology of South West Angola, between Kunene and Lunda Axis. *Transactions of The Geological Society of South Africa, 36, 137 – 176.*

Becker, T., Schreiber, U., Kampunzu, A. B. & Armstrong, R. 2006. Mesoproterozoic rocks of Namibia and their plate tectonic setting. *Journal of African Earth Sciences*, 46: 112-140.

Bizimis M, Salters, V.J.M, and Dawson, J.B., 2003. The brevity of carbonatite sources in the mantle: evidence from Hf isotopes. Contribution: *Mineralogy and Petrology* 145:281-300.

Brandt, S., Klemd, R and Okrusch, M., 2000. Evidence for Ultra-high –temperature metamorphism in the Pre-Pan –African Epupa Complex, NW Namibia. *Geoluanda 2000. Abstract* Vol. 33 -34.

Brandt, S., 2003. Metamorphic evolution of Ultra-high –temperature granulite facies and upper amphibolite facies rocks of the Epupa Complex, NW Namibia, PhD Thesis, University of Wurzburg.

Brandt, S., Will, T.M., and Klemd, R., 2007.Ultrahigh-temperature metamorphism and anticlockwise PT paths of sapphire bearing orthpyroxene-sillimanite gneisses from the Proterozoic Epupa Complex, NW Namibia. *Precambrian Research*, 153,143-178.

Bybee, G.M., Hayes, H. Owen-Smith, T.M., Lehmann, J., Ashwal L.D., Brower A. M., Hill, C.M., Corfu, F., and Manga, M.,(2019). Proterozoic massif-type anorthosites as the archetypes of long-lived (≥ 100 Myr) Magmatic systems—new evidence from the Kunene Anorthosite Complex (Angola), Precambrian Research doi: *https://doi.org/10.1016/j.precamres.2019.105393*

Chakhmouradian, A.R., 2006. High-field-strength elements in carbonatitic rocks: Geochemistry, crystal chemistry and significance for constraining the sources of carbonatites. Chemical Geology 235: 138–160.

Chakhmouradian, A. R. and Williams, C. T., 2004. Mineralogy of High-field strength elements (Ti, Nb, Zr, Ta, Hf) in phoscoritic and carbonatitic rocks of the Kola Peninsula, Russia. *Mineralogical society Series*,10.

Chakhmouradian, A.R.; Reguir, E.P.; Zaitsev, A.N.; Couëslan, C.; Xu, C.; Kynický, J.; Mumin, A.H. and Yang, P., 2017. Apatite in carbonatitic rocks: Compositional variation, zoning, element partitioning and petrogenetic significance. *Lithos*, 274, 188–213.

Date, A. R. and Jarvis, K. E., 1989. The application of IC-PMS in the earth sciences. Blackie, Glasgow.

Carvalho, H., Tassinari C., Alves P. H., Guimaraes, F and Simoes, M.C., 2000. Geochronological review of the Precambrian in western. Angola: links with Brazil. *Journal of African Earth Science*. 31,383-402.

Do Cabo V.N., 2014. Geological, mineralogical and geochemical characterization of the Heavy Rare Earth rich carbonatites at Lofdal, Namibia. PhD Thesis, University of Exeter, 548p.

Drüppel, K., 1999. Petrologie und Geochemie von Anorthositen des Kunene-Intrusiv-20 Komplexes, NW Namibia. Diploma Thesis, University of Würzburg.

Drüppel, K., Littmann, S., Romer, R.and Okrusch, M., 2001. Fenitizing Processes Induced by Ferrocarbonatite Magmatism at Swartbooisdrif, NW Namibia. *Journal of Petrology*, Vol. 46, 377–406.

Drüppel, K., Littmann, S., Rome, R.L., and Okrusch, M. 2007. Petrology and isotope geochemistry of the Mesoproterozoic anorthosite and related rocks of the Kunene Intrusive Complex, NW Namibia. *Precambrian Research*, 156: 1-36.

Edahbi, M., Plante, B., Benzaazoua , M., Kormos, l. and Pelletier, M., 2018. Rare Earth Elements (La, Ce, Pr, Nd, and Sm) from a Carbonatite Deposit: Mineralogical Characterization and Geochemical Behavior. *Minerals*, 8, 55.

European Commission, 2014. Report on critical raw materials for the EU. *http://ec.europa.eu/enterprise/policies/raw-materials/fi les/docs/crm-report-on-critical-raw-materials_en.pdf*> Accessed August 6, 2018.

Falshaw, S., 2012. The Geology and Rare Metal Metallogenesis of the Epembe Carbonatite dyke, North West Namibia. Msc. Thesis, University of Exeter, Camborne School of Mines, Penryn, UK.

Ferguson, J., McIver, J.R. and Danchlin, R.V., 1975. Fenitisation associated with the alkaline carbonatite complex of Epembe, South West Africa. *Transactions of the Geological Society of South Africa*, 78, 111-121.

Gaillard, F., Pichavant, M. and Scaillet B., 2003. Experimental determination of activities of FeO and Fe2O3 components in hydrous silicic melts under oxidizing conditions. *Geochimica et Cosmochim-ica Acta,* 67, pp.22, 4389-4409.

Gittins, J., 1989. The origin and evolution of carbonatite magmas. In Bell, K., *Carbonatites: genesis and evolution.* London. Unwin Hyman, 580-600.

Gittins, J. and Harmer R. E., 1997. What is ferrocarbonatite? A revised classification. *Journal of African Earth Sciences,* 25, 159-168.

Gittins, J. and Harmer, R. E., 2003. Myth and reality in the carbonatite-silicate rock 'association'. *Periodico di Mineralogical*, 72, 17-26.

Goodenough, K.M., Wall, F. and Merriman, D., 2017.The Rare Earth Elements: Demand, Global Resources, and Challenges for Resourcing Future Generations. *Natural Resources Research*, 27, 201-216.

Hatch, G.P., 2012. Dynamics in the global market for rare earths. *Elements 8*: 341–346.

Harker, A., (1909). The Natural History of Igneous Rocks. Macmillan. New York.

Harmer, R. E. and Gittins, J., 1998. The case for primary, mantle derived carbonatite magma. *Journal of Petrology*, 39, 1895 – 1903.

Hensen, G. N.,1980. Rare earth elements in petrogenetic studies of igneous systems. Review of *Earth and Planetary Sciences*, 8, 371-406.

Hurst, C., 2010. China's rare earth element industry: what can the west learn*?* Institute for the analysis of global security *(IAGS), 42 pp.*

Jones, A. P., Genge, M. and Carmody, L., 2013. Carbonate Melts and Carbonatites. *Reviews in Mineralogy & Geochemistry*, 75: 289-322.

Kanazawa, Y. and Kamitani, M., 2006. Rare earth minerals and resources in the world. *Journal of Alloys and Compounds*, 408, 1339-1343.

Kapustin, Y. l., 1966. Geochemistry of Rare Earth Elements in carbonatites. *Geochemistry internationals*, 3, 1054 – 1064.

Kjarsgaard, B. A. and Hamilton, D.L., 1989. The genesis of carbonatites by immiscibility. In Bell, K., . *Carbonatite: genesis and evolution* (pp388 -404). London: Unwin Hyman.

Kjarsgaard B, A., 1998. Rare earth element in Sovitic carbonatites and their mineral phases, *Journal of petrology*, 39, number 11 & 12, pp.2105-2121.

Köstlin, E. C., 1967. The geology of part of the Kunene basic complex, Kaokoveld, South West Africa. M.Sc. Thesis, University of Cape Town, Cape Town, 92 pp

Köstlin, E.C., 1974. The Kunene basic Complex, northern South West Africa. In: Kröner, A. Contribution to the Precambrian geology of southern Africa. University of Cape Town Bulletin, 15 pp. 123 – 135.

Kunene Resource Holdings (Pty), 2016. Technical report, Unpublished Report, 92 pp.

Knudsen, C., 1989. Pyrochlore group minerals from the Qaqarssuk carbonatite complex. *Berlin-Heidelberg: Springer-Verlag,* pp .80 – 99.

Kuhn, J. and Gevers, H., 2015. Rare Earth Elements; from Mineral to Magnet. *GSDR 2015 Brief* ,Wageningen University and Research Centre, 10pp.

Kynicky, J., Smith, M. P. and Xu, C., 2012. Diversity of rare earth deposits: The key example of China. *Elements*, 8(5) ,361–367.

Lee, W. J. and Wyllie P. J., 1998. Processes of crystal carbonatite formation by liquid immiscibility and differentiation, elucidated by modal system. *Journal of Petrology*, 39, 2005-2013.

Le Bas, M.J., 1987. Nephelinites and carbonatites. In: Fitton, J. G & Upton, B. G. J. (eds) Alkaline Igneous rocks. Geological Society, London*, Special Publications*, 30, 53-83.

Le Bas M., J, Xueming, Y., Taylor R. N., Spiro, B., Milton, J. A. and Peishan, Z. 2007. New evidence from a calcite-dolomite carbonatite dyke for themagmatic origin of the massive Bayan Obo ore-bearing dolomite marble, Inner Mongolia, China. *Mineralogy and Petrology* 90:223–248.

Long, K.R.; Van Gosen, B.S.; Foley, N.K. and Cordier, D., 2017. The Principal Rare Earth Elements Deposits of the United States. Available online: https://pubs.usgs.gov/sir/2010/5220/ (accessed on 31 July 2018).

Lottermoser, B. G., 1992. Rare Earth Elements and hydrothermal of ore formation processes: *Ore Geology Revies*, 7, P.25-41.

Maier, W.D., Teigler, B and Miller, R. McG., 2002. The Kunene Anorthosite Complex and its satellite

intrusions, in: The Geology of Namibia: Archean to Mesoproterozoic. Ministry of Mines and Energy, *Geological Survey*, 1, 9-1.

Maier, W.D., Rasmussen, B., Fletcher, I.R., Li, C. Y., Barnes, S-J. and Huhma. H., 2013. The Kunene Anorthosite Complex, Namibia, and Its Satellite Intrusions: Geochemistry, Geochronology, and Economic Potential. *Journal of Economic geology*, 108 (5), 953 - 986.

Mariano, A. N. and Mariano A., 2013. A Preliminary mineralogical study of selected rocks from the Ta rich carbonatite occurrences, Epembe complex, Namibia. *Confidential Repor*t for: Kunene Resources Pty. Ltd.

Mayer, A., Hofmann, A.W., Sinigoi,S. and Morais, E., 2004. Mesoproterozoic Sm-Nd and U-Pb ages for the

Kunene Anorthosite Complex of SW Angola. *Precambrian Research*, 133, 187 – 206.

Martin, H., 1965. The Precambrian geology of South West Africa and Namaqualand. Bulletin of the *Precambrian Research Unit*, University of Cape Town, Bulletin Number 161, 159 pp.

McCourt, S., Armstrong, R.A., Jelsma, H. and Mapeo, R.B.M. 2013. New U–Pb SHRIMP ages from the

McDonough, W.F. and Sun, S.S., 1995. The Composition of the Earth; *Chemical Geology*, v. 120, 223-253.

Lubango region, SW Angola: insights into the Palaeoproterozoic evolution of the Angolan Shield, southern Congo Craton, Africa. *Journal of the Geological Society of Lodondon*, 170, 353 – 363.

Mehmood, M., 2018. Rare Earth Elements-A Review. *Journal of Ecology & Natural Resources*, 2(2).

Menge, G. F. W., 1986. Sodalite-carbonatite deposits of Swartbooisdrift, southwest Africa/Namibia. Anhaeusser C.R, Moske S. Minerals Deposit of Southern Africa. Johannesburg, Journal of The *Geological Society of South Africa*, 2261 – 2268.

Menge, G. F. W., 1996. The eastern portion of the Kunene complex, its satellite intrusions and the alkaline suite between Epembe and Swartbooisdrif. *Unpublished Report*, 128 pp.

Menge, G.F.W., 1998. The antiformal structure and general aspects of the Kunene Comlpex. *Zeitschrift der Deutschen Geologischen*, 149, 431 – 448.

Mitchell, R.H., 1995.Kimberlites, Orangeites and Related Rocks. *Plenum Press*, New York, N.Y, 410pp.

Mitchell, R.H., 2005. Carbonatite and carbonatites. *Canadian Mineralogist*, 43, 2049 – 2068.

Miller, R.M. and Burger, A.J., 1983.U-Pb Zircon Age of the Early Damaran Naauwpoort Formation. In: Miller, R.G. (Ed*.),* Evolution of the Damara Orogen of South West Africa-Namibia. Geological Society of South Africa *Special Publication* 11, pp. 267–272.

Miller, R. McG, 2008. The Geology of Namibia. Geological Survey of Namibia*,* Windhoek *1-3,* 1-1 – 28-11. 68

Morrison, W.M. and Tang, R., 2012. China's Rare Earth Industry and Export Regime. Economic and Trade Implications for the United States. Congressional Research Service. https://www.fas.org/sgp/crs/row/R42510.pdf Accessed August 4, 2018.

Nelson, D., Chivas A., Chappell B. and McCulloch, M., 1988. Geochemical and isotopic systematics in carbonatites and implications for the evolution of ocean-island sources. *Geochimica et Cosmochimica Acta,* 52:1- 17.

Nelson S.A.,2012. Magmatic differentiation. *Paper*. Tulane University. https://www.tulane.edu/~sanelson/eens212/magmadiff.htm

Orris, G.J. and Grauch, R.I., 2002. Rare Earth Element Mine, Deposits, and Occurrences; USGC (*Science for a Changing World*): Reston, *Open File Report*, U.S. Geological Survey, USA.

Pell, J. and Hey, T., 1989. Carbonatites in a continental margin environment - the Canadian Cordillera. In Carbonatites - Genesis and Evolution (K. Bell, Ed.), Unwin Hyman, London,200-220.

Peter, J. M., Theodore, J. A. and Hoover D. B., 1986. Summary of relevant geologic, geoenvironmental, and geophysical information. In Singer, Carbonatite Deposits, U.S Geological Survey *Bulletin*, 47-49

Pirajno, F., 2004. Hotspots and mantle plumes: Global intraplate tectonics, magmatism and ore deposits. *Mineralogy and Petrology,* 82, 183-216.

Rock, N.M.S., 1987. The need for standardization of normalized multi-element diagrams in Geochemistry: a comment. *Geochemical Journal,* v 21, 75 - 84,

Rollinson, H.R., 1993. Using Geochemical Data: Evaluation, Presentation, and Interpretation. Longman Scientific & Technical Ltd., Harlow, 352 pp.

Seth, B., Armstrong, R.A., Brandt, S., Villa, I.M. and Kramers, J.D., 2003. Mesoproterozoic U-Pb and Pb-Pb ages of granulites in NW Namibia: reconstructing a complex orogenic cycle. *Precambrian Research*, 126:147-168.

Schneider, G., 2004. The roadside of geology of Namibia. Gebrüder Borntraeger, Berli-Stuttgar.t

Shelley, D., 1993. Igneous and Metamorphic rocks under microscope, a classification, texture, microstructure and minerals preferred orientations Chapman and Hall.

Simon, S.J., 2017. Epembe Niobium-Tantalum Deposit, NW Namibia: U-Pb Age and Resource Estimation. Msc.Thesis, *China University of Mining and Technology*, Xuzhou, China, 96pp.

Simon, S.J., Wei, C.T., Ellmies, R., Yang, H., and Soh Tamehe, L. 2017. New SIMS U-Pb age on zircon from. The Epembe carbonatite dyke, NW Namibia: Implications for Mesoproterozoic evolution of carbonatites at the southern margin of the Congo Craton. *Journal of African Earth Sciences*, 135: 108-114.

Smith, M. P., Moore, K., Kavecsanszki, D., Finch, A. A., Kynicky, J. and Wall, F., 2016 From mantle to critical zone: A review of large and giant sized deposits of the rare earth elements. *Geoscience Frontiers*, 7(3), 315–334.

Streckeisen, A.L., 1979. Classification and nomenclature of volcanic rocks, lamprophyres, carbonatites, and melilitic rocks: Recommendations and suggestions of the IUGS subcommission on the systematics of igneous rocks. *Geology*, 7, 331–335.

Thompson, W., Lombard, A., Santiago, E. and Singh, A. 2011. Mineralogical studies in assisting beneficiation of rare earth element minerals from carbonatite deposit. 10th International Congress for Applied Mineralogy (ICAM). Trondheim, p. 665 – 672.

Trommpette, R., 1994. Geology of Western Gondwana (200-500Ma). Pan-African-Brasiliano aggregation of South America and Africa. *Balkema,* Rotterdam, 350 pp.

Turker, R.D., Belkin, H.E., Schulz, K.J., Peters, S.G., Horton, F., Buttleman, K. and Scott, E.R., 2012. A major light rare earth element (Lree) resource in the Khanneshin carbonatite Complex, southern Afghanistan*. Journal of Economic Geology*, 207, 197 – 205.

Veksler, I. V., Nielsen, T.F. and Sokolov S.V., 1989(a). Mineralogy of crystalized melt inclusion from Gardiner and Kavdor ultra-mafic alkaline complexes: implications on carbonatite genesis. *Journal of Petrology* 39, 2015 – 2031.

Unger, G., Zimmermann, R. and Gloaguen, R., 2018. 3D Modeling of the Epembe (Namibia) Nb-Ta-P-(LREE) Carbonatite Deposit: New Insights into Geometry Related to Rare Metal Enrichment. *Minerals*, 8 (12), 600.

U.S. Geological Survey 2011. Minerals Year Book—Rare Earths. Available online: https://minerals.usgs.gov/minerals/pubs/commodity/rare_earths/mcs-2011-raree.pdf (accessed on 30 July 2018).

U.S. Geological Survey 2014. Fact Sheet 2014 –3078; available at (ISSN 2327– 6932 online) Home page: https://pubs.usgs.gov/fs/2014/3078/pdf/fs2014-3078.pdf.

Verplanck P.L and Gosen B.S., 2011. Carbonatite and Alkaline Intrusion-Related Rare Earth Element Deposits –A deposit Model. U.S. Geological Survey. *Open File Geological Reports* 2011-1256, 5P.

Verplanck, P. L., Mariano, A. N. and Mariano, A., 2016. Rare earth element ore geology of carbonatites. In P. Verplanck &M. Hitzman (Eds.), Rare earth and critical elements in ore deposits Reviews in Economic Geology, 18, pp. 5–32. Littleton, *Colorado: Society of Economic Geologists*.

Viladkar, S. G. and Pawaskar, P. B., 1989. Rare earth element abundances in carbonatites and fenites of the Newania complex, Rajasthan, India. *Bulletin of the Geological Survey of Finland* 61, 113–122.

Wall, F., 2014. Rare earth elements. In: Gunn, G. (ed.), Critical Metals *Handbook*, John Wiley and Sons Ltd., Hoboken, pp. 312-339.

Walters, A. and Lusty P., 2010. Rare Earth Elements. British Geological Survey. 45 p. www.MineralsUK.com.

Walters, A. S., Goodenough, K.M., Hughes, H.S.R., Roberts, N.M.W., Gunn, A.G., Rushton, J and Lacinska , A., 2013. Enrichment of Rare Earth Elements during magmatic and post-magmatic processes: a case study from the Loch Loyal Syenite Complex, northern Scotland Contribution *Mineralogy and Petrology* ,166,1177–1202.

White, W.M, 2005. Geochemistry: an online textbook, Cornell University, available at:http:/www.geo.cornell.edu/geology/classes/geo455/chapters.HTML.

Williams-Jones, A.E.; Migdisov, A.A. and Samson, I.M., 2012. Hydrothermal mobilisation of the rare earth elements., a Tale of "Ceria" and "Yttria". *Elements*, 8, 355–360.

Winter, J. D., 2010. Principles of igneous and metamorphic petrology. *Pearson education, Inc.*

Woolley, A. R., 1982. A discussion of carbonatite evolution and nomenclature and the generation of sodic and potassic fenites. *Mineralogical Magazine*,46, 7-13.

Woolley, A. R. and Kempe, D. R. C., 1989. Carbonatites: Carbonatites: nomenclature, average chemical compositions, and element distribution. In: Bell, K. (Ed.) Carbonatites: Genesis and Evolution. Unwin Hyman Ltd. London p.1-14.

Woolley, A.R., 1991. The spatial and temporal distribution of carbonatites. In Carbonatites: Genesis and Evolution (K. Bell, ed.), Unwin Hyman, London, pp. 15-35.

Woolley, A.R., 1991. Extrusive carbonatites from the Uyaynah Area, United Arab Emirates. *Journal of*

petrology, 32, 1143- 1167.

Woolley, A.R., Bergman, S.C., Edgar, A.D., Le bas, M.J., Mitchell, R.H., Rock, N.M.S. and Scott, S, B.H., 1996. Classification of lamprophyres, lamproites, kimberlites, and the kalsilitic, melilitic, and leucitic rocks. *Canadian Mineralogist*. 34, 175-186.

Woolley, A.R. and Church, A.A., 2005. Extrusive carbonatites: A brief review. *Litho*s, 85, 1 – 14.

Woolley, A.R. and Kjarsgaad., B. A., 2008. Paragenetic types of carbonatites as indicated by the diversity and relative abundances of associated silicate rocks: evidence from global database. *Canadian Mineralogist,* 46, 741 -752.

Wyllie, P.J., 1995. Experimental petrology of upper-mantle materials, process and products*. Journal of Geodymic,* 20(4):429- 468.

Wyllie, P. J.,and Biggar, G. M., 1966. Fractional crystallization in the "carbonatite systems" CaO-MgO-CO_2-H_2O and CaO-CaF_2-P_2O_5-CO_2-H_2O: International Mineralogical Association, IMA Volume, *Mineralogical Society of India*, p. 92-105.

Xie, F., Zhang, T. A., Dreisinger, D. and Doyle, F. 2014. A critical review on solvent extraction of rare earths from aqueous solutions. *Minerals Engineering*, 56, 10-28.

Yaxley ,G.M. and, Brey ,G.P., 2004. Phase relations of carbonate-bearing eclogite assemblages from 2.5 to 5.5 GPa: implications for petrogenesis of carbonatites. Contribution *Mineralogy and Petrology* 146(5), 606-619.

Zimmermann, R., Brandmeier, M., Andreani, L. and Gloaguen, R., 2015. Hyperspectral remote sensing exploration of carbonatite– an example from Epembe, Kunene region, Namibia: *Remote Sensing,* Helmholtz Institute Freiberg for Resource Technology, 8, 21pp.

Zhou, B., I., D, Li Z. A, and Chen, C. 2017. Global Potential of Rare Earth Resources and Rare Earth Demand from Clean Technologies, *Minerals*, 7,203.

APPENDICES

Appendix A: Sample preparation:

Crushing and milling was done at the GSN laboratories. Prior to crushing the Geo-crusher machine and specifically its crushing surfaces were thoroughly cleaned with the shop-vac and scrubbing brush to avoid any possible contamination of samples. Also a portion of pure quartz was run through the machines as part of the cleaning process. The same process was carefully followed every single time of sample changes. Samples were crushed to about 0.5- 15mm.



Figure 7-1 *Crushing processes. A) A researcher is crushing samples using a Geo-crusher in the GSN laboratory; B) Sample sizes after crushing that were sending to the milling machine.*

Once the samples are crushed, they were then milled in the pulveriser machine (RS 200) (Fig. 1Cb) using steals bowls. Prior to milling, samples were homogenised through a splitter; they were than milled to finer powder of about minus (-) 64 microns which is ideal for both X-RF and ICP-MS. Batches of (200g each) sixteen (16) pulp samples were send for analysis at Wits University. Analysis was done free of charge at the university's lab(Earth Lab) were control samples were prohibited due to cost involved, therefore all 16 samples submitted are primary samples and no control samples for Quality Assurance and Quality control (QA/QC) were inserted. However, the labs do have their own control samples.



Figure 7-2 *Milling process. A) Samples were milled using a pulveriser machine (RS 200) at GSN laboratory; B) pulp samples (-64 microns) that were send for ICP-MS and X-RF study.*

Samples were then examined for trace-element and REEs using Inductively Coupled Plasma Mass Spectrometry (ICP-MS) techniques, which was done through University of Witwatersrand. The ICP-MS is defined by Date and Jarvis, 1989 as an extension of the induced coupled plasma emission spectrometry. The system is designed with a very low detection limit and is thus used for trace elements and isotopic analysis due to its high accuracy and precision (Jenner et al, 1990). This system works by removing ions from the plasma through a pinhole-sized hole Ions are then forced into a vacuum system and focused by an ion lens into the mass spectrometer.

Appendix B: Geological map

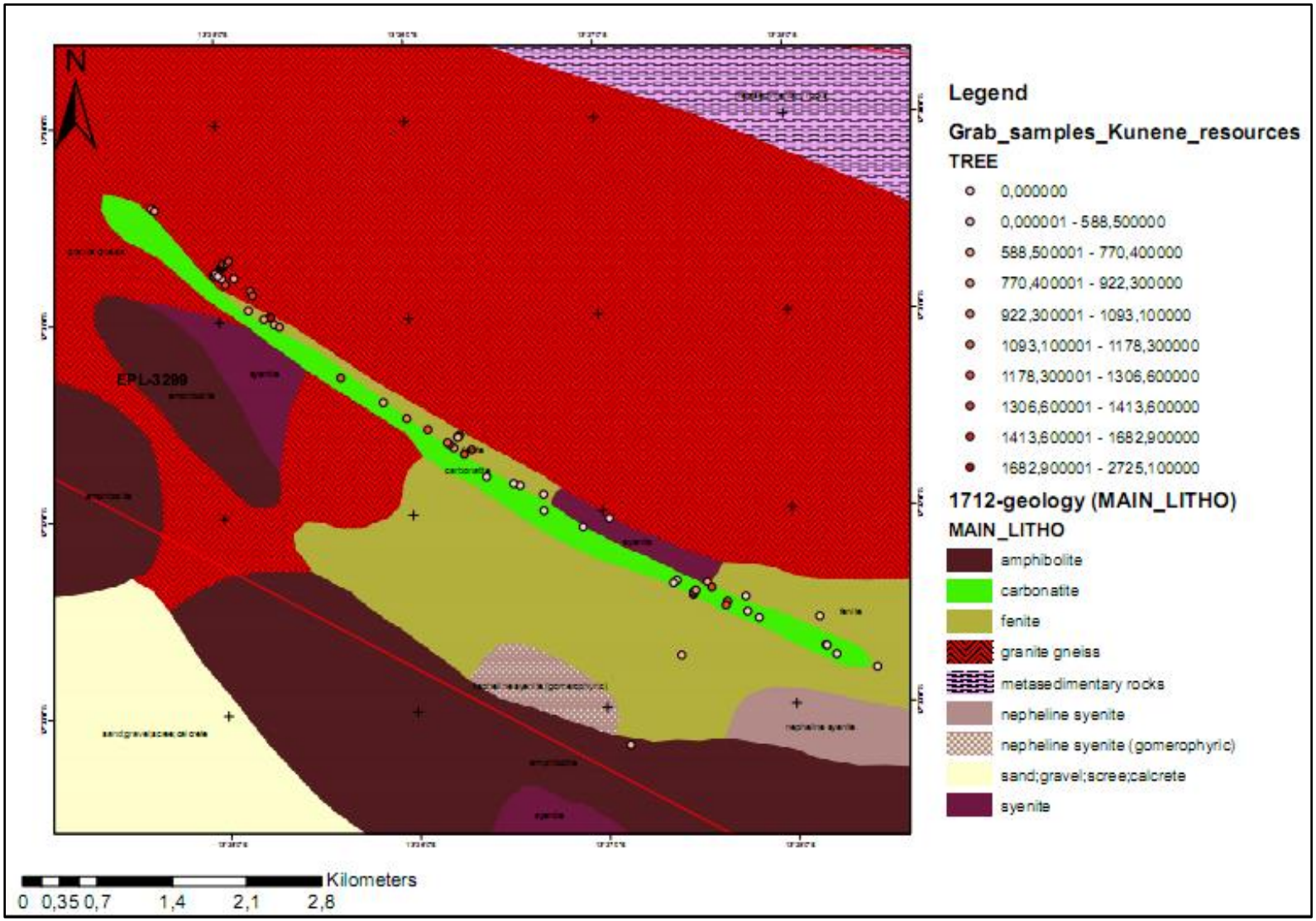


Figure 7-3 *Geological map of 1:250k maps of the study are*

Appendix C: Ortho-ASTER 3ALevel1

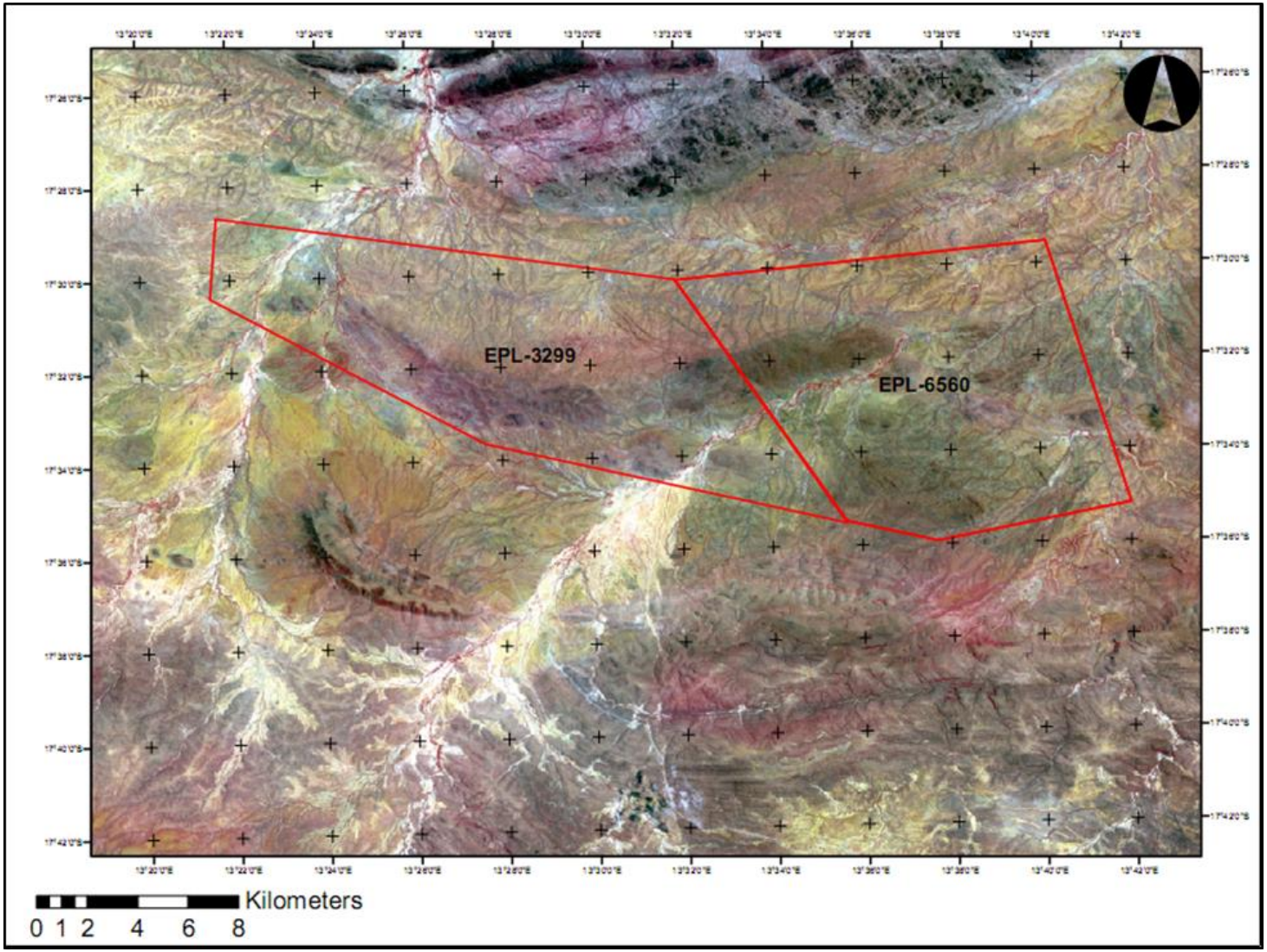


Figure 7-4 *Processed Ortho-Aster 3ALevel 1 RGB_321 of the study area*

Appendix D: List of collected field samples from Epembe carbonatite

Table 7-1 List of collected field samples from Epembe carbonatite

Sample ID	GPS location		Elevation (m)	Rock Unit	Date Acquired
	Southing	Easting			
EPB 1	-17.513038	13.417057	1104	carbonatite	14/11/2017
EPB 2	-17.512212	13.417140	1144	carbonatite	14/11/2017
EPB 3	-17.512993	13.418096	1146	carbonatite	14/11/2017
EPB 4	-17.514365	13.419709	1142	carbonatite	14/11/2017
EPB 5	-17.515262	13.421041	1122	gneissic granite/Fenite	14/11/2017
EPB 6	-17.524261	13.431686	1147	carbonatite	14/11/2017
EPB 7	-17.523495	13.430534	1137	carbonatite	14/11/2017
EPB 8	-17.531856	13.442560	1189	carbonatite	14/11/2017
EPB 9	-17.538297	13.453993	1196	carbonatite	14/11/2017
EPB 10	-17.542553	13.463739	1193	Syenite	14/11/2017
EPB 11	-17.541974	13.463835	1201	carbonatite	14/11/2017
EPB 12	-17.544146	13.467014	1168	carbonatite	14/11/2017
EPB 13	-17.509573	13.411296	1093	carbonatite	15/11/2017
EPB 14	-17.511419	13.412942	1091	carbonatite	15/11/2017
EPB 15	-17.518588	13.423310	1112	carbonatite	15/11/2017
EPB 16	-17.520683	13.418768	1122	nepheline Syenite	15/11/2017

Appendix E: Description of field samples

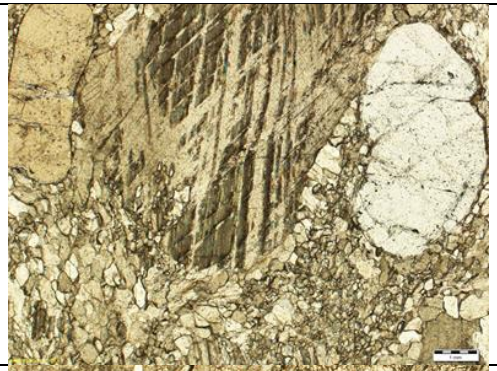
Table 7-2 Description of field samples

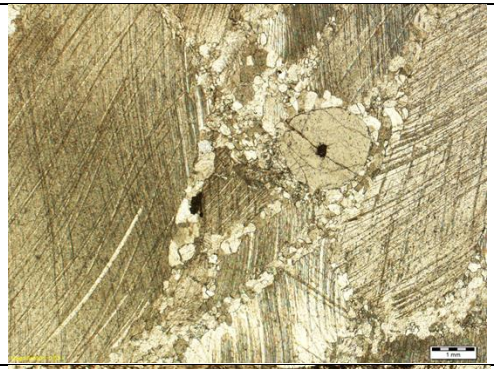
SAMPLE ID	Rock Unit	OUTCROP/SAMPLE DESCRIPTION
EPB1	carbonatite	
EPB2	carbonatite	Pinkish- Grey in colour, dominated by dark green minerals (name?). Also have some shiny calcite (probably from precipitation of hydrothermal fluids)
EPB3	carbonatite	Carbonatite, grey, hard and medium grained, dominated by light brown (goldish) sheeted mineral (looks like mica).
EPB4	carbonatite	Grey, medium grained with very course grained hard (resistant) dark, euhedral mineral. Also some calcite is visible
EPB5	gneissic granite/Fenite	Gneissic granite/fenite (altered granite gneiss). The outcrop is characterized by carbonatite vein cutting through granitic gneiss. Very highly fractured and altered. The outcrop shows some shearing evidence as shown by lineation. (In situ lineation)

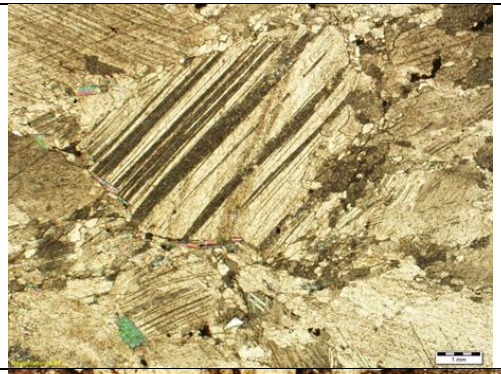
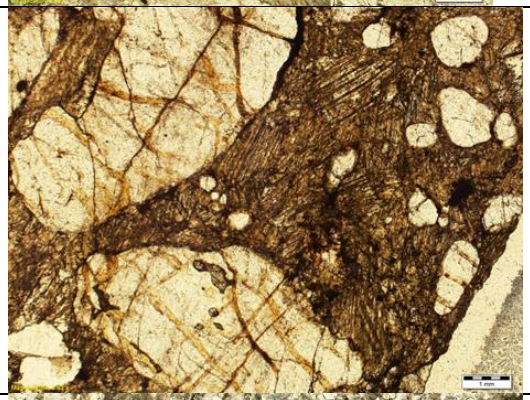
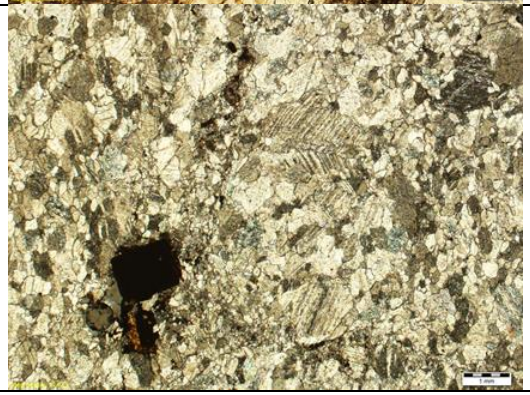
		which is sign of movement. Lineation measurement (dip:33degree and dip direction: 233 degree
EPB6	carbonatite	carbonatite ,very much foliated(which is a metamorphic structure – stress imprint) dominated by a mineral with characteristic of weathering resistant
EPB7	carbonatite	Pinkish-grey in colour(some evidence of calcite replacement by iron), appears massive and not foliated implying there is a change in some mineralogy ratio
EPB8	carbonatite	Carbonatite, massive and hard (very dolomitic), fine to medium grained, more silica with traces of greenish minerals (probably epidote).also some goldish shiny mica
EPB9	carbonatite	Carbonatite with a weathering pattern of calcrete (roughness)
EPB10	syenite	Syenite , hard light grey, medium-course grained
EPB11	carbonatite	Carbonatite with a calcitc texture
EPB12	carbonatite	
EPB13	carbonatite	Pure grey un mineralized carbonatite with traces of black colured mineral (amphibole).at some place of this point/site, stains of malachite is recorded. From flat area
EPB14	carbonatite	Carbonatite from a flat area
EPB15	carbonatite	
EPB16	nepheline syenite	Nepheline Syenite, dark grey (more mafic), jointed. From a flat area

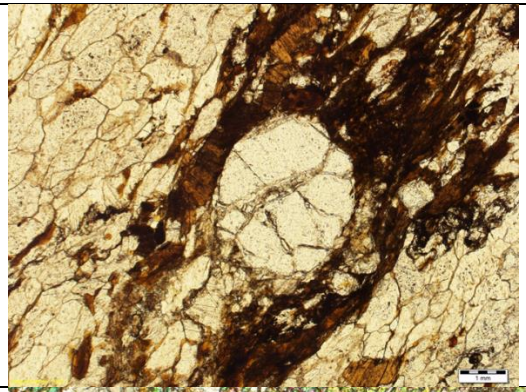
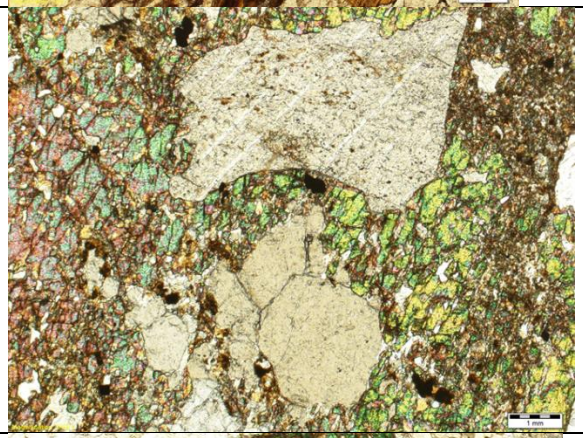
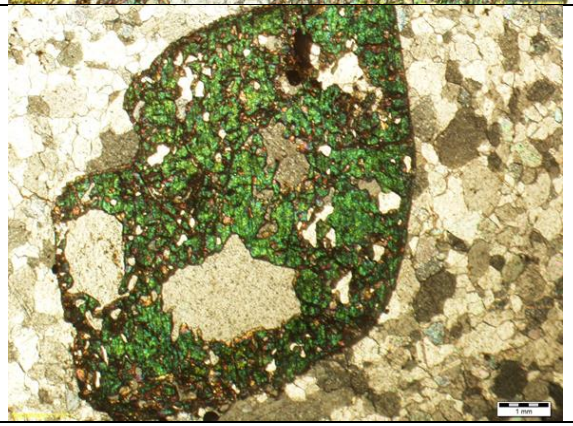
Appendix F: Mineralogy and textural characteristic of Epembe carbonatite from thin section analysis

Table 7-3 Mineralogy and textural characteristic of Epembe carbonatite from thin section analysis

Sample #	Photomicrograph	Major Minerals	Accessory Minerals	Texture and Characteristic
EPB02(XLP,4X)		Calcite	Apatite Plagioclase quartz	Coarse grained primary calcite with well-developed cleavages (multiple twinning) and porphyritic apatite are the dominant minerals in a fined matrix of secondary calcite and feldspars with minor quartz seen as interstitial minerals of variable sizes forming flow bands around the big grains. Calcite and apatite are typically oriented and shows some spatial association with each other suggesting similar time of crystallisation.
EPB02(XLP,4X)		Calcite	Apatite Plagioclase Quartz Biotite Hematite magnetite	Sub-rounded to oval shaped apatite suspended in fine ground mass of secondary calcite, biotite….Apatite is highly fractured and stained with iron (Fe) oxide along the fractures which are signs of late hydrothermal activities.

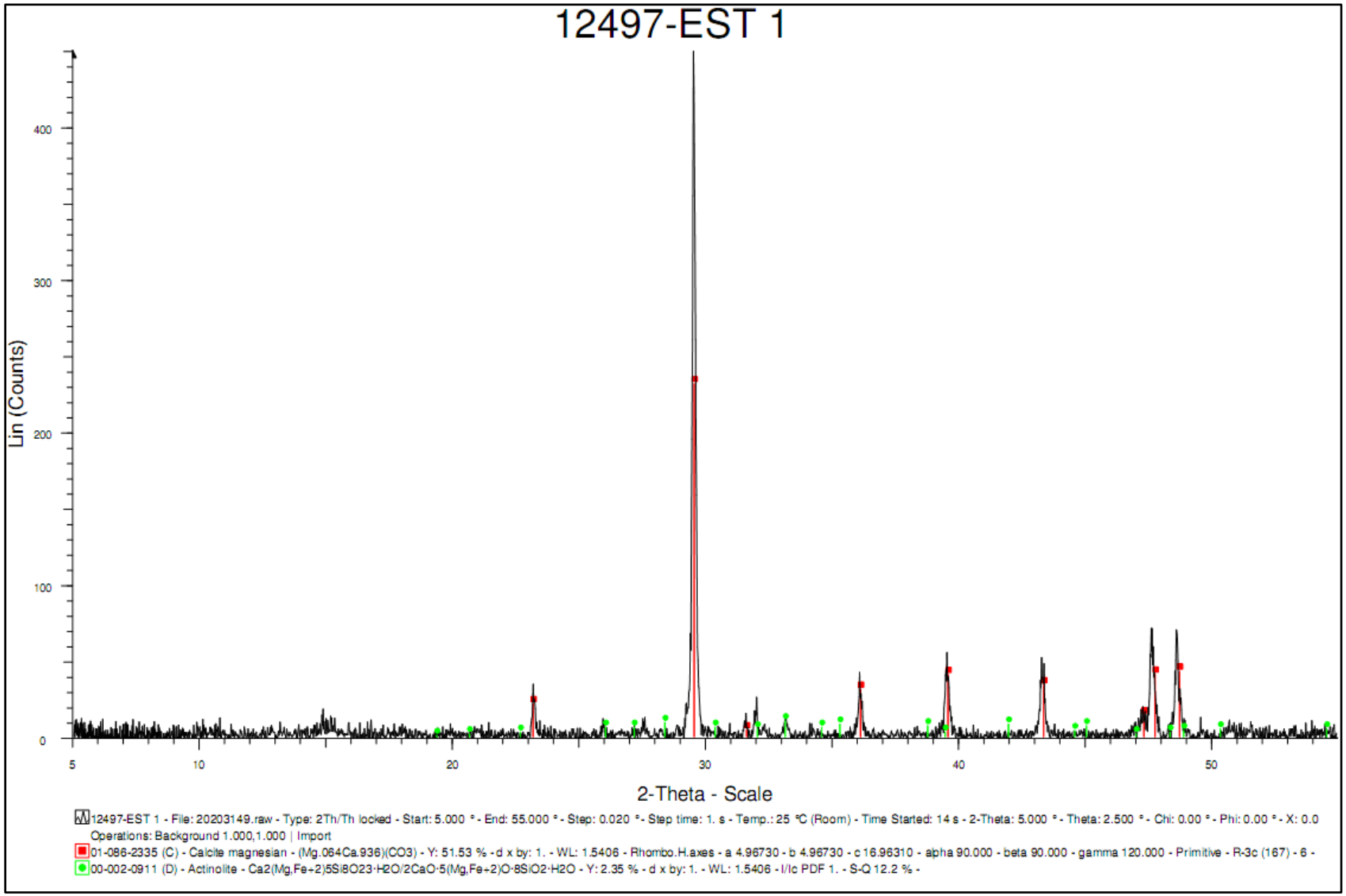
EPB03(XLP,4X)		Calcite	Apatite Pyrochlore Plagioclase quartz	Similar mineralogy to EPB02. Barren very course grained calcite with apatite which is hosting pyrochlore, suggesting that apatite had crystalised first than the pyrochlore. Pyrochlore appears as honey brown/or yellow and sometimes as opaque crystals suspended in small late vein
EPB04		Calcite	Apatite aegirine	Abundant coarse and sub-rounded apatite (yellowish green in colour) grains, highly fractured and compacted together with some inclusion of aegirine (peacock colured)
EPB06(XPL, 5X)		Calcite	Microcline plagioclase Dolomite Biotite Aegirine Magnetite	Medium to fine grained granular groundmass (gm) of anhedra feldspars, interstitial calcite, dolomite and minor amount of quartz forming equigranular texture seen also as un-oriented, interlocking grains. Fine grained grain implies that those minerals crystalised fast as compared to coarse grained that have crystalised with time

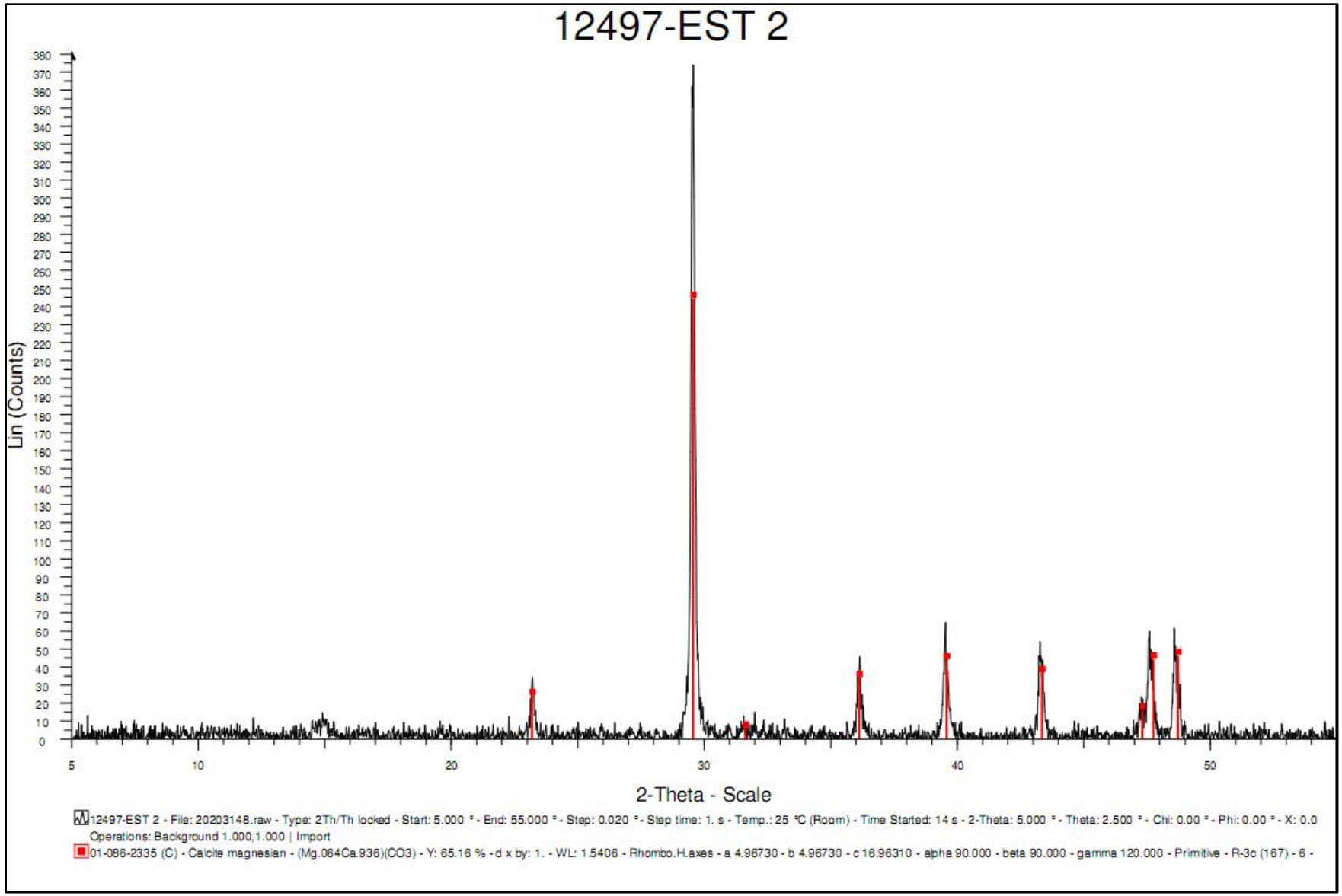
EPB07		Calcite	Plagioclase K-feldspar Biotite Aegirine Chlorite Magnetite hematite	Similar mineralogy and texture to **EPB02** and EPB03
EPB08 (PPL, 4X)		Calcite	Apatite	Apatite with calcite replacement. Iron (Fe) oxides exploiting cleavage planes within the calcite matrix and ovoid fractured crystals of apatite
EPB09(XPL,4X)		Calcite	Pyrochlore microcline Plagioclase (albite)	Brown red to opaque subhedral pyrochlore suspended in the ground mass of medium (0.1-0.8mm) to fine grained microcline and albite which are found in similar amounts. The minerals do not display specific orientation

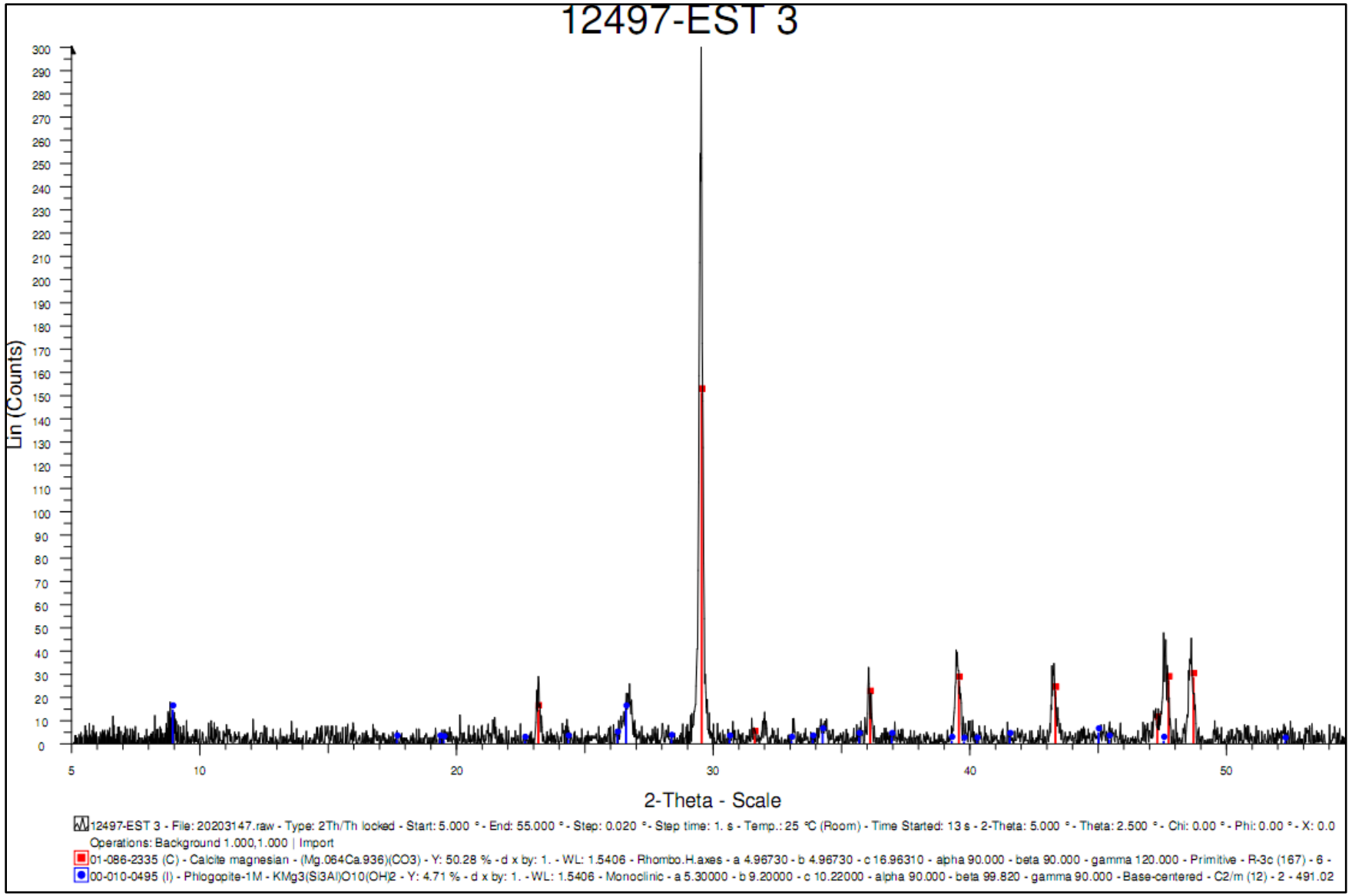
EPB12(PPL,4X)		Calcite	Biotite Apatite Aegirine Feldspars	Coarse grained ovoid apatite in the groundmass of calcite, aegirine, and feldspars all located in the vein
EPB13 (XPL,4X)		Calcite	Aegirine Feldspars Magnetite Hematite Biotite	Aegirine is typically brown green in colour, appearing as large aligned phenocrysts hosting calcite and apatite (calcite and apatite replacing aegirine?) Medium grained to opaque Magnetite and hematite together with feldspar, quarts and biotite disseminated within the aegirine.
EPB13 (XPL,4X)				Xenocrysts of aegirine within a mosaic calcite matrix, aegirine being replaced by calcite

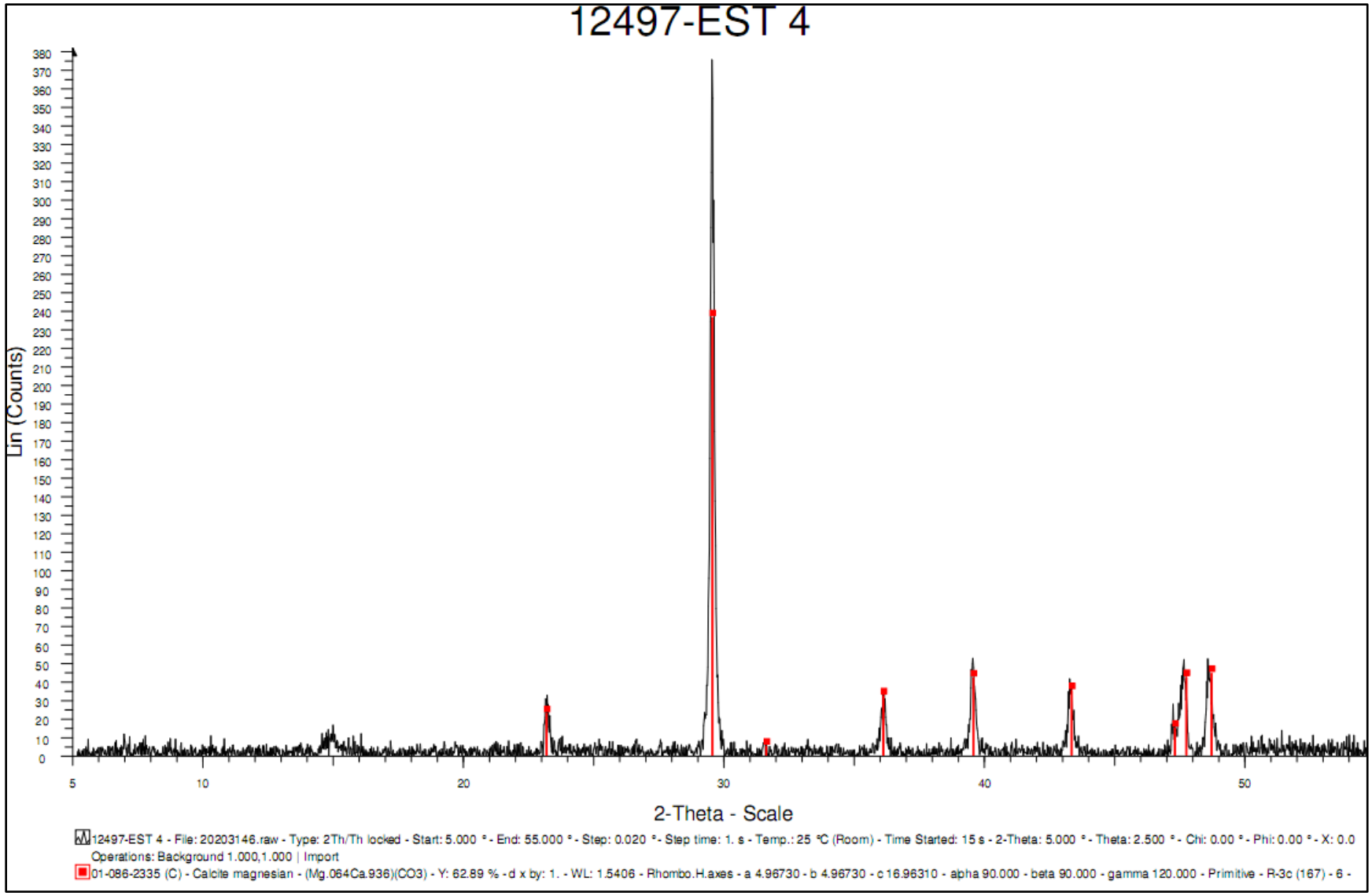
EPB15 (XPL,4X)			Apatite	Fractured apatite in the matrix of calcite, feldspar, biotite, hematite, magnetite flowing around the oval apatite grain.

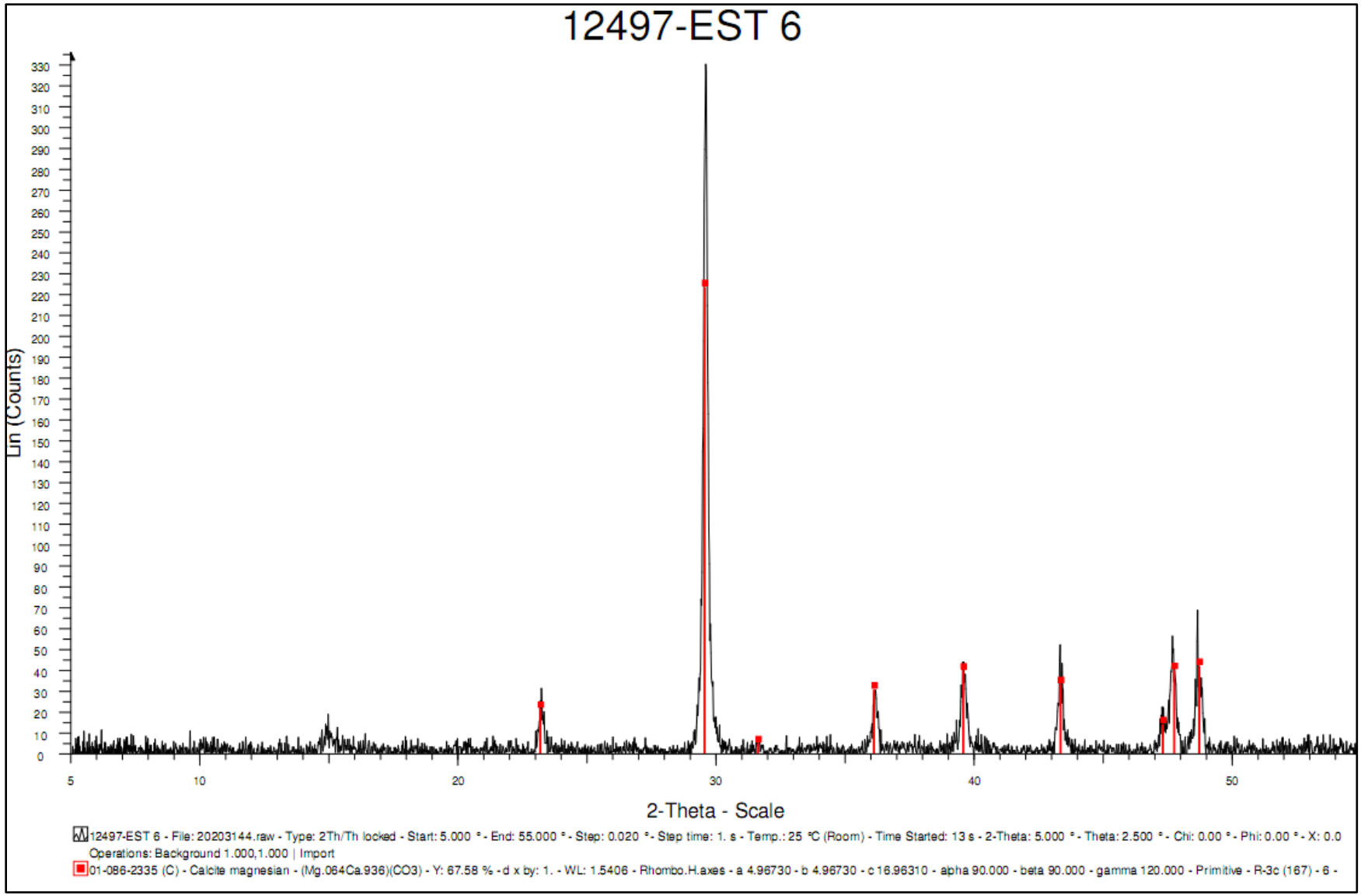
Appendix G: XRD results

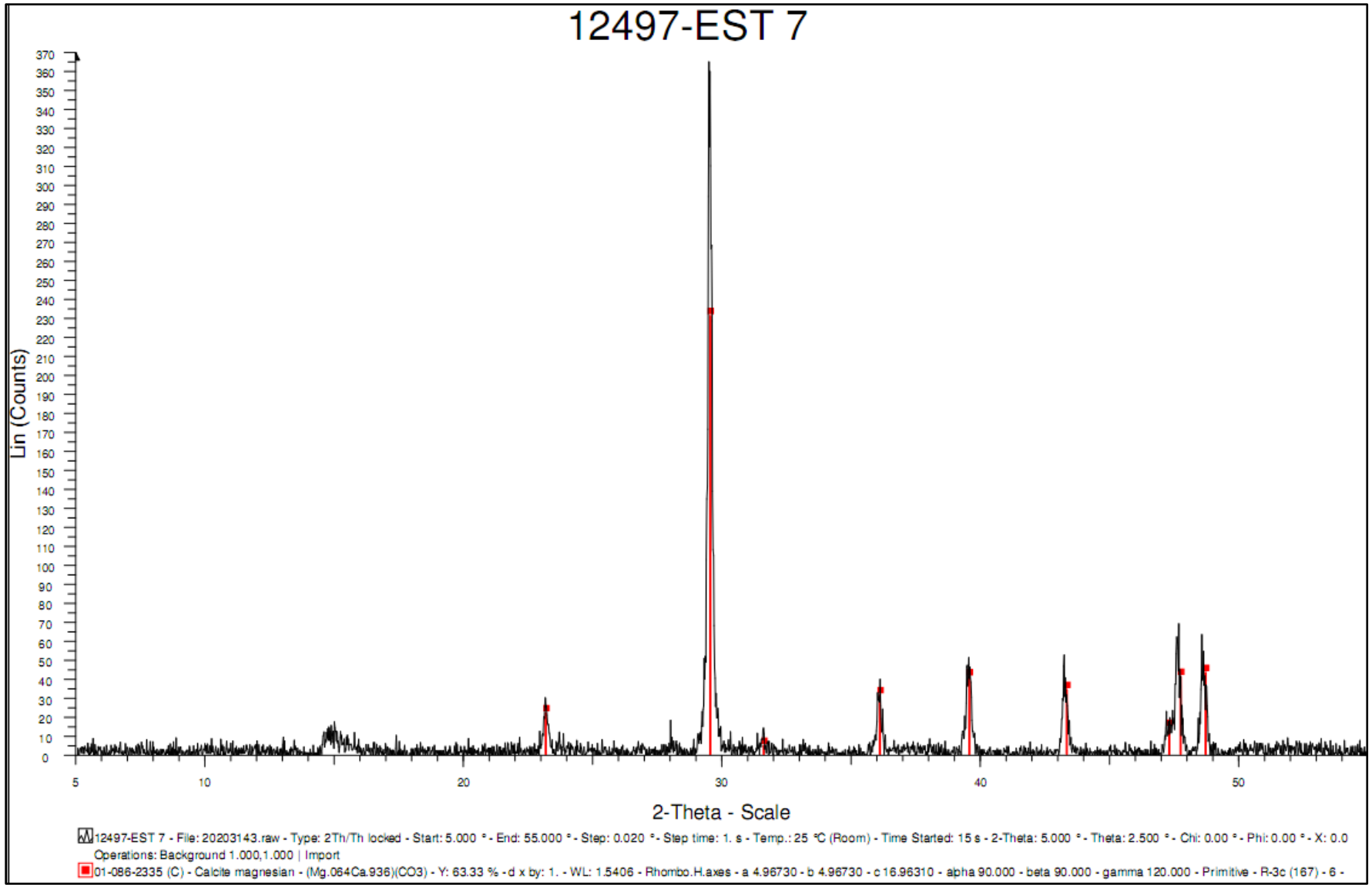


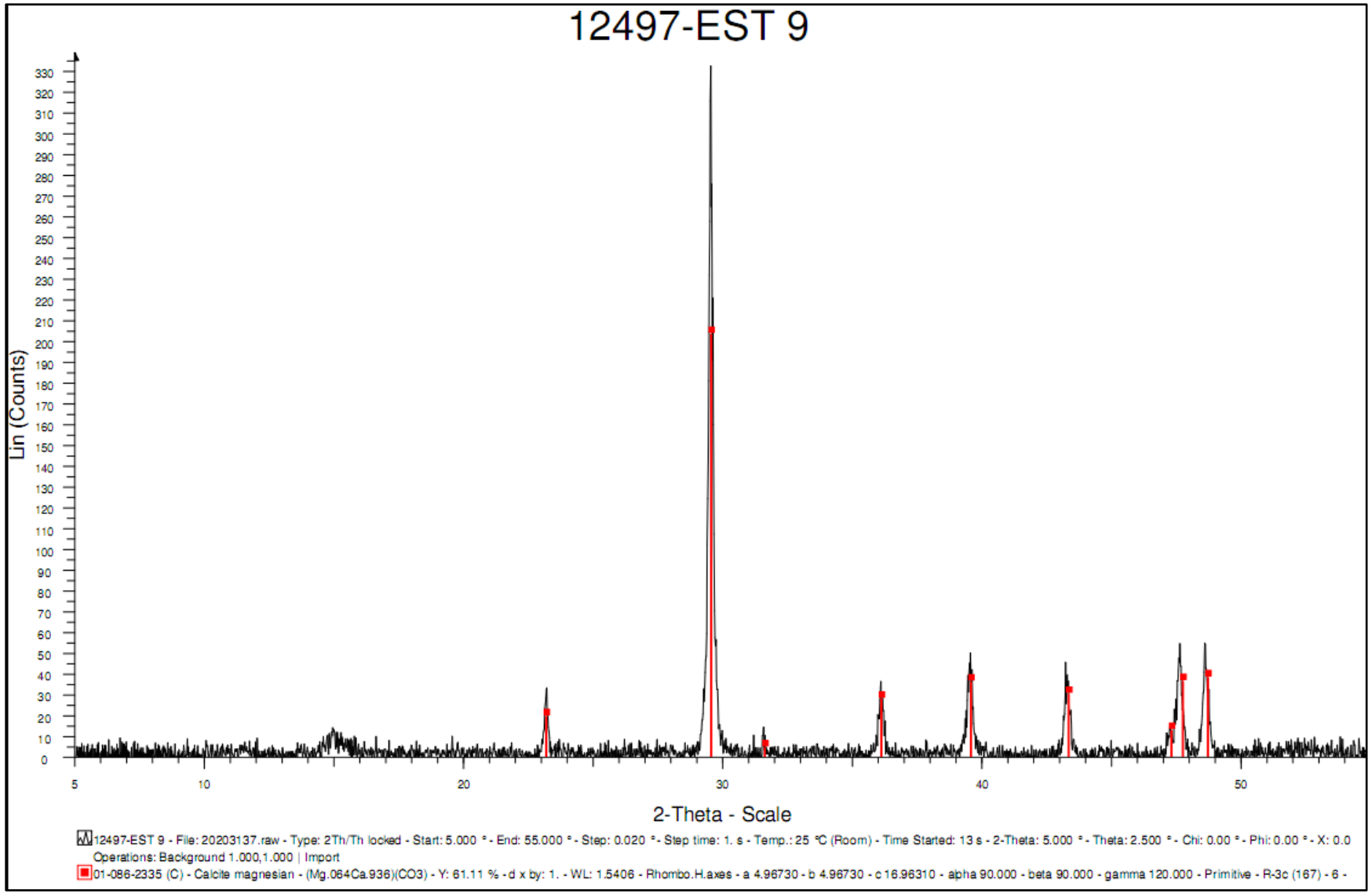

12497-EST 2
Lin (Counts)
2-Theta - Scale
12497-EST 2 - File: 20203148.raw - Type: 2Th/Th locked - Start: 5.000 ° - End: 55.000 ° - Step: 0.020 ° - Step time: 1. s - Temp.: 25 °C (Room) - Time Started: 14 s - 2-Theta: 5.000 ° - Theta: 2.500 ° - Chi: 0.00 ° - Phi: 0.00 ° - X: 0.0
Operations: Background 1.000,1.000 | Import
01-086-2335 (C) - Calcite magnesian - (Mg.064Ca.936)(CO3) - Y: 65.16 % - d x by: 1. - WL: 1.5406 - Rhombo.H.axes - a 4.96730 - b 4.96730 - c 16.96310 - alpha 90.000 - beta 90.000 - gamma 120.000 - Primitive - R-3c (167) - 6 -

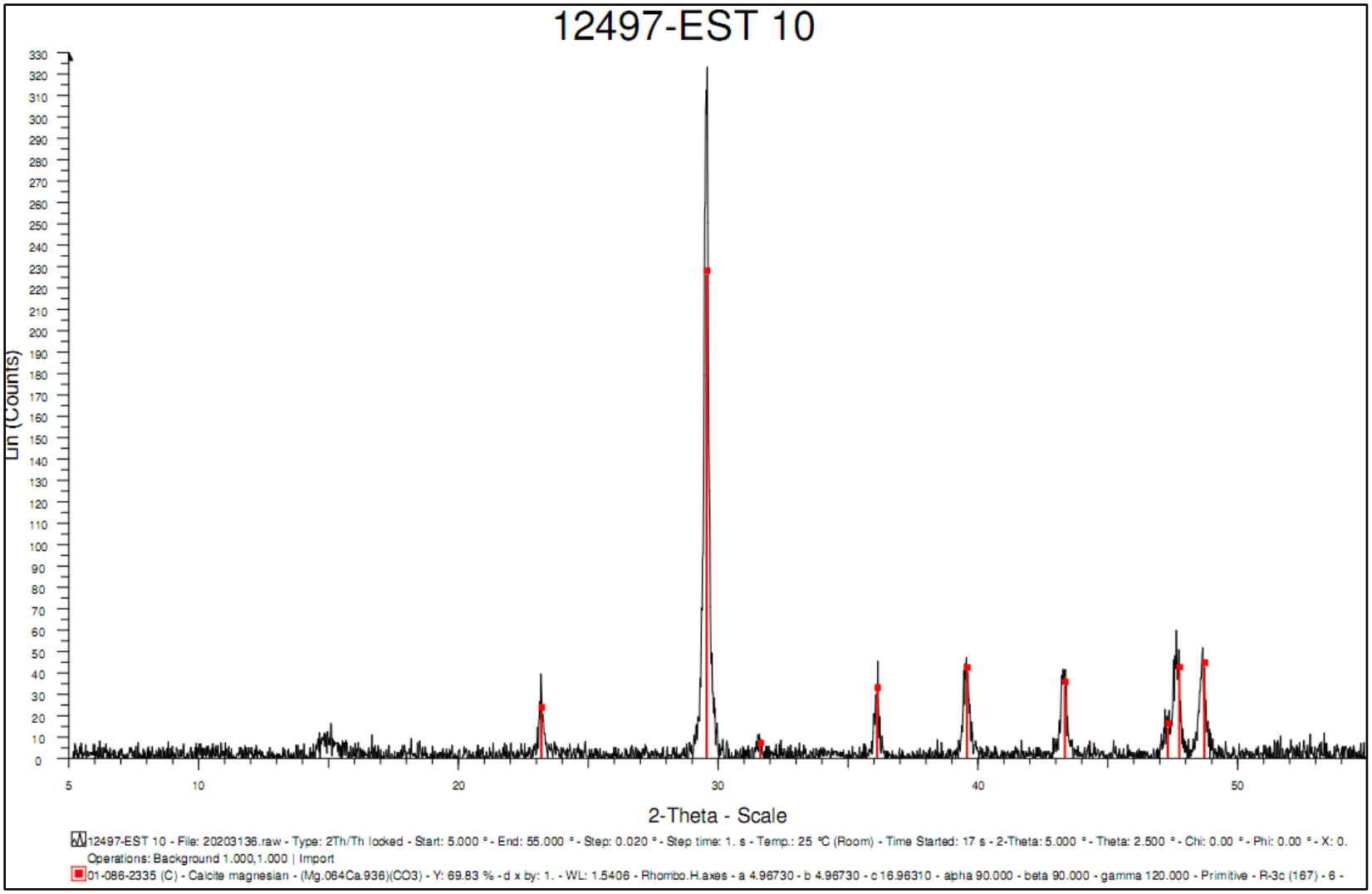

12497-EST 3
Lin (Counts)
2-Theta - Scale
12497-EST 3 - File: 20203147.raw - Type: 2Th/Th locked - Start: 5.000 ° - End: 55.000 ° - Step: 0.020 ° - Step time: 1. s - Temp.: 25 °C (Room) - Time Started: 13 s - 2-Theta: 5.000 ° - Theta: 2.500 ° - Chi: 0.00 ° - Phi: 0.00 ° - X: 0.0
Operations: Background 1.000,1.000 | Import
01-086-2335 (C) - Calcite magnesian - (Mg.064Ca.936)(CO3) - Y: 50.28 % - d x by: 1. - WL: 1.5406 - Rhombo.H.axes - a 4.96730 - b 4.96730 - c 16.96310 - alpha 90.000 - beta 90.000 - gamma 120.000 - Primitive - R-3c (167) - 6 -
00-010-0495 (I) - Phlogopite-1M - KMg3(Si3Al)O10(OH)2 - Y: 4.71 % - d x by: 1. - WL: 1.5406 - Monoclinic - a 5.30000 - b 9.20000 - c 10.22000 - alpha 90.000 - beta 99.820 - gamma 90.000 - Base-centered - C2/m (12) - 2 - 491.02

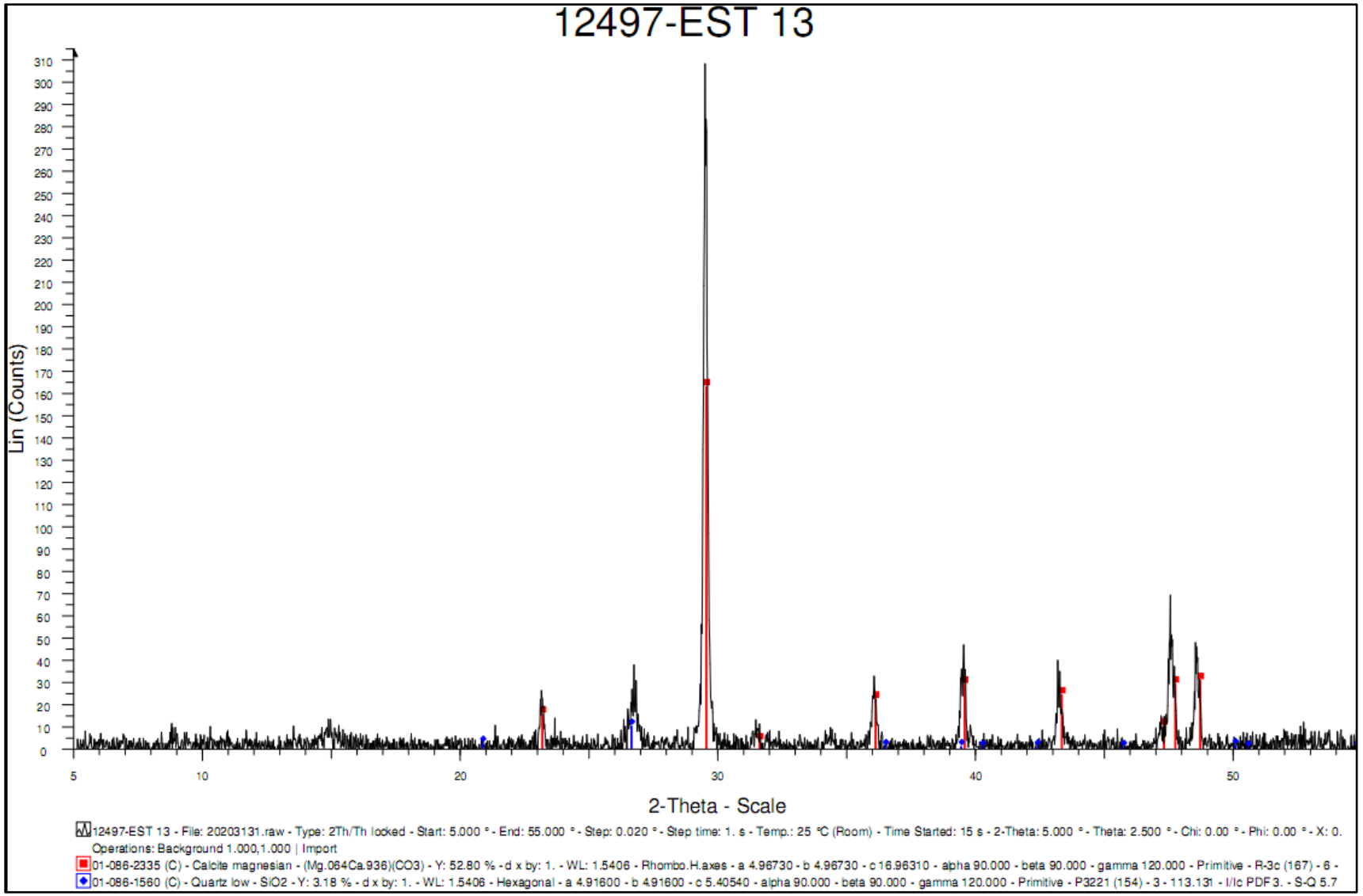

12497-EST 4
Lin (Counts)
2-Theta - Scale
12497-EST 4 - File: 20203146.raw - Type: 2Th/Th locked - Start: 5.000 ° - End: 55.000 ° - Step: 0.020 ° - Step time: 1. s - Temp.: 25 °C (Room) - Time Started: 15 s - 2-Theta: 5.000 ° - Theta: 2.500 ° - Chi: 0.00 ° - Phi: 0.00 ° - X: 0.0
Operations: Background 1.000,1.000 | Import
01-086-2335 (C) - Calcite magnesian - (Mg.064Ca.936)(CO3) - Y: 62.89 % - d x by: 1. - WL: 1.5406 - Rhombo.H.axes - a 4.96730 - b 4.96730 - c 16.96310 - alpha 90.000 - beta 90.000 - gamma 120.000 - Primitive - R-3c (167) - 6 -

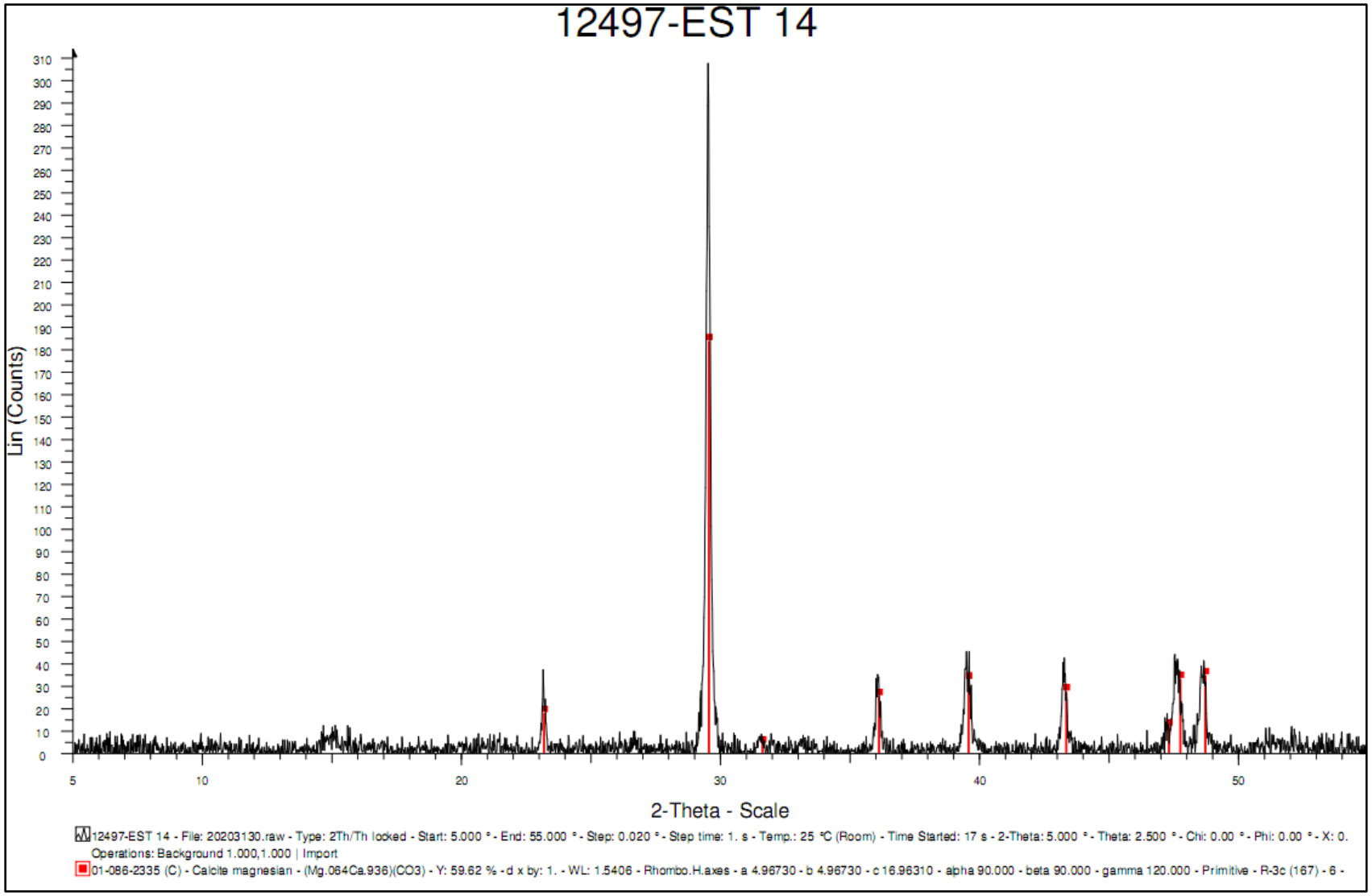

12497-EST 6
Lin (Counts)
2-Theta - Scale
12497-EST 6 - File: 20203144.raw - Type: 2Th/Th locked - Start: 5.000 ° - End: 55.000 ° - Step: 0.020 ° - Step time: 1. s - Temp.: 25 °C (Room) - Time Started: 13 s - 2-Theta: 5.000 ° - Theta: 2.500 ° - Chi: 0.00 ° - Phi: 0.00 ° - X: 0.0
Operations: Background 1.000,1.000 | Import
01-086-2335 (C) - Calcite magnesian - (Mg.064Ca.936)(CO3) - Y: 67.58 % - d x by: 1. - WL: 1.5406 - Rhombo.H.axes - a 4.96730 - b 4.96730 - c 16.96310 - alpha 90.000 - beta 90.000 - gamma 120.000 - Primitive - R-3c (167) - 6 -

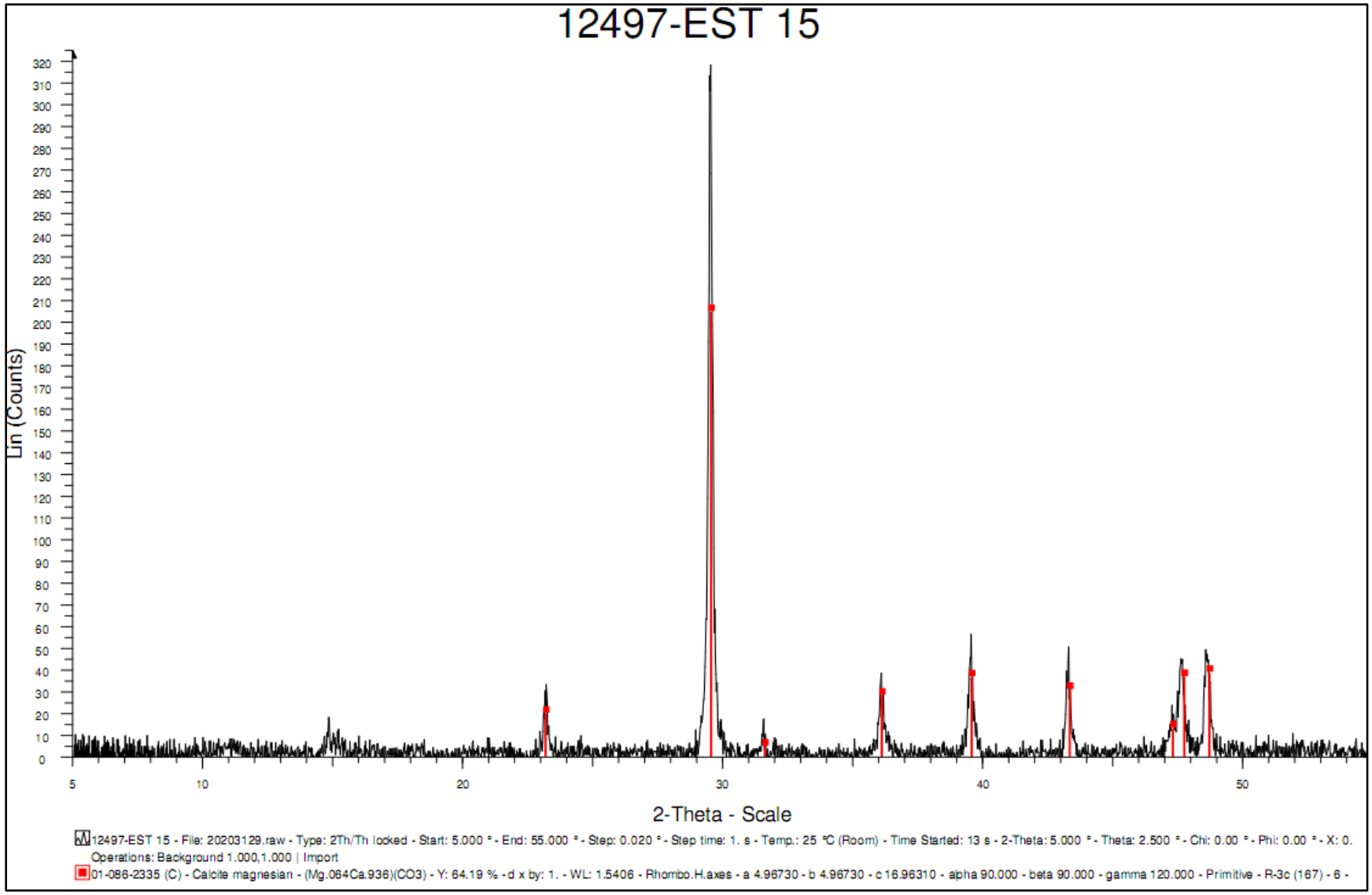

12497-EST 7
Lin (Counts)
2-Theta - Scale
12497-EST 7 - File: 20203143.raw - Type: 2Th/Th locked - Start: 5.000 ° - End: 55.000 ° - Step: 0.020 ° - Step time: 1. s - Temp.: 25 °C (Room) - Time Started: 15 s - 2-Theta: 5.000 ° - Theta: 2.500 ° - Chi: 0.00 ° - Phi: 0.00 ° - X: 0.0
Operations: Background 1.000,1.000 | Import
01-086-2335 (C) - Calcite magnesian - (Mg.064Ca.936)(CO3) - Y: 63.33 % - d x by: 1. - WL: 1.5406 - Rhombo.H.axes - a 4.96730 - b 4.96730 - c 16.96310 - alpha 90.000 - beta 90.000 - gamma 120.000 - Primitive - R-3c (167) - 6 -

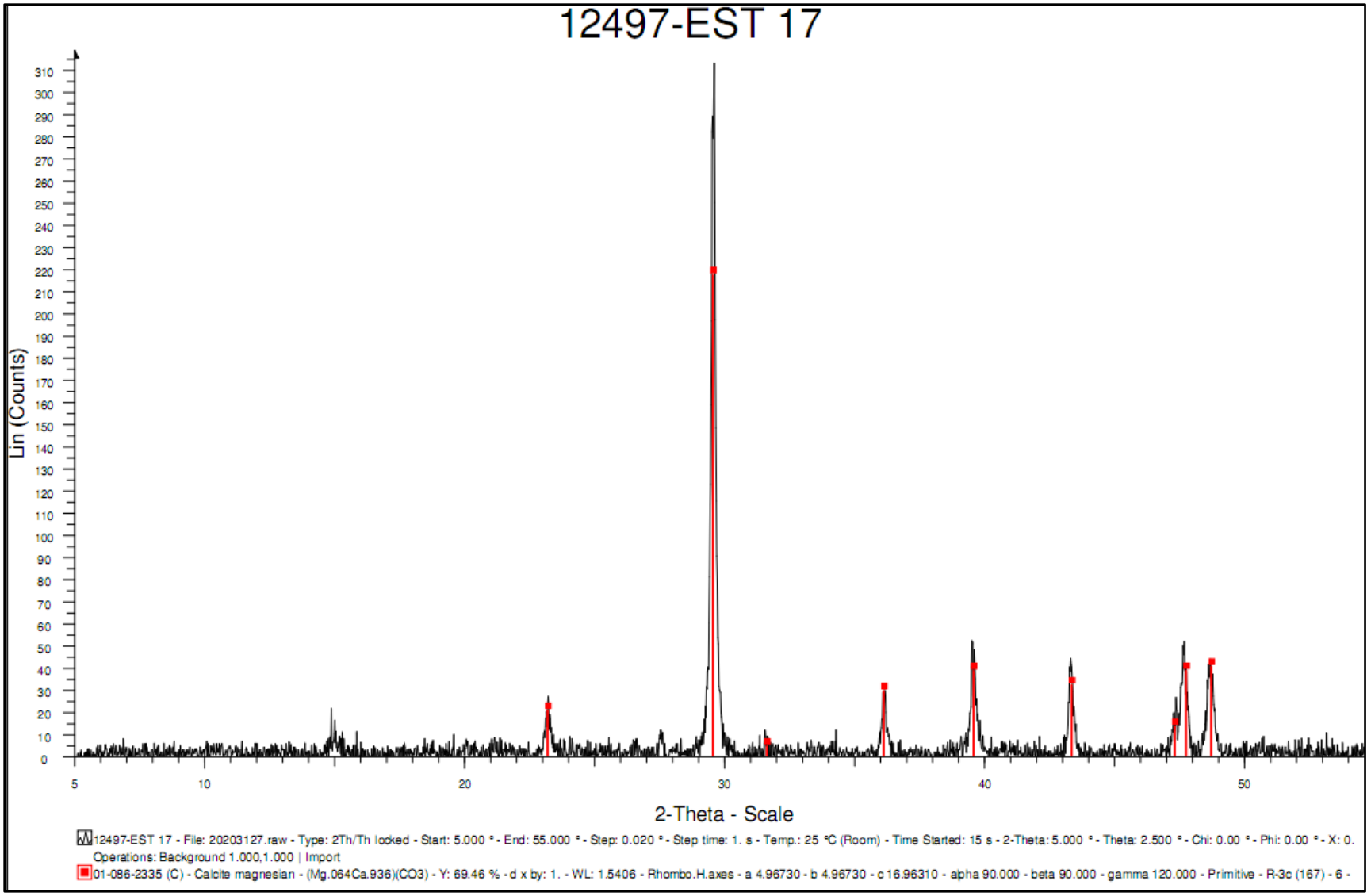

12497-EST 9
Lin (Counts)
2-Theta - Scale
12497-EST 9 - File: 20203137.raw - Type: 2Th/Th locked - Start: 5.000 ° - End: 55.000 ° - Step: 0.020 ° - Step time: 1. s - Temp.: 25 °C (Room) - Time Started: 13 s - 2-Theta: 5.000 ° - Theta: 2.500 ° - Chi: 0.00 ° - Phi: 0.00 ° - X: 0.0
Operations: Background 1.000,1.000 | Import
01-086-2335 (C) - Calcite magnesian - (Mg.064Ca.936)(CO3) - Y: 61.11 % - d x by: 1. - WL: 1.5406 - Rhombo.H.axes - a 4.96730 - b 4.96730 - c 16.96310 - alpha 90.000 - beta 90.000 - gamma 120.000 - Primitive - R-3c (167) - 6 -

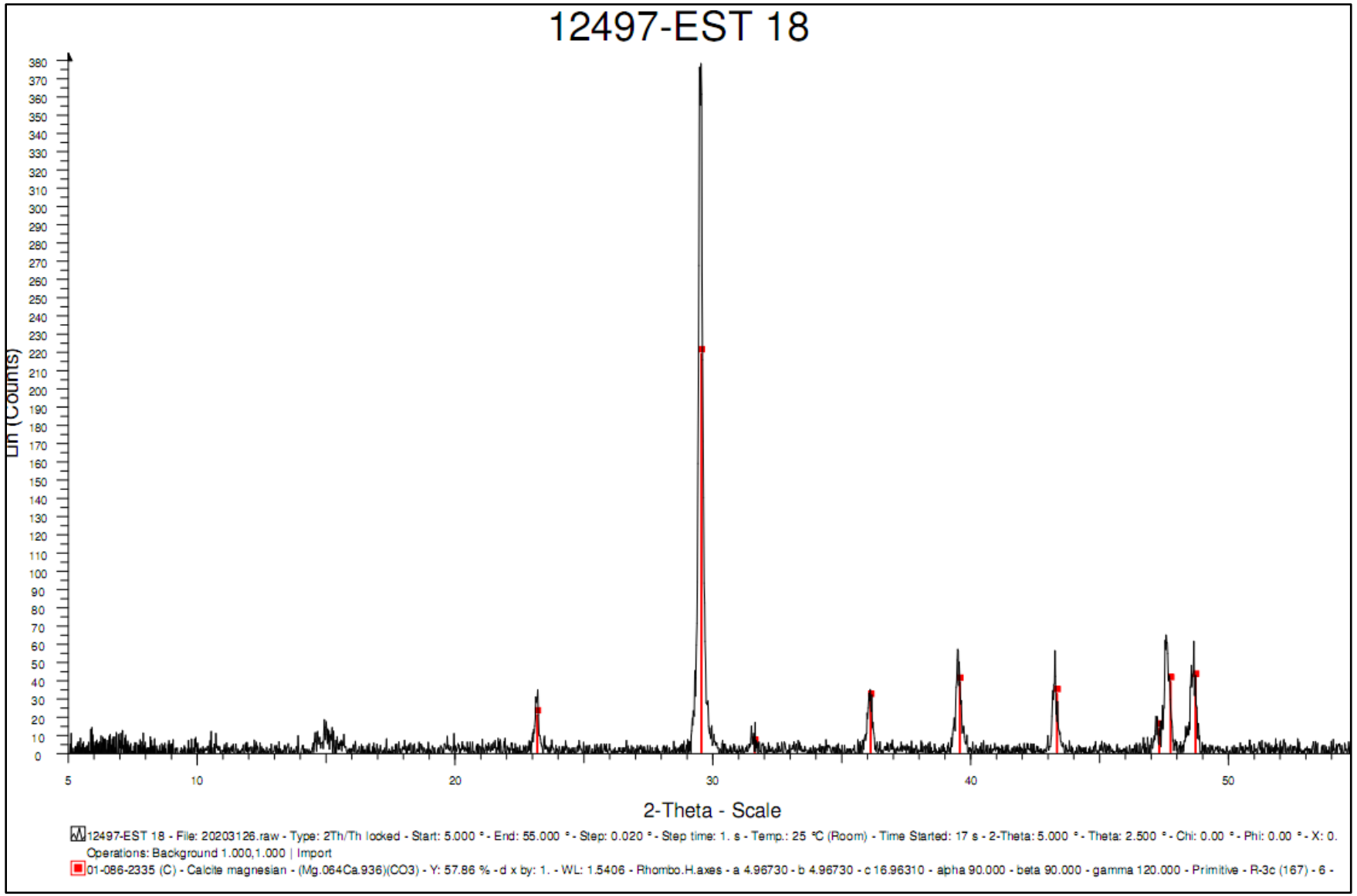

12497-EST 10
Lin (Counts)
2-Theta - Scale
12497-EST 10 - File: 20203136.raw - Type: 2Th/Th locked - Start: 5.000 ° - End: 55.000 ° - Step: 0.020 ° - Step time: 1. s - Temp.: 25 °C (Room) - Time Started: 17 s - 2-Theta: 5.000 ° - Theta: 2.500 ° - Chi: 0.00 ° - Phi: 0.00 ° - X: 0.
Operations: Background 1.000,1.000 | Import
01-086-2335 (C) - Calcite magnesian - (Mg.064Ca.936)(CO3) - Y: 69.83 % - d x by: 1. - WL: 1.5406 - Rhombo.H.axes - a 4.96730 - b 4.96730 - c 16.96310 - alpha 90.000 - beta 90.000 - gamma 120.000 - Primitive - R-3c (167) - 6 -


12497-EST 13
Lin (Counts)
2-Theta - Scale
12497-EST 13 - File: 20203131.raw - Type: 2Th/Th locked - Start: 5.000 ° - End: 55.000 ° - Step: 0.020 ° - Step time: 1. s - Temp.: 25 °C (Room) - Time Started: 15 s - 2-Theta: 5.000 ° - Theta: 2.500 ° - Chi: 0.00 ° - Phi: 0.00 ° - X: 0.
Operations: Background 1.000,1.000 | Import
01-086-2335 (C) - Calcite magnesian - (Mg.064Ca.936)(CO3) - Y: 52.80 % - d x by: 1. - WL: 1.5406 - Rhombo.H.axes - a 4.96730 - b 4.96730 - c 16.96310 - alpha 90.000 - beta 90.000 - gamma 120.000 - Primitive - R-3c (167) - 6 -
01-086-1560 (C) - Quartz low - SiO2 - Y: 3.18 % - d x by: 1. - WL: 1.5406 - Hexagonal - a 4.91600 - b 4.91600 - c 5.40540 - alpha 90.000 - beta 90.000 - gamma 120.000 - Primitive - P3221 (154) - 3 - 113.131 - I/Ic PDF 3. - S-Q 5.7


12497-EST 14
Lin (Counts)
2-Theta - Scale
12497-EST 14 - File: 20203130.raw - Type: 2Th/Th locked - Start: 5.000 ° - End: 55.000 ° - Step: 0.020 ° - Step time: 1. s - Temp.: 25 °C (Room) - Time Started: 17 s - 2-Theta: 5.000 ° - Theta: 2.500 ° - Chi: 0.00 ° - Phi: 0.00 ° - X: 0.
Operations: Background 1.000,1.000 | Import
01-086-2335 (C) - Calcite magnesian - (Mg.064Ca.936)(CO3) - Y: 59.62 % - d x by: 1. - WL: 1.5406 - Rhombo.H.axes - a 4.96730 - b 4.96730 - c 16.96310 - alpha 90.000 - beta 90.000 - gamma 120.000 - Primitive - R-3c (167) - 6 -


12497-EST 15
Lin (Counts)
2-Theta - Scale
12497-EST 15 - File: 20203129.raw - Type: 2Th/Th locked - Start: 5.000 ° - End: 55.000 ° - Step: 0.020 ° - Step time: 1. s - Temp.: 25 °C (Room) - Time Started: 13 s - 2-Theta: 5.000 ° - Theta: 2.500 ° - Chi: 0.00 ° - Phi: 0.00 ° - X: 0.
Operations: Background 1.000,1.000 | Import
01-086-2335 (C) - Calcite magnesian - (Mg.064Ca.936)(CO3) - Y: 64.19 % - d x by: 1. - WL: 1.5406 - Rhombo.H.axes - a 4.96730 - b 4.96730 - c 16.96310 - alpha 90.000 - beta 90.000 - gamma 120.000 - Primitive - R-3c (167) - 6 -


12497-EST 17
Lin (Counts)
2-Theta - Scale
12497-EST 17 - File: 20203127.raw - Type: 2Th/Th locked - Start: 5.000 ° - End: 55.000 ° - Step: 0.020 ° - Step time: 1. s - Temp.: 25 °C (Room) - Time Started: 15 s - 2-Theta: 5.000 ° - Theta: 2.500 ° - Chi: 0.00 ° - Phi: 0.00 ° - X: 0.
Operations: Background 1.000,1.000 | Import
01-086-2335 (C) - Calcite magnesian - (Mg.064Ca.936)(CO3) - Y: 69.46 % - d x by: 1. - WL: 1.5406 - Rhombo.H.axes - a 4.96730 - b 4.96730 - c 16.96310 - alpha 90.000 - beta 90.000 - gamma 120.000 - Primitive - R-3c (167) - 6 -


12497-EST 18
Lin (Counts)
2-Theta - Scale
12497-EST 18 - File: 20203126.raw - Type: 2Th/Th locked - Start: 5.000 ° - End: 55.000 ° - Step: 0.020 ° - Step time: 1. s - Temp.: 25 °C (Room) - Time Started: 17 s - 2-Theta: 5.000 ° - Theta: 2.500 ° - Chi: 0.00 ° - Phi: 0.00 ° - X: 0.
Operations: Background 1.000,1.000 | Import
01-086-2335 (C) - Calcite magnesian - (Mg.064Ca.936)(CO3) - Y: 57.86 % - d x by: 1. - WL: 1.5406 - Rhombo.H.axes - a 4.96730 - b 4.96730 - c 16.96310 - alpha 90.000 - beta 90.000 - gamma 120.000 - Primitive - R-3c (167) - 6 -

Appendix H: Analytical Results

Major element analysis

		SiO2	Al2O3	Fe2O3	MnO	MgO	CaO	Na2O	K2O	TiO2	P2O5	Cr2O3	NiO	LOI	Total	
PN/EK	EST1	5.28	1.28	4.41	0.28	0.35	48.98	0.22	0.55	0.13	3.62	0.02	0.00	34.71	99.82	
PN/EK	EST2	3.71	0.52	2.89	0.25	0.23	49.47	0.44	0.19	0.09	2.81	0.02	0.00	36.78	97.41	
PN/EK	EST3	10.89	4.45	10.33	0.25	1.33	38.01	0.21	1.52	1.06	3.43	0.02	0.00	28.18	99.66	
PN/EK	EST4	3.91	1.17	2.25	0.24	0.33	50.00	0.11	0.59	0.14	2.22	0.03	0.00	37.14	98.13	
PN/EK	EST5	67.81	15.37	3.32	0.05	0.88	1.49	5.10	5.62	0.74	0.32	0.02	0.00	0.67	101.39	
PN/EK	EST6	1.73	0.16	0.97	0.31	0.25	55.31	0.05	0.02	0.03	0.46	0.02	0.00	40.83	100.14	
PN/EK	EST7	1.99	0.52	1.67	0.31	0.23	53.90	0.03	0.15	0.03	0.53	0.02	0.00	40.29	99.66	
PN/EK	EST8	2.62	0.65	1.36	0.29	0.19	51.54	0.01	0.42	0.06	1.18	0.02	0.00	39.88	98.23	
PN/EK	EST9	1.30	0.35	1.18	0.31	0.26	54.69	0.04	0.17	0.03	0.16	0.02	0.00	41.56	100.08	
PN/EK	EST10	54.57	19.96	2.24	0.07	0.34	4.48	7.01	6.65	0.25	0.37	0.02	0.00	4.79	100.77	
PN/EK	EST11	6.26	1.61	5.83	0.25	0.76	46.18	0.19	0.91	0.33	0.75	0.02	0.00	36.08	99.17	
PN/EK	EST12	2.41	0.79	3.29	0.38	0.59	52.33	0.03	0.36	0.14	2.30	0.03	0.00	37.53	100.18	
PN/EK	EST13	3.42	0.63	3.10	0.29	0.27	49.41	0.34	0.28	0.05	1.50	0.03	0.00	38.11	97.43	
PN/EK	EST14	7.90	2.27	1.55	0.34	0.20	48.83	0.26	1.44	0.03	1.66	0.02	0.00	34.41	98.92	
PN/EK	EST15	1.51	0.50	1.22	0.26	0.19	54.45	0.01	0.15	0.05	0.34	0.02	0.00	41.04	99.74	
PN/EK	EST16	55.64	20.21	5.73	0.09	1.44	2.73	9.64	1.77	0.62	0.23	0.02	0.00	3.03	101.15	
	CRMs															
		SiO2	Al2O3	Fe2O3	FeO	MnO	MgO	CaO	Na2O	K2O	TiO2	P2O5	Cr2O3	NiO	TOTAL	LOI
NIM-P		51.2	4.28	1.28	10.35	0.23	25.32	2.61	0.34	0.08	0.1949	0.03	3.5273	0.0757	99.51	-0.23
NIM-D		39.11	0.33	1.71	13.83	0.22	43.78	0.3	0.03	0	0.0267	0.01	0.3985	0.2619	100.01	-0.51
W2		53.1	15.49	1.1	8.9	0.16	6.46	10.94	2.22	0.63	1.0767	0.13	0.0215	0.0089	100.24	0.19
NIM-S		64.04	17.34	0.14	1.12	0.01	0.46	0.68	0.37	15.46	0.0504	0.12	0.007	0.001	99.8	0.42
GSP2		67.32	15.07	0.5	4.02	0.04	0.97	2.13	2.82	5.46	0.669	0.3	0.0114	0	99.31	0.87
BCR2		55.11	13.71	1.4	11.36	0.2	3.65	7.18	3.16	1.81	2.2824	0.36	0.0235	0.0008	100.26	0.1
NIM-N		53.4	16.75	0.91	7.38	0.18	7.6	11.58	2.42	0.25	0.2001	0.02	0.0165	0.0159	100.73	0.04
NIM-G		76.6	12.23	0.2	1.58	0.02	0.04	0.8	3.31	5.09	0.0994	0.02	0.0077	0.0011	99.98	0.73
PCC1		43.97	0.74	0.86	7	0.12	45.79	0.59	0.07	0	0.0153	0.01	0.4051	0.3293	99.91	5.09
BHVO2		50.23	13.71	1.25	10.1	0.17	7.33	11.43	2.2	0.52	2.7467	0.28	0.0579	0.0138	100.04	-0.48
AGV2		60.43	17.25	0.68	5.54	0.1	1.81	5.28	4.24	2.94	1.0428	0.48	0.0137	0.0037	99.81	1.8
G2		69.7	15.45	0.27	2.16	0.03	0.77	1.96	4.1	4.54	0.4925	0.14	0.0097	0.0022	99.61	0.64
DTS1		40.83	0.26	0.87	7.05	0.12	50.15	0.16	0.06	0.01	0.0112	0.02	0.5774	0.3138	100.41	-0.02

Trace element analysis

	EST01	EST02	EST03	EST04	EST05	EST06	EST07	EST08	EST09	EST10	EST11	EST12	EST13	EST14	EST15	EST16
Li	1.858	0.487	4.534	1.365	6.399	0.486	1.206	0.745	0.34	8.151	2.01	1.711	0.512	0.768	0.726	46.175
P	18076.91	11637.61	12778.69	8314.227	1158.75	2024.969	2546.249	5109.313	751.433	1314.421	3516.495	11330.12	7512.338	7694.047	1491.791	1110.539
Sc	4.381	7.029	3.956	3.657	4.29	1.193	0.779	1.765	0.45	0.161	1.856	2.355	6.384	1.513	1.066	1.609
Ti	674.363	381.25	5122.755	644.722	4018.862	43.6	137.704	217.331	69.002	863.493	1535.985	600.214	184.22	113.748	144.343	3749.906
V	161.806	89.28	116.548	33.896	51.452	2.716	8.253	17.288	5.447	12.07	47.352	28.598	148.95	3.723	19.426	58.218
Cr	12.129	9.571	8.323	6.045	84.731	4.622	13.254	3.819	3.958	48.698	8.622	8.453	23.905	10.361	5.343	67.253
Co	7.554	3.247	11.466	4.39	5.915	2.643	2.201	4.063	2.189	2.174	7.918	10.621	5.669	4.271	3.437	8.96
Ni	19.65	17.753	11.879	17.321	7.318	19.844	21.219	16.585	19.299	3.707	24.067	31.679	21.518	27.206	30.215	11.91
Cu	9.265	7.893	7.433	4.552	32.448	9.732	6.293	9.38	3.513	4.239	17.728	19.227	6.881	5.983	4.492	9.815
Zn	13.745	12.868	99.359	15.1	42.483	6.709	6.369	518.026	10.571	25.551	59.37	27.725	8.971	54.41	5.985	93.408
Ga	12.474	7.06	16.115	8.218	22.929	3.29	3.709	4.662	4.973	28.295	15.182	8.218	6.332	6.625	3.792	27.555
Rb	17.994	6.352	20.9	20.863	223.121	0.99	3.408	7.237	9.58	56.34	77.383	13.53	7.188	21.388	3.717	124.77
Sr	4232.201	12315.44	7544.458	8641.792	444.701	5108.843	4538.515	8954.933	5381.323	782.809	8282.465	3354.482	9446.242	7502.439	4832.948	1074.916
Y	83.483	75.31	54.563	72.66	19.439	76.135	70.685	74.326	91.074	3.432	69.774	86.18	67.435	63.277	52.53	10.574
Zr	125.733	99.527	114.128	94.076	461.5	2.606	2.453	116.125	3.072	199.56	224.418	34.962	72.877	6.865	7.636	292.52
Nb	1532.567	1090.018	2022.64	159.584	20.895	7.687	40.046	280.704	45.169	26.217	150.534	225.125	64.152	51.784	24.802	141.536
Ba	96.631	134.621	205.813	142.226	2637.837	53.782	516.205	135.755	110.28	669.348	182.432	saturated	141.361	247.497	98.64	633.981
Sn	18.085	17.932	11.401	4.234	2.69	0.242	1.702	3.676	0.965	0.211	4.624	1.044	16.983	1.435	1.052	3.201
Cs	0.632	0.237	1.35	0.705	3.978	0.024	0.201	0.072	1.877	1.378	2.946	0.956	0.148	0.12	0.119	5.2
La	176.877	159.36	151.284	166.471	157.415	131.631	123.828	109.644	163.835	13.112	167.194	172.029	133.58	76.812	141.432	26.982
Ce	347.772	296.856	267.934	307.59	290.656	260.133	241.302	210.867	341.538	32.607	290.229	saturated	257.332	168.92	254.796	53.401
Pr	39.423	32.687	30.414	33.868	28.65	26.032	26.524	23.069	35.445	2.492	31.946	40.212	29.802	21.57	28.563	6.682
Nd	159.157	132.662	136.065	136.478	102.654	100.016	112.511	94.816	149.781	10.578	130.901	saturated	128.712	82.438	103.42	27.589
Sm	28.765	23.413	20.856	22.544	15.603	16.177	18.168	17.689	25.297	1.998	20.777	28.641	21.631	17.87	17.796	5.362
Eu	8.587	6.929	6.143	6.689	3.241	4.51	5.247	5.325	6.896	0.715	6.189	8.593	6.426	5.459	5.002	1.495
Gd	29.341	24.159	20.795	23.704	12.795	17.954	19.319	19.319	26.827	1.785	21.868	30.044	22.335	18.458	18.21	4.411
Tb	3.489	2.752	2.284	2.695	1.096	2.199	2.265	2.322	3.043	0.183	2.432	3.517	2.634	2.361	2.07	0.533
Dy	18.096	14.235	11.167	13.911	4.682	12.345	12.362	13.152	16.077	0.933	12.614	18.095	14.027	12.612	10.5	2.784
Ho	2.979	2.427	1.819	2.362	0.67	2.288	2.185	2.33	2.798	0.151	2.139	3.101	2.404	2.284	1.859	0.473
Er	6.781	5.72	4.334	5.703	1.745	5.961	5.488	5.53	6.818	0.366	5.355	7.429	5.762	5.383	4.678	1.221
Tm	0.931	0.801	0.582	0.791	0.201	0.948	0.847	0.821	0.95	0.05	0.745	1.042	0.827	0.808	0.682	0.185

Yb	5.664	5.11	3.607	5.07	1.277	6.49	5.629	5.205	6.09	0.304	4.779	6.509	5.159	5.122	4.369	1.26
Lu	0.769	0.697	0.495	0.716	0.171	0.967	0.812	0.735	0.86	0.041	0.684	0.914	0.735	0.733	0.644	0.187
Hf	5.04	5.68	3.05	2.099	10.621	0.124	0.133	2.088	0.194	3.555	3.948	0.841	3.593	0.19	0.288	4.956
Ta	76.502	187.417	367.275	33.412	1.145	0.485	10.757	54.006	8.356	1.131	12.841	48.354	8.417	2.16	3.018	6.429
W	0.651	0.116	0.27	0.188	0.399	0.142	0.227	0.122	0.237	0.156	0.365	0.267	0.103	0.217	0.148	0.512
Pb	5.81	6.74	6.206	5.023	27.346	6.501	2.988	143.836	6.989	2.873	4.757	19.164	7.041	23.243	1.741	11.599
Th	21.895	6.372	8.062	2.082	72.776	0.401	0.341	3.22	3.282	0.937	3.052	2.257	0.413	0.757	0.964	4.438
U	26.739	331.901	480.062	25.154	7.431	2.184	6.19	67.622	10.671	2.333	6.001	50.28	9.091	1.923	2.096	4.096

CRMs	BCR2	BHVO2														
Li	10.233	4.843														
P	1575.964	1174.301														
Sc	32.782	30.278														
Ti	13003.75	15622.5														
V	420.252	324.177														
Cr	14.514	286.54														
Co	36.814	45.74														
Ni	14.12	111.97														
Cu	22.734	123.837														
Zn	136.987	115.438														
Ga	22.442	21.244														
Rb	49.69	9.245														
Sr	330.444	371.386														
Y	32.073	22.255														
Zr	191.001	162.553														
Nb	12.455	16.868														
Ba	655.746	125.869														
Sn	2.828	2.259														
Cs	1.248	0.104														
La	25.221	15.166														
Ce	52.25	35.801														
Pr	6.346	4.964														
Nd	27.568	23.516														
Sm	6.4	5.711														
Eu	2.005	1.91														
Gd	6.57	5.838														